This is to certify that the

thesis entitled

A TWO-DIMENSIONAL SOIL PHYSICAL MODEL
OF MOISTURE AND TEMPERATURE INTERACTIONS
IN THE SEED ZONE USING A FINITE ELEMENT FORMULATION

presented by

Don E. Holzhei

has been accepted towards fulfillment
of the requirements for

Ph.D. degree in Agricultural Engineering

Thomas H Burkhardt
Major professor

Date August 7, 1984

# A TWO-DIMENSIONAL SOIL PHYSICAL MODEL OF MOISTURE AND TEMPERATURE INTERACTIONS IN THE SEED ZONE USING A FINITE ELEMENT FORMULATION

by

Don Earl Holzhei

A DISSERTATION

Submitted to

Michigan State University

in partial fulfillment of the requirements

for the degree of

DOCTOR OF PHILOSOPHY

Department of Agricultural Engineering

1984

# ABSTRACT

## A TWO-DIMENSIONAL SOIL PHYSICAL MODEL OF MOISTURE AND TEMPERATURE INTERACTIONS IN THE SEED ZONE USING A FINITE ELEMENT FORMULATION

by

Don E. Holzhei

The objective of this study was the formulation of finite element model that could be used to analyze the moisture and temperature regime around a planted seed periodically for three or more days after planting. The model developed from this study was unique due to the combination outlined below:

1. Studied simultaneous moisture and temperature interactions
2. Incorporated soil air mass flow convection with diffusion mechanisms
3. Exhibited two-dimensional and time-dependent regimes
4. Considered heterogeneous soil grid with varying structure and texture
5. Included soil moisture hysteresis
6. Interfaced with a diurnal meteorological model imposed on the soil surface
7. Utilized the Galerkin approximation to the finite element numerical solution
8. Applied to seed furrow geometry and tillage practice studies

The grid was composed of triangular elements of varying size, extending horizontally from the furrow centerline to a point midway between rows, and vertically to a depth of 30 cm. The seed was considered as a passive point in the grid. The computer program was written in FORTRAN for an IBM 360/40 computer. The model was validated using published field data.

Simulations were run studying the following parameters:

1. Sandy loam vs. clay loam

2. Tilled vs. undisturbed soil profile

3. Bulk density comparisons in the tilled soil layer (representing different tillage treatments)

4. Seed furrow geometry

5. Average May vs. hot June conditions for Michigan

This study concludes with suggestions regarding the need for future work. Refinement of this model and its expansion to include a broader scope of conditions is prerequisite to linking this two-dimensional model to a three-dimensional seed-soil interface model. The latter is a vital component of a larger seed germination model proposed in a long-range plan.

Approved: Thomas H Burkhardt
Major Professor

Donald W. Edwards
Department Chairman

## ACKNOWLEDGMENTS

The author sincerely appreciates the guidance, patience, and cooperation over the years of his committee chairman, Dr. Thomas Burkhardt. His gratitude is also extended to his committee members Dr. G. Merva, Dr. L. Segerlind, Dr. A. Smucker and Dr. A. Srivastava for their time and counseling.

The author is indebted to Betty Nicholson and Susan Schroeder of Computer Services at Delta College for their tireless processing of computer runs throughout the development. Acknowledgment is due Marnie Laurion of MSU for the final typing of this dissertation.

Finally, the author wishes particularly to thank his wife, Kathleen Ann, for her encouragement and support over a period of eight years, without who's selfless devotion this dissertation quite likely may not have been brought to fruition.

TABLE OF CONTENTS

Page

LIST OF FIGURES . . . . . viii

LIST OF TABLES . . . . . x

LIST OF VARIABLES . . . . . xii

1. INTRODUCTION . . . . . 1

1.1 Computer Modeling of Soils . . . . . 1

1.2 Long Range Goal . . . . . 4

1.3 Objective of this Study . . . . . 7

1.4 Soil Model . . . . . 7

1.5 Summary . . . . . 10

2. THEORY AND LITERATURE REVIEW . . . . . 11

2.1 Moisture and Heat in the Soil . . . . . 11

2.2 Explanation of Philip-DeVries Equations . . . . . 12

2.2.1 Moisture Equation . . . . . 12

2.2.2 Temperature Equation . . . . . 13

2.3 Assumptions . . . . . 13

2.3.1 Assumptions Made by Philip and DeVries . . 13

2.3.2 Additional Assumptions and Considerations . 15

2.4 Simplified Equations . . . . . 17

2.5 Theory Incorporation of Air Mass Effects . . . . . 19

2.5.1 Air Velocity Due to Pressure Gradients . . 19

2.5.2 Air Velocity Due to Density Gradients . . . 21

2.5.3 Modification of Heat Equation . . . . . 24

2.5.4 Modification of Moisture Equation . . . . . 27

2.5.5 Evaluation of the Velocity Gradient . . . . 30

2.6 Summary . . . . . 31

3. MODEL FOR NUMERICAL SOLUTION . . . . . 32

3.1 Background of Finite Element Modeling . . . 32

3.2 Model Development . . . . . 34

3.3 Integration of Terms in the Model . . . . . 47

3.3.1 Area Integrals . . . . . 47

3.3.2 Line Integrals . . . . . 48

3.3.3 Time Integrals . . . . . 49

3.4 Set of Algebraic Equations . . . . . 50

3.5 Summary . . . . . 56

4. SOIL PARAMETERS . . . . . 57

4.1 Moisture Diffusivity $D_\theta$ . . . . . 57

4.1.1 Moisture Characteristic Slope $\frac{\partial \psi}{\partial \theta}$ 57

4.1.2 Hydraulic Conductivity K . . . . . 58

4.1.3 Hysteresis Effects . . . . . 59

4.2 Moisture Diffusivity $D_T$ . . . . . 60

4.2.1 Factor f . . . . . 61

4.2.2 Moisture Content $\theta_{lk}$ . . . . . 61

4.2.3 Atmospheric Diffusion $D_{atm}$ . . . . . 62

4.2.4 Air Pore Temperature Gradient Ratio $(\nabla T)a/(\nabla T)$ . . . . . 62

4.2.5 Theory Modification . . . . . 63

4.3 Thermal Conductivity $\lambda$ . . . . . 64

4.3.1 Soil Temperature Gradient Ratios $k_s$ . 65

4.3.2 Temperature Gradient Ratio of the Dispersed Fluid $k_{av}$ or $k_l$ . . . . . 66

4.3.3 Thermal Conductivity of Air-filled Pores $\lambda_{av}$ . . . . . 67

4.4 Heat Capacities C and Cg . . . . . 68

4.5 Vapor Content $\theta_v$ . . . . . 69

4.6 Velocity Gradient $\partial V/\partial z$ . . . . . 70

4.6.1 Pressure Changes Components $\partial V_p/\partial z$ . . . . . 70

4.6.2 Density Changes Component $\partial V_d/\partial z$ . . . . . 74

4.7 Summary . . . . . 75

5. SURFACE CONDITIONS . . . . . 76

5.1 Evaporation at the Surface . . . . . 76

5.2 Heat Flux at the Surface . . . . . 80

5.3 Summary . . . . . 82

6. COMPUTER IMPLEMENTATION . . . . . 84

6.1 Finite Element Grid of Soil Furrow Profile . 84

6.2 Boundary and Initial Conditions . . . . . 88

6.3 Specific Inputs to the Model . . . . . 89

6.4 Computer Flow Diagram . . . . . 89

6.5 Computer Program Listing . . . . . 90

6.6 Summary . . . . . 91

7. PARAMETER SENSITIVITY ANALYSIS . . . . . 92

7.1 Soil Moisture Diffusivity $D_\theta$, Matric Potential $\psi$, and Hydraulic Conductivity K . 92

7.2 Soil Moisture Diffusivity $D_T$ . . . . . 97

7.3 Soil Thermal Conductivity $\lambda$ . . . . . 99

7.4 Soil Heat Capacity C . . . . . 102

7.5 Velocity Gradients $\partial Vp/\partial z$ and $\partial Vd/\partial z$ of Soil Air . . . . . 102

7.6 Evaporation and Soil Heat Gain at the Surface . . . . . 103

8. MODEL VALIDATION . . . . . 106

8.1 The Bruce Study . . . . . 106

8.2 Model Refinements . . . . . 107

8.2.1 Finite Element Formulation . . . . . 110

8.2.2 Soil Air Mass Flow . . . . . 110

8.2.3 Surface Conditions Model . . . . . 111

8.2.4 Bruce Data . . . . . 111

8.2.5 Moisture Diffusivity Due to Vapor . . 113

8.3 Comparisons Between the Model and Published Data . . . . . 114

8.4 Summary . . . . . 116

9. SIMULATIONS . . . . . 117

9.1 Model Parameters . . . . . 117

9.1.1 Soil Profile . . . . . 117

9.1.2 Undisturbed Soil . . . . . 117

9.1.3 Tilled Soil . . . . . 122

9.1.4 Meteorological Inputs . . . . . 124

9.2 Simulation Results . . . . . 127

9.2.1 Temperature and Moisture in Undisturbed Metea Sandy Loam . . . . 127

9.2.2 Temperature and Moisture in Undisturbed Brookston Clay Loam . . . 130

9.2.3 Comparisons Between Undisturbed and Tilled Metea Loam . . . . . 133

9.2.4 Tilled Density and Tillage Passes Comparisons in Metea Loam . . . . . 136

9.2.5 Minimum Tillage Furrow Shape Comparisons . . . . . 136

9.2.6 Varying Meteorological Conditions . . 142

9.3 Summary . . . . . 142

10. CONCLUSIONS AND FUTURE WORK . . . . . 145
10.1 Summary . . . . . 145
10.2 Conclusions . . . . . 146
10.3 Future Work . . . . . 147
10.3.1 Second Validation . . . . . 147
10.3.2 Refinement of Parameters . . . . . 148
10.3.3 Model Expansion . . . . . 149
10.3.4 The Three-Dimensional Seed Model . . 150
10.3.5 The Three-Dimensional Soil Model . . 150
10.3.6 The Seed-Soil System Model . . . . . 151
LIST OF REFERENCES . . . . . 152
APPENDIX A-COMPUTER FLOW DIAGRAM
APPENDIX B-COMPUTER PROGRAM LISTING
APPENDIX C-CONVERSION TABLE
APPENDIX D-METEOROLOGICAL INPUT CALCULATIONS

## LIST OF FIGURES


| Figure | | Page |
|---|---|---|
| 1.1 | Seed-Soil System Model for Germination . . . . | 6 |
| 1.2 | Soil Model Decision Tree Diagram . . . . . | 8 |
| 2.1 | Infinitesimal Element of Soil for Heat Flow . | 24 |
| 2.2 | Infinitesimal Element of Soil for Mass Flow . | 28 |
| 3.1 | Gray and Pinder Model . . . . . | 35 |
| 6.1 | Finite Element Domain of Soil Profile . . . . | 85 |
| 6.2 | Finite Element Grid for Validation . . . . . | 86 |
| 6.3 | Finite Element Grid for Simulation . . . . . | 87 |
| 7.1 | Moisture Characteristic Curves for Adelanto Loam . . . . . | 93 |
| 7.2 | Hydraulic Conductivity for Adelanto Loam . . . | 94 |
| 7.3 | Moisture Diffusivity $D_\theta$ for Adelanto Loam . . | 95 |
| 7.4 | Thermal Conductivity of Quartz Sand at 20°C . | 100 |
| 7.5 | Thermal Conductivity of Quartz Sand at 40°C . | 101 |
| 7.6 | Daily Evaporation for a Loam in Binghamton, NY, in June . . . . . | 104 |
| 8.1 | June 18 Temperatures comparing Model with Bruce Data . . . . . | 108 |
| 8.2 | June 18 Moistures comparing Model with Bruce Data . . . . . | 109 |
| 8.3 | June 18 Noon Moistures comparing Liquid and Vapor Diffusivities . . . . . | 115 |
| 9.1 | Moisture Characteristic Curve for Metea Sandy Loam . . . . . | 118 |
| 9.2 | Moisture Characteristic Curve for Brookston Clay Loam . . . . . | 120 |
| 9.3 | Effect of Soil Structure on Moisture Characteristics . . . . . | 122 |
| 9.4 | Ghosh Argument for One $\psi_e$ . . . . . | 123 |

9.5 Temperatures in Undisturbed Metea Sandy Loam for May . . . . . 128

9.6 Noon Moistures in Undisturbed Metea Sandy Loam for May . . . . . 129

9.7 Temperatures in Undisturbed Brookston Clay Loam for May . . . . . 131

9.8 Noon Moistures in Undisturbed Brookston Clay Loam for May . . . . . 132

9.9 Moistures at Selected Depths in Metea Sandy Loam comparing Undisturbed and Tilled . . . . 134

9.10 Noon Moisture Profiles in Metea Sandy Loam . . 135

9.11 Third Day Temperatures in Metea Sandy Loam comparing Undisturbed and Tilled . . . . . 137

9.12 Third Day Moistures in Metea Sandy Loam comparing Tilled Densities . . . . . 138

9.13 Minimum Tillage Furrows Modeled . . . . . 139

9.14 Moistures at Seed Point in Metea Sandy Loam comparing Furrow Shapes . . . . . 140

9.15 Third Day Moistures in Metea Sandy Loam comparing Meteorological Conditions . . . . . 143

9.16 Third Day Moistures in Metea Sandy Loam comparing Meteorological Conditions . . . . . 144

A.1 Computer Flow Diagram

D.1 Global Irradiance Cycle Computation

## LIST OF TABLES


| Table | | Page |
|---|---|---|
| 4.1 | Moisture contents at $K = K_s/1000$ for several soils (Mualem (1978)) | 62 |
| 4.2 | Thermal conductivities of several elements, J/m·sec·°C | 66 |
| 4.3 | Soil temperature gradient ratios | 66 |
| 4.4 | Heat capacities, $J/m^3 \cdot °C$ | 69 |
| 4.5 | Air permeabilities, K*, m/sec | 71 |
| 4.6 | Volume surface mean diameters, mm | 72 |
| 4.7 | Air pressure wave measurements (Farrell, et al. (1966)) | 74 |
| 5.1 | Surface roughness, Zo, cm | 79 |
| 5.2 | Soil surface albedo | 81 |
| 6.1 | Depth of influence | 84 |
| 6.2 | Boundary and initial conditons for the model | 88 |
| 7.1 | Soil moisture properties | 97 |
| 7.2 | Moisture diffusivities, $m^2 \cdot sec^{-1}/(°C \text{ or } \theta)$ | 98 |
| 7.3 | Velocity gradients, m/sec·m | 103 |
| 7.4 | Aerodynamic resistance for $\Delta T = 4°C$ | 105 |
| 9.1 | Soil conditions in Northern locations pertinent to model | 121 |
| 9.2 | Meteorological statistics from Bishop Airport (1941-1970) | 125 |
| 9.3 | Diurnal meteorological statistics for 1981 from Bishop Airport | 125 |
| 9.4 | Mean weekly solar radiation over East Lansing, langley/day | 126 |
| 9.5 | Meteorological inputs used in the simulations | 127 |

B.1 Computer program

C.1 Conversion table

## LIST OF VARIABLES

$a$ = volumetric air content, $m^3$ of air/$m^3$ total volume

al = albedo, reflectivity coefficient of soil surface

$a_o$ = amplitude of pressure waves of air moving horizontally

$c_l$ = specific heat of liquid water, J $kg^{-1}$ $C^{-1}$

$c_p$ = specific heat of water vapor at constant pressure, J $kg^{-1}$ $C^{-1}$

$C$ = volumetric heat capacity of moist porous medium, J $m^{-3}$ $C^{-1}$

$C_{s,l,g}$ = volumetric heat capacity of soil, liquid, and gas constituents of a soil medium

$D_{atm}$ = molecular diffusion coefficient of water vapor in air, $4.42 \times 10^{-4} T^{2.3}/P$, $cm^2$ $sec^{-1}$, or $5.801 \times 10^{-11} T^{2.3}$, $m^2$ $sec^{-1}$

$D_T$ = thermal moisture diffusivity, $D_{Tl}+D_{Tv}$, $m^2$ $sec^{-1}$ $C^{-1}$

$D_{Tl}$ = liquid diffusivity due to temperature gradients, $k\gamma\psi$, $m^2$ $sec^{-1}$ $C^{-1}$

$D_{Tv}$ = vapor diffusivity due to temperature gradients, $fD_{atm}\nu\beta h(\nabla T)_a/\rho_l \nabla T$, $m^2$ $sec^{-1}$ $C^{-1}$

$D_\theta$ = isothermal moisture diffusivity, $D_{\theta l} + D_{\theta v}$, $m^2$ $sec^{-1}$

$D_{\theta l}$ = liquid diffusivity due to moisture gradients, $K\partial\psi/\partial\theta_l$, $m^2$ $sec^{-1}$

$D_{\theta v}$ = vapor diffusivity due to moisture gradients, $\alpha a D_{atm} \nu g \rho_v (\partial\psi/\partial\theta_l)/\rho_l RT$, $m^2$ $sec^{-1}$

$\partial\psi/\partial\theta$ = slope of soil moisture characteristic curve, m $H_2O$

$E$ = evaporation rate, $msec^{-1}$

$E_m$ = mass evaporation rate, kg $m^{-2} sec^{-1}$

f = factor accounting for liquid island effect, describing effective space available for flow, exclusive of tortuosity,

= S for $\theta_l < \theta_{lk}$

= $a + a\theta_l/(S-\theta_{lk})$ for $\theta_l > \theta_{lk}$

g = acceleration due to gravity, 9.81, $msec^{-2}$

h = relative humidity

$H_a$ = absolute humidity of air, kg $m^{-3}$

$H_o$ = saturation absolute humidity at the surface temperature, kg $m^{-3}$

$H_s$ = absolute humidity of air at the soil surface, kg $m^{-3}$

j = mechanical equivalent of heat, $4.18 \times 10^7$, erg $cal^{-1}$

$\vec{k}$ = unit vector in vertical direction

K = unsaturated hydraulic conductivity, m $sec^{-1}$

$K_s$ = hydraulic conductivity at saturation, m $sec^{-1}$

K* = air permeability, cm $sec^{-1}$/cm $H_2O$ $cm^{-1}$

L = heat of vaporization, $2.45115 \times 10^6$, J $kg^{-1}$

p = partial pressure of water vapor, mm Hg

P = total gas pressure, mm Hg

$Q_A$ = sensible heat flux to the air, W $m^{-2}$

$Q_{RG}$ = total global short wave irradiance from sun and atmosphere, W $m^{-2}$

$Q_{RL}$ = incoming long wave radiation from sky, W $m^{-2}$

$Q_{RN}$ = net irradiance, W $m^{-2}$

$Q_s$ = sensible heat flux in soil, W $m^{-2}$

$R$ = gas constant of water vapor, $4.615 \times 10^{6}$ erg $g^{-1}C^{-1}$ or 0.11 cal $g^{-1}C^{-1}$

$R_a$ = adiabatic or neutral value of $R_c$, sec $m^{-1}$

$R_c$ = aerodynamic resistance, sec $m^{-1}$

$R_i$ = Richardson Number

$S$ = porosity, $m^3/m^3$

$S_a$ = wind speed, measured at 2m elevation, m $sec^{-1}$

St = stability correction factor

$t$ = time, sec

$T$ = temperature, °K or °C

$T_a$ = air temperature, °C

$T_s$ = surface temperature, °C

$V_d$ = vertical air mass velocity due to density gradients

$V_p$ = vertical air mass velocity due to pressure gradients

$x$ = horizontal coordinate, m

$z$ = vertical coordinate, m

$z_o$ = surface roughness, m

$\alpha$ = tortuosity factor for diffusion of gases in soils, 0.67

$\beta$ = $d\rho_o/dT$, $1.05 \times 10^{-3}$ @ 20C, kg $m^{-3}$ $C^{-1}$ or = dimensionless empirical constant in soil $\psi$-$\theta$ relationship

$\gamma$ = temperature coefficient of surface tension of water, $-2.09 \times 10^{-3}$ @ 20C, $C^{-1}$

$\varepsilon$ = emissivity of soil surface (dimensionless)

$\theta$ = total volumetric content of moisture, $\theta_l + \theta_v$, $m^3/m^3$ soil volume

$\theta_e$ = volumetric moisture content at air entry point (at "knee" of $\psi$-$\theta$ curve)

$\theta_l$ = volumetric liquid content, $m^3/m^3$ soil volume

$\theta_{lk}$ = value of $\theta_l$ at which "liquid continuity" fails

$\theta_H$ = moisture content at a point between wilting and hygroscopic levels where soil is considered dried

$\theta_v$ = volumetric vapor content, $m^3$ of precipitable water/$m^3$ soil volume

$\lambda$ = thermal conductivity of soil, weighted average over its constituents, $\Sigma x_i k_i \lambda_i / \Sigma x_i k_i$, (where $x_i$ = volume fraction, $k_i$ = ratio of temperature gradient across ith constituent to overall gradient), J $m^{-1}$ $sec^{-1}$ $C^{-1}$

$\lambda_a$ = thermal conductivity of dry air, J $m^{-1} sec^{-1}$ $C^{-1}$

$\lambda_{av}$ = thermal conductivity of air-vapor mixture, $\lambda_a + \lambda_v$, J $m^{-1} sec^{-1} C^{-1}$

$\lambda_l$ = thermal conductivity of liquid, J $m^{-1} sec^{-1} C^{-1}$

$\lambda_s$ = thermal conductivity of soil, J $m^{-1} sec^{-1} C^{-1}$

$\lambda_v$ = thermal conductivity of vapor, apparent in an air filled pore due to vapor diffusion, $h\nu\beta LD_{atm}$, J $m^{-1} sec^{-1} C^{-1}$

$\lambda_{1,2,3}$ = % sand, silt, and clay, respectively, in soil volume

$\nu$ = P/(P-p), mass flow factor due to diffusion within an air pore

$\rho_B$ = soil bulk density, kg $m^{-3}$

$\rho_l$ = density of liquid water, kg $m^{-3}$

$\rho_o$ = density of saturated water vapor, kg $m^{-3}$

$\rho_v$ = density of water vapor, $\rho_o \exp(\psi g/RT)$, $\rho_o h$, kg $m^{-3}$

$\sigma$ = Stefan-Boltzmann constant, $5.67 \times 10^{-8}$, W $m^{-2} K^{-4}$

$\psi$ = soil moisture potential, matric, m $H_2O$ bars or atmospheres

$\psi_e$ = air entry value of matric potential, obtained from $\psi$-$\theta$ curve, evaluated at $\theta_e$

$\psi_s$ = matric potential at the soil surface, m $H_2O$

$\omega$ = frequency of air pressure waves moving horizontally, $sec^{-1}$

$(\nabla T)_a$ = average temperature gradient in air-filled pores, C $m^{-1}$

# 1. INTRODUCTION

## 1.1 Computer Modeling of Soils

The computer has become an extremely powerful tool in design and research. It allows the engineer to analyze a part or product providing information which may not have been obtainable before, or only obtainable with a costly prototype exposed to extensive testing. Software programs using numerical methods such as finite elements are used to perform stress analysis, vibration analysis, or kinematic analysis. Manufactured products and natural processes alike have been modeled to predict their response to an external stimulus through the method of simulation. This adds to the understanding of complex interrelationships and provides a better basis for decision-making for equipment or process managers.

One area which can benefit substantially from computer modeling is that of soils research. Specifically, a better understanding of the immediate environment around a seed after it has been planted and during the germination and emergence periods could:

1. serve as an educational tool for study by students from many disciplines,

2. aid the researcher in the study of different tillage methods such as minimum-till, ridge tilling or slot mulch tilling,

3. aid the farmer in crop residue management,

4. aid the machinery manufacturer in tillage equipment design.

Agricultural and engineering students can all benefit from such a soil model by observing moisture and temperature changes in the soil profile which could not be fully appreciated in a lecture on the subject nor by extensive soil testing in the lab.

Researchers should be able to determine, for a given climate, seed and soil combination, whether the seed displays more or less viability during the germination process for one tillage treatment over another. Studies could be made on the immediate seed environment, how it is affected by the tillage treatment and climate over a period of days, and how it in turn affects the seed and its chances for survival. Complex soil moisture-temperature interactions can be studied, such as the effect of a tilled soil layer on the impedance to moisture flow as the layer heats up and dries, the effects of bulk density on heat and moisture, and hysteretic effects due to diurnal variations.

The farmer could use the model on a home computer for managerial decisions on his operation. Example could be "If I plant corn shallow with conventional tillage, expecting a rain, but instead it stays dry for six days, what happens to the moisture at the seed level, and will I still get an acceptable germination?" "If I plant sugar beets now, and it freezes two nights in a row, what can I expect for a germination response?" "With the present soil

condition and weather, how long can I delay planting and still be assured of an acceptable stand?"

The planter/tillage equipment manufacturer could use the model to study furrow depths and shapes, soil aggregation, and seed placement relative to the furrow to gain insight as to which tillage implement combinations are best suited for specific regions, soils, and crop cultures. With the model the manufacturer could determine whether furrow shape or width is the prime factor in moisture retention at the seed level and what bulk density above and below the seed is optimum for seed germination.

Much has been published on soils, and on crop response to soil, meteorological and tillage conditions. Through the decades the body of knowledge of soils and crops has grown considerably, and recently some models of systems and subsystems have been proposed. Some of these models have been parochial in nature, concentrating on a subsystem artificially isolated from other pertinent factors in the total system. Hillel (1977) made detailed computer simulations of heat and moisture interactions in the soil, but confined his study to one-dimensional flow using relatively large soil increments in the model. More recently Cruse, et al. (1980) developed a model to predict temperatures at the 5-cm. depth as affected by tillage, but that model did not incorporate direct interactions with moisture. Gray and

Pinder (1974) applied the finite element analysis to transient groundwater flow, but it was confined to isothermal conditions.

Other models have been broadly-based crop growth models to predict growth response to macro-meteorological and soil conditions, but do not incorporate the intricate heat-moisture-oxygen-crop interactions in the soil. Examples of these are the CORNGRO (Tscheschke and Gilley (1979)) and SORGF (Arkin, et al. (1980)) models.

## 1.2 Long Range Goal

The long range goal surrounding this study was to develop a model of the soil environment around a planted seed with sufficient detail to understand all pertinent climate-soil-seed interactions in the system. The intended use of the model would be to study the seed-soil interactions for the duration of the germination period to predict seed viability in response to factors such as:

1. soil texture
2. meteorological conditions
3. tillage methods and soil structure
4. cropping management

Thus this model could be used to determine whether a given tillage practice, under specified weather conditions, would provide a suitable environment for seed germination.

The emergence of the seedling is also crucial to developing a healthy crop stand. This emergence period

would require a seedling model different from the seed model and would necessitate incorporation of soil chemistry for surface crusting conditions. Since germination and emergence mechanisms are significantly different and do not occur at the same time, the author decided a completely separate emergence system model could sometime in the future be interfaced with the germination system model of Figure 1.1.

Figure 1.1 represents the long range goal. A two-dimensional soil physical model views the soil profile in a vertical plane sliced across the furrow with the seed considered as a passive point in the profile. Meteorological diurnal data from the meteorological model are superimposed onto the soil surface through a soil surface interface model. At each time step, physical variables such as moisture and temperature are computed throughout the profile. The computed variables near the seed are then transferred into the grid of a 3-D soil model which forms a shell around an active spherical seed model. The 3-D soil model interacts with the seed model within each time step. It extends only far enough to incorporate the seed's sphere of influence, and includes a seed-soil interface boundary across which moisture, heat and oxygen exchange. The 3-D soil model thus models only the immediate environment around the seed, whereas the 2-D soil model models the entire soil profile.

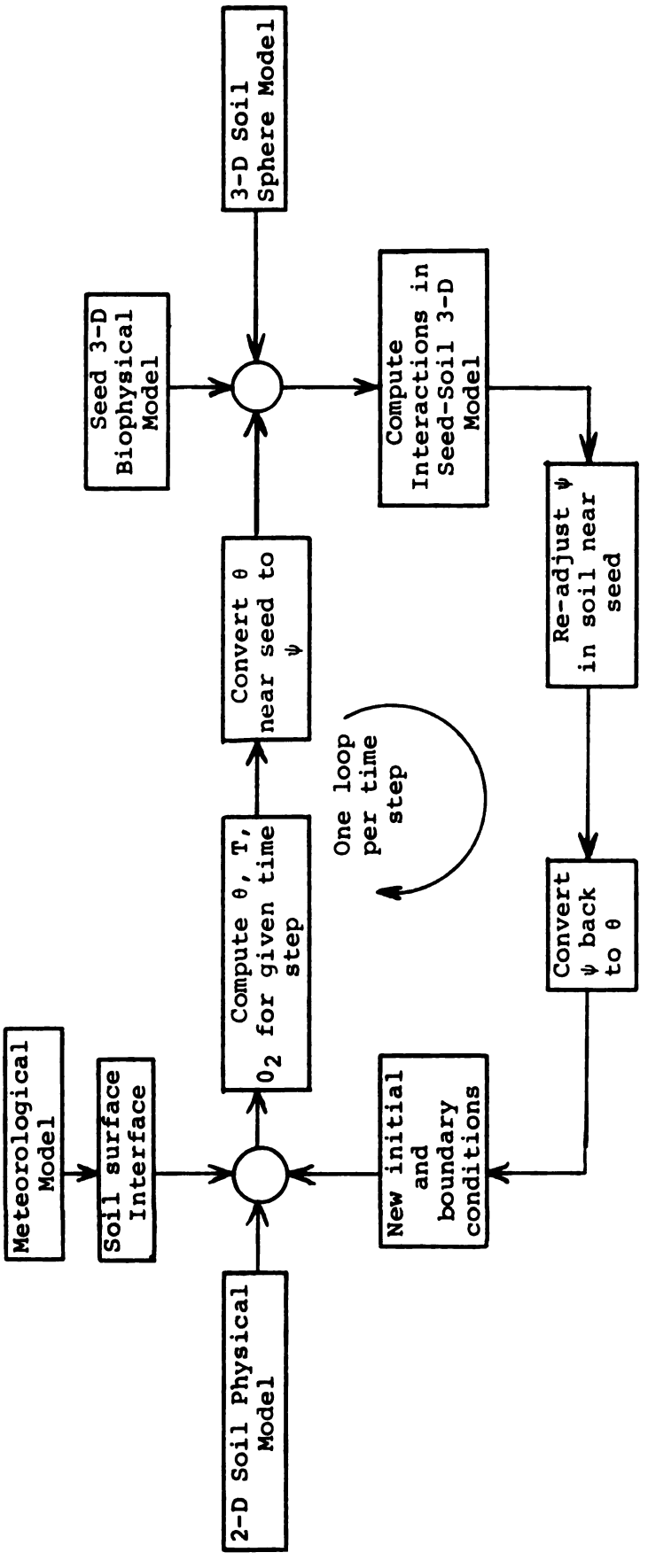


Figure 1.1. Seed-Soil System Model for Germination

After the 3-D soil model has equilibriated for the given time step, the new physical variables are re-introduced back into the 2-D soil model as initial and boundary conditions for the next time step.

## 1.3 Objective of This Study

The system model in Figure 1.1 represents many man-years of development. To fulfill the requirements of a Ph.D. dissertation within a reasonable time span, it was necessary to concentrate on developing a portion of the system model. This portion would require the following:

1. It must be self-sustaining, that is, embody a sufficiently comprehensive system within itself to be verifiable with actual field data.

2. It must be easily interfaced with the rest of the total system as other models are developed.

The objective of this study was to develop, verify and experiment with the 2-D soil model coupled with the meteorological and surface interface models, considering the seed as a passive point in the profile. The scope of this model development is clarified in the next section.

## 1.4 Soil Model

In order to narrow the scope of development of the 2-D soil model to a manageable level, certain assumptions and simplifications had to be made. Figure 1.2 delineates these decisions in a decision tree diagram form. Remarks concerning the decisions are numbered along the side of Figure

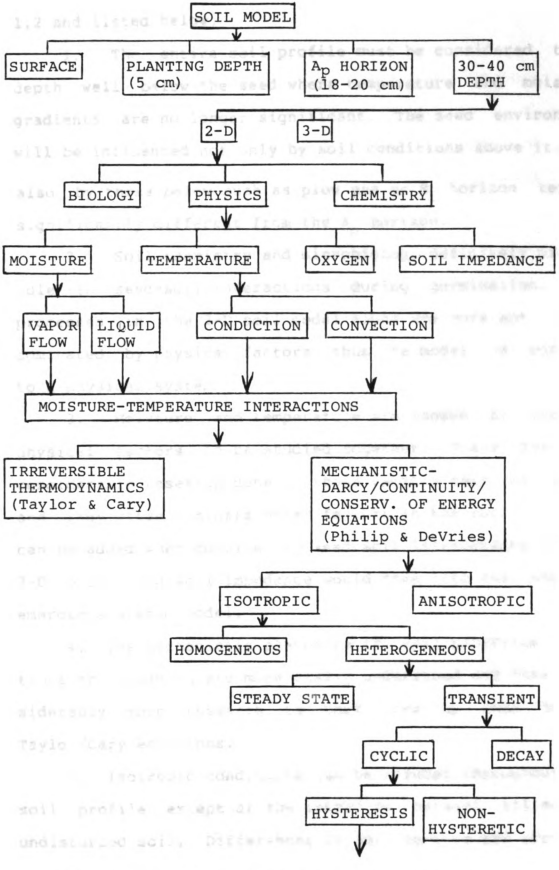


**Figure 1.2. Soil Model Decision Tree Diagram**

1.2 and listed below.

1. The entire soil profile must be considered to a depth well below the seed where temperature and moisture gradients are no longer significant. The seed environment will be influenced not only by soil conditions above it, but also by those below such as plow pan or $B_1$ horizon texture significantly different from the $A_p$ horizon.

2. Soil chemistry and microbiology definitely play a role in seed-soil interactions during germination. But processes in the 2-D soil model alone are more apt to be dominated by physical factors, thus the model was confined to a physical system.

3. Moisture and temperature are chosen as the two physical factors to be studied together. There has been considerable research done on these factors over the years, and they often dominate other factors in the soil. Oxygen can be added when considering seed-soil interactions in the 3-D model, and soil impedance would come into the separate emergence system model.

4. The mechanistic phenomena the Philip/DeVries equations are based on are more easily understood and have considerably more research to back them up than do the Taylor/Cary equations.

5. Isotropic conditions can be assumed throughout the soil profile except at the interface between tilled and undisturbed soil. Differences in soil texture and structure throughout the profile makes it heterogeneous.

## 1.5 Summary

This chapter outlined a long range goal for seed germination modeling, and the short range objective of this dissertation to develop the 2-D soil model. Chapter 2 lays the theoretical foundation for this soil model. Chapter 3 develops the partial differential equations into a matrix of algebraic equations suitable for modeling on a computer. The soil model calls for soil parameters. Expressions for these are developed in Chapter 4 to the point of requiring model inputs which are easily measured. The meteorological model and soil surface interface model with surface evaporation and heat flux are developed in Chapter 5. Grids for the finite element solution and initial and boundary conditions are outlined in Chapter 6 for computer implementation. Chapter 7 discusses the sensitivity of soil parameters to computer inputs and surface conditions. Chapter 8 compares the model results with field data for verification of the model. Chapter 9 displays a variety of simulation results demonstrating the versatility of the soil model. Chapter 10 presents conclusions and proposes future work beyond the scope of this dissertation which will meet the long range goal outlined in Figure 1.1.

# 2. THEORY AND LITERATURE REVIEW

## 2.1 Moisture and Heat in the Soil

The theory of moisture and heat interactions in the soil was first advanced in the 1950's by Philip and DeVries (1957) and DeVries (1958, 1963). They made use of the continuity equation, Darcy's law and the diffusion equation applied to separate liquid and vapor mechanisms to obtain two diffusion-type equations as follows:

**Moisture:**

$$(1 + D_{\theta v}/(\alpha \nu D_{atm}) - \rho_v/\rho_l)\,\partial\theta_l/\partial t + ((S-\theta_l)h\beta/\rho_l)\,\partial T/\partial t = \quad [1]$$

$$\nabla(D_\theta \nabla\theta_l) + \nabla(D_T \nabla T) + \partial K/\partial z$$

**Temperature:**

$$(C + L(S-\theta_l)h\beta)\,\partial T/\partial t + (L\rho_l D_{\theta v}/(\alpha \nu D_{atm}) - L\rho_v + \rho_l j^{-1} g$$

$$(\psi - T\partial\psi/\partial T))\ \ \partial\theta_l/\partial t = \nabla(\lambda \nabla T) + L\rho_l \nabla(D_{\theta v} \nabla\theta_l) + \rho_l c_l((D_{\theta l} \nabla\theta_l$$

$$+ D_{Tl} \nabla T + K\vec{k})\nabla T) + \rho_l c_p((D_{\theta v} \nabla\theta_l + D_{Tv} \nabla T)\nabla T) \qquad [2]$$

where $D_{\theta v}$ = vapor diffusivity due to moisture gradients

$\alpha$ = tortuosity factor for diffusion of gases in soils

$\nu$ = mass flow factor due to diffusion within an air pore

$D_{atm}$ = molecular diffusion coefficient of water vapor in air

$\rho_v$ = density of water vapor

$\rho_\ell$ = density of liquid water

$\theta_l$ = volumetric liquid content

$h$ = relative humidity

$S$ = porosity

$D_\theta$ = isothermal moisture diffusivity

$D_T$ = thermal moisture diffusivity

K = unsaturated hydraulic conductivity

z = vertical coordinate in soil profile

C = volumetric heat capacity of moist porous medium

L = heat of vaporization

$\beta$ = change in density of saturated water vapor with temperature

$\psi$ = soil moisture matric potential

$c_l$ = specific heat of liquid water

$c_p$ = specific heat of water vapor at constant pressure

$\lambda$ = soil thermal conductivity

## 2.2 Explanation of Philip-DeVries Equations

### 2.2.1 Moisture Equation.

The terms $(D_{\theta v}/\alpha v D_{atm} - \rho_v/\rho_l)\frac{\partial \theta_l}{\partial t}$ and $((S-\theta_l)h\beta/\rho_l)\ \frac{\partial T}{\partial t}$ of equation [1] are products of differentiation to satisfy the continuity principle and represent the time rate of change of the volumetric vapor content $\theta_v$. This is applicable where changes in liquid and vapor content are of the same order (dry soils, high temperatures). The remaining term on the left, $\partial\theta_l/\partial t$, represents the time rate of change of volumetric liquid content of the differential element, also satisfying the law of conservation of mass.

The first term on the right, $\nabla(D_\theta\ \nabla\theta_l)$, is an expression for the total moisture flux due to liquid moisture gradients alone. The second term, $\nabla(D_T\nabla T)$, expresses the total moisture flux due to thermal gradients alone. Both fluxes are assumed additive, and are based on diffusivities which are

in turn based on the assumption that the liquid and vapor mechanisms within each gradient influence are additive. The last term on the right, $\partial K/\partial z$, evolves from a consideration of the gravity effect on moisture movement in the expression for total moisture potential, $\phi = \psi$ matric $- z$.

2.2.2 Temperature Equation. This equation is based on the conservation of heat principle and recognizes the total heat content of a volume of soil is made up of the heat capacity of the soil particles plus the latent heat of the water vapor plus the sensible heat of the liquid and vapor separately minus the differential heat of wetting.

The terms $L(S-\theta_\ell)h\beta\frac{\partial T}{\partial t}$ and $(L\rho_\ell D_{\theta v}/\alpha\nu D_{atm} - L\rho_v)\frac{\partial \theta_\ell}{\partial t}$ of equation [2] represent the heat transfer due to moisture changes between the liquid and vapor phases. The term $(\rho_\ell j^{-1} g(\psi - T\partial\psi/\partial T))\frac{\partial \theta_\ell}{\partial t}$ represents the differential heat of wetting. The term $\nabla(\lambda\nabla T)$ represents heat transfer due to pure conduction. The term $L\rho_\ell\nabla(D_{\theta v}\nabla\theta_\ell)$ represents the transfer of latent heat by vapor movement. The terms $\rho_\ell c_\ell((D_{\theta\ell}\nabla\theta_\ell + D_{T\ell}\nabla T + K\hat{k})\nabla T)$ and $\rho_\ell c_\rho((D_{\theta v}\nabla\theta_\ell + D_{Tv}\nabla T)\nabla T)$ represent the transfer of sensible heat in the liquid and vapor form, respectively.

## 2.3 Assumptions

### 2.3.1 Assumptions Made by Philip and DeVries.

a. Moisture vapor flows through dry soil by a series-parallel path around and through liquid islands via

an evaporation-diffusion-condensation-evaporation mechanism, accounted for by the factor f in the expression for the vapor diffusivity $D_{Tv} = fD_{atm}\, \nu\beta h(\nabla T)_a/\rho_\ell \nabla T$.

b. Liquid and vapor diffusivities due to a potential gradient are additive.

c. Moisture flux due to a temperature gradient is additive with that due to a moisture gradient.

d. Temperature gradient across an individual air pore may be appreciably higher than the average across the soil matrix at that point. This is incorporated as a pore-soil temperature gradient ratio $(\nabla T)_a/\nabla T$ into the expression for the thermal vapor diffusivity $D_{Tv}$.

e. Parameters can be evaluated and are assumed reasonably constant in the 10°C to 30°C range.

f. In the thermal vapor diffusivity term, as $\theta$ increases above the critical level $\theta_{lk}$ where liquid continuity results, the effective cross-section for combined liquid-vapor transfer will decrease steadily.

g. All processes of heat transfer and sources and sinks are evenly distributed throughout the soil volume.

h. Heat transfer by convection and radiation is negligible.

i. Heat capacity of the soil is the weighted average

of the capacities of the solid, liquid and gas constituents.

j. Thermal conductivity of the soil is the weighted average, accounting for particle shape, of the several constituents. Further, the thermal conductivity of the air constituent equals that of dry air plus that of the vapor. The vapor term takes into account the vapor distillation due to temperature gradients in the air-filled pores. This leads to an apparent increase in the thermal conductivity of the air-filled pores.

k. Generation of heat due to viscosity of the moving liquid is negligible.

l. A unique relation exists between $\psi$ and $\theta$, (no hysteresis).

### 2.3.2 Additional Assumptions and Considerations

There are additional simplifying assumptions recognized by DeVries (1958) which hold true for most soil conditions at virtually no loss to generality.

a. Sensible heat transfer by vapor diffusion is usually negligible. This is the last term in equation [2].

b. Changes of moisture contained in the vapor phase over time ($\partial\theta_v/\partial t$) are often assumed negligible. This is because vapor content is usually small compared with liquid content, and the relative

humidity is essentially constant at 100% throughout the moisture range until the wilting point is reached. This is then true in moist soils under moderate or low temperatures. This affects many of the terms on the left hand side of both equations.

With the environmental and time conditions outlined in Chapter One, further assumptions were made by the author:

a. Heat of wetting, significant when irrigating hot and dry soils, is negligible under these conditions.

b. Soil is sufficiently moist throughout the period so that vapor content is very small compared with liquid content. Thus assumption (b) above is further justified.

c. Sensible heat transfer by liquid movement is negligible. DeVries already alluded to this to be the case for most conditions. It will be further justified if the moisture content is always considered below field capacity. In this region the heat flux due to pure conduction would be the dominant term.

d. Gravity effects on liquid flow are negligible. At moisture contents below the field capacity, as the soil dries the matric potential becomes large compared to gravity potential. Even in a fairly wet soil, consideration of only a few centimeters of soil depth in the seed zone would produce negligible hydraulic head.

e. Vapor diffusivity due to moisture gradients ($D_{\theta v}$) is negligible. DeVries (1958) showed this to be significant only at the extreme low end of the total moisture range, but virtually zero compared to $D_{\theta l}$ throughout the useful part of the range.

## 2.4 Simplified Equations

Utilizing all of the above assumptions, the heat-moisture equations reduce to:

**Moisture:** $$\partial\theta/\partial t = \nabla\cdot(D_T\nabla T) + \nabla\cdot(D_\theta\nabla\theta_l) \qquad [3]$$

**Temperature:** $$C\,\partial T/\partial t = \nabla\cdot(\lambda\nabla T) \qquad [4]$$

A number of investigators have scrutinized the thermal conductivity expression proposed by Philip and DeVries (Hadas, 1969; Kimball, et al., 1976; Hadas, 1977a, b; Sepaskhah and Boersma, 1979). Others have tested the theory under varying conditions and proposed further modifications (Woodside and Kuzmak, 1958; Hadas, 1968; Laroussi, et al., 1975; Malik, et al., 1979; Jury and Letey, 1979). In most cases the investigations have supported the theory and have clarified the limits or proposed modifications to diffusivities or the conductivity term.

However, Hadas (1968, 1969, 1977a) has questioned specifically the assumptions (h) and (l) listed in Section 2.3.1. The two diffusion-type equations do not predict adequately the moisture-heat interactions under diurnal temperature conditions in natural soils.

The equations are based on negligible heat convection. However, near the surface, heat and vapor flow due to air mass movement through the soil may be appreciable. In fact, Ojeniyi and Dexter (1979) state that much of the drying of tilled soil in the field occurs as a result of convective transport of air through large pores produced by the tillage. This air mass movement would be induced by air pressure gradients arising from wind gustiness at the surface and by air density gradients arising from reversed temperature gradients in the top few centimeters of the soil in the evening and early morning hours.

Hadas (1969, 1977a) and others have proposed a mass enhancement factor $\xi$ fitted into the vapor thermal conductivity term to account for this: $\lambda_{av} = \lambda_a + \xi \lambda_v$

More recently Hadas (1977a) recognized the probable inadequacy of this method and suggested in its place a third equation be added to the theory to account for these diurnal effects near the surface. Similarly, Farrell et al. (1966) had proposed a mass velocity squared term be added to the vapor diffusivity to account for increased vapor movement near the surface.

Both of the above methods involve correction terms to bring theory in line with experimental data. An alternative method is to return to the basic study of heat and mass flow through a differential volume of soil. Below is presented the development of this alternate method to incorporate air mass movement effects in the surface soil layers.

## 2.5 Theory Incorporation of Air Mass Effects

Luikov (1966) developed a set of three equations using the thermodynamic approach to explain heat and mass transfer through capillary-porous bodies under the influence of temperature, mass and gas pressure gradients:

$$\begin{aligned} \partial T/\partial t &= K_1 \nabla^2 T \\ \partial \theta/\partial t &= K_2 \nabla^2 \theta + K_3 \nabla^2 T + K_4 \nabla^2 p \\ \partial p/\partial t &= K_5 \nabla^2 p \end{aligned} \qquad [5]$$

Where the $K_i$ terms are phenomenological transfer coefficients. These equations still do not include density gradient effects. To incorporate density effects, a fourth equation would have to be added of the type: $\partial \rho_g/\partial t = K_6 \nabla^2 \rho_g$ where $\rho_g$ = density of the gas.

Since this would produce a number of transfer coefficients for which there is little if any experimental data, a different direction is proposed.

Both pressure and density gradients give rise to vertical momentum of the air-vapor (gas) mixture in the soil, especially in tilled, porous, drier top layers of soil. If the net velocity of the gas due to these gradients can be calculated at any point in the soil at any time, then this velocity can be incorporated into an expanded expression of the original two heat-mass equations, as suggested by several investigators.

### 2.5.1 Air Velocity Due To Pressure Gradients.

Several investigators have studied this phenomenon. Fukuda (1955)

developed a mathematical equation, based on the Darcy law and supported by data, for calculating the transmission of air pressure and air mass movement through the soil due to surface pressure disturbances. His governing equation was of the form:

$$\partial p/\partial t = (k/a)\partial(p\partial p/\partial z)/\partial z$$

where p = air pressure, k = air permeability, and a = volumetric air content, or air porosity. His direct solution was for a vertical periodic pressure disturbance at the surface.

Hanks and Woodruff (1958) discussed, but did not prove, that vapor transfer would be also enhanced by a "mixing effect" caused by pressure fluctuations in addition to air mass actually leaving the soil as in Fukuda's model.

Farrell, et al. (1966) expanded on Fukuda's model, incorporating a second spatial dimension, and allowing for variable soil depth to an impermeable layer and variable wave length of the surface disturbance. Horizontal effects were found to be negligible. Their macroscopic vertical air velocity expression $V_p$ was:

$$V_p = -(K^*\lambda^* a_o/\varepsilon)\exp(-\lambda^* z)[\cos(\omega t-\gamma^* z-2\pi y/L^*) + r\sin(\omega t-\gamma^* z-2\pi y/L^*)] \qquad [6]$$

where $\lambda^*$ and $\gamma^*$ are derived from: $\lambda^{*2} = \gamma^{*2} + (2\pi/L^*)^2$

$$\lambda^* = \varepsilon/2K^* p_o \gamma^*$$

and:

$\varepsilon$ = soil porosity

$p_o$ = mean atmospheric pressure, cm $H_2O$

L = wavelength of horizontal pressure waves, cm

y = horizontal coordinate, cm

z = depth, cm

r = $\gamma^*/\lambda^*$

$K^*$ = air permeability, cm $sec^{-1}$/cm $H_2O$ $cm^{-1}$

$a_o$ = amplitude of pressure waves of air moving horizontally, cm

$\omega$ = frequency of air pressure waves moving horizontally, $sec^{-1}$

t = time, sec

2.5.2 Air Velocity Due To Density Gradients. Luikov (1966) and Hollman (1976) gave a brief discussion of free convection in enclosed spaces. Their treatment was of two horizontal plates closed around the edges with the bottom plate heated. Earlier investigators had shown fluid flow in this free convection mode to be a pattern of mushroom clouds, or "Benard cells", positioned perpendicular to the plates. Fluid moves up from the hot plate inside each cell and as it cools at the cold plate it falls back down around the outside of each cell. Although this continuous circulation of fluid "pumps" heat across the plates by free convection, Hollman (1976) outlined that it is often treated as conduction. An apparent thermal conductivity $k_e$ representing convection was identified in the Nusselt Number $Nu = k_e/k$, where Nu is a function of both the Grashof and Prandtl Numbers. Knowing geometrical and fluid parameters, this apparent conductivity can be calculated.

Hadas (1977a) proposed that free convection in air-

filled pores in soil may be similar to this process. A closer analysis would show that, although this may be the dominant mechanism in wet or deep layered soils where air pores are isolated from each other, it is probably not the dominant mechanism in drier, porous, well-tilled soil layers near the surface. Here the pores would provide a more continuous medium for air mass flow. This is evidenced by field measurements of appreciable moisture movement back towards the surface during temperature reversals in the drier surface layers.

Assuming this latter condition, density gradients would then give rise to buoyant forces pushing the air mass vertically through the soil. The following analysis is based on this assumption.

According to Gebhart (1961), the difference between the weight of a small volume of fluid and the buoyant force on it due to a density gradient is the net force

$$F = g\beta^{*}\rho_{v}(T-T_{\infty})$$

where: $F$ = force/unit volume, N $m^{-3}$

$g$ = gravitational constant, m $sec^{-2}$

$\beta^{*}$ = coefficient of thermal expansion, $°K^{-1}$

$\rho_{v}$ = fluid density, kg $m^{-3}$

$T$ = temperature of the fluid volume under consideration, °K

$T_{\infty}$ = temperature of the total fluid medium, °K

The actual path of this small volume of gas follows a tortuous route on its way to the surface. If we assume the macroscopic kinetic and potential energy of the volume is conserved, then a relation between the net force and velocity can be obtained.

The change in potential energy of the gas volume across a vertical increment of soil of depth $\Delta z$ can be expressed as:

$$\Delta \text{ P.E.} = g\beta^{*}\rho_{v}\Delta T\Delta Z$$

The change in kinetic energy of this same volume across this same soil increment can be expressed as:

$$\Delta \text{ K.E.} = \frac{1}{2}\rho_{v}\,(V_{du}^{2} - V_{d\ell}^{2})$$

where: $\Delta T$ = change in temperature across the soil increment

$V_{du}$ = macroscopic velocity at upper layer of soil increment

$V_{dl}$ = macroscopic velocity at lower layer of soil increment

Equation the two energy terms and rearranging:

$$V_{du} = \sqrt{2g\beta^{*}\Delta T\Delta z + V_{dl}^{2}} \qquad [7]$$

Equation [7] requires the knowledge of the macroscopic velocity of air at the lower boundary of the soil increment and the temperature gradient across the increment. Thus, the velocity of air due to density gradients will depend on where the element in question is positioned vertically within the soil profile.

2.5.3 Modification of Heat Equation. The total air velocity is, from equations (6) and (7),

$$V = V_p + iV_d \qquad [8]$$

where $i = \begin{cases} 1 \text{ if temperature gradients are reversed (hot sublayer)} \\ 0 \text{ if temperature gradients are normal (hot surface)} \end{cases}$

This is now incorporated into the heat equation by returning to a basic study of an infinitesimal element of soil composed of solid, liquid and gas (air-vapor) constituents, as shown in Figure 2.1.

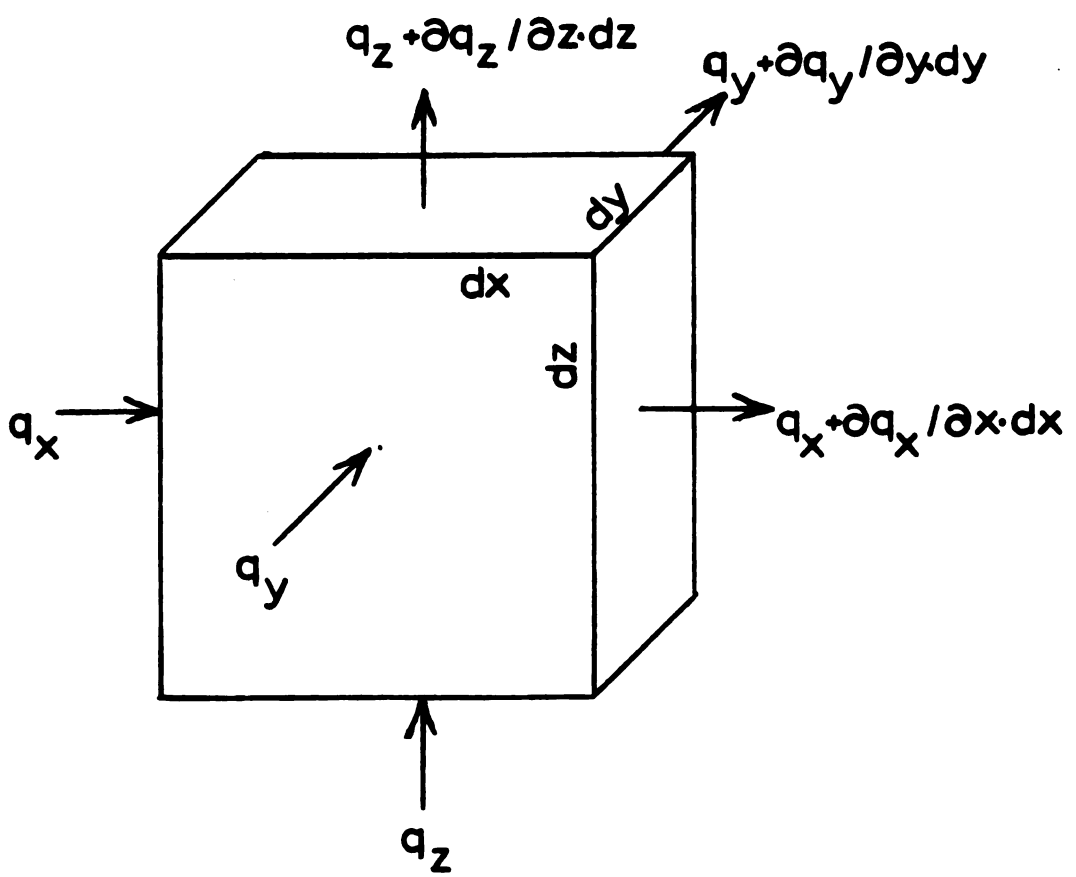


Figure 2.1. Infinitesimal Element of Soil for Heat Flow

Referring to Figure 2.1., the total heat flux per unit area of this element in direction n is:

$q_n = q_n$ conduction $+ q_n$ free convection $+ q_n$ forced convection

$= q_n$ conduction $+ q_n$ convection

and generally, $q_n$ conduction $= -\lambda_n \partial T/\partial n$

If the total convection term ($q_n$ convection) is abbreviated $q_{cn}$, then the difference in rate of heat flow per unit area along the x axis is:

$$- \frac{\partial}{\partial x} \left(-\lambda_x \frac{\partial T}{\partial x} + q_{cx}\right) dx$$

The net rate of gain in this element of volume dxdydz due to this flux is:

$$\frac{\partial}{\partial x} \left(\lambda_x \frac{\partial T}{\partial x} + q_{cx}\right) dx \; (dydz)$$

$$\text{or} \quad \left(\frac{\partial}{\partial x} \left(\lambda_x \frac{\partial T}{\partial x}\right) + \frac{\partial}{\partial x} \left(q_{cx}\right)\right) dxdydz$$

Similar expressions can be obtained for heat flux along the y and z axes. A general expression would be of the form

$$(\nabla \cdot (\lambda \nabla T) + \nabla q_c) dxdydz$$

If only the x and z directions are considered, and convective currents are confined to the z direction, then the net rate of gain becomes:

$$\left(\frac{\partial}{\partial x} \left(\lambda_x \frac{\partial T}{\partial x}\right) + \frac{\partial}{\partial z} \left(\lambda_z \frac{\partial T}{\partial z}\right) + \frac{\partial q_{cz}}{\partial z}\right) dxdydz$$

The time rate of change of stored energy in the element is:

$$m \cdot c \cdot DT/Dt$$

where m = mass of element

c = mass heat capacity of element

DT /Dt = particle derivative of temperature of element

$= \partial T/\partial t + u\partial T/\partial x + v\partial T/\partial y + w\partial T/\partial z$

u,v,w, = velocity components of the element in the x,y,z directions, respectively

The element's solid and liquid constituents are at zero velocity, but the gas is not. Thus, the stored energy term can be expanded to reflect both temperature and momentum changes.

$$m \cdot c \cdot \frac{DT}{Dt} = m_s c_s \frac{DT_s}{Dt} + m_l c_l \frac{DT_l}{Dt} + m_g c_g \frac{DT_g}{Dt}$$

where s,l,g = solid, liquid and gas subscripts.

Letting $\rho$ = m/dxdydz and assuming $\rho_g$ = constant at these low velocities, the time rate of change of stored energy becomes:

$$(\rho_s c_s \frac{DT_s}{Dt} + \rho_l c_l \frac{DT_l}{Dt} + \rho_g c_g \frac{DT_g}{Dt})\ dxdydz$$

and since the only velocity consideration is that of the gas in the vertical (z) direction, and assuming all constituents are in thermal equilibrium at any one point, the expression reduces to:

$$(\rho_s c_s \frac{\partial T}{\partial t} + \rho_l c_l \frac{\partial T}{\partial t} + \rho_g c_g (\frac{\partial T}{\partial t} + w \frac{\partial T}{\partial z}))dxdydz$$

Equating this time rate of change of stored energy to the net rate of energy gain:

$$\rho_s c_s \frac{\partial T}{\partial t} + \rho_l c_l \frac{\partial T}{\partial t} + \rho_g c_g (\frac{\partial T}{\partial t} + w \frac{\partial T}{\partial z}) = \frac{\partial}{\partial x}(\lambda_x \frac{\partial T}{\partial x}) + \frac{\partial}{\partial z}(\lambda_z \frac{\partial T}{\partial z}) + \frac{\partial}{\partial z}(q_{cz}) \qquad [9]$$

The heat flux per unit area due to convection, $q_{cz}$, at any point can be expressed as the heat capacity of the fluid at that temperature times the velocity, or

$$q_{cz} = C_g w T$$

where $C_g$ = volumetric heat capacity of the gas. The change of the convective heat flux with depth z is:

$$\frac{\partial}{\partial z}(q_{cz}) = C_g w \frac{\partial T}{\partial z} + wT \frac{\partial C_g}{\partial z} + C_g T \frac{\partial w}{\partial z}$$

Assuming the relative humidity of the air at a constant 100% throughout the depth considered, then $\frac{\partial C_g}{\partial z} = 0.$

Substituting the above expression and corresponding volumetric heat capacities ($C = \rho c$) for the solid and liquid constituents brings equation (9) to:

$$(C_s+C_l+C_g)\frac{\partial T}{\partial t} + C_g w \frac{\partial T}{\partial z} = \frac{\partial}{\partial x}(\lambda_x \frac{\partial T}{\partial x}) + \frac{\partial}{\partial z}(\lambda_z \frac{\partial T}{\partial z}) + C_g w \frac{\partial T}{\partial z} + C_g T \frac{\partial w}{\partial z}$$

Letting C = volumetric heat capacity of the composite element, substituting the macroscopic gas velocity V for w, and further assuming an isotropic soil medium ($\lambda x = \lambda z = \lambda$), the heat equation finally becomes:

$$C \frac{\partial T}{\partial t} = \frac{\partial}{\partial x}(\lambda \frac{\partial T}{\partial x}) + \frac{\partial}{\partial z}(\lambda \frac{\partial T}{\partial z}) + C_g T \frac{\partial V}{\partial z} \qquad [10]$$

### 2.5.4 Modification of the Moisture Equation

The infinitesimal element of soil in Figure 2.2 is now analyzed for mass continuity. The mass flow rate is of the form:

$$\dot{m} = \frac{\text{mass of water}}{\text{area} \cdot \text{time}} = \frac{\rho \text{ water} \cdot \text{volume water}}{\text{area} \cdot \text{time}}$$

A volumetric liquid flow rate per area can be expressed as a diffusivity times a gradient: gradients occur in soil due to both temperature and moisture. Then the expression for $\dot{m}_x$ becomes:

$$\rho_\ell \left[ D_{Tx} \frac{\partial T}{\partial x} + D_{\theta x} \frac{\partial \theta}{\partial x} \right]$$

and the change in mass flow through the element in the x direction would be:

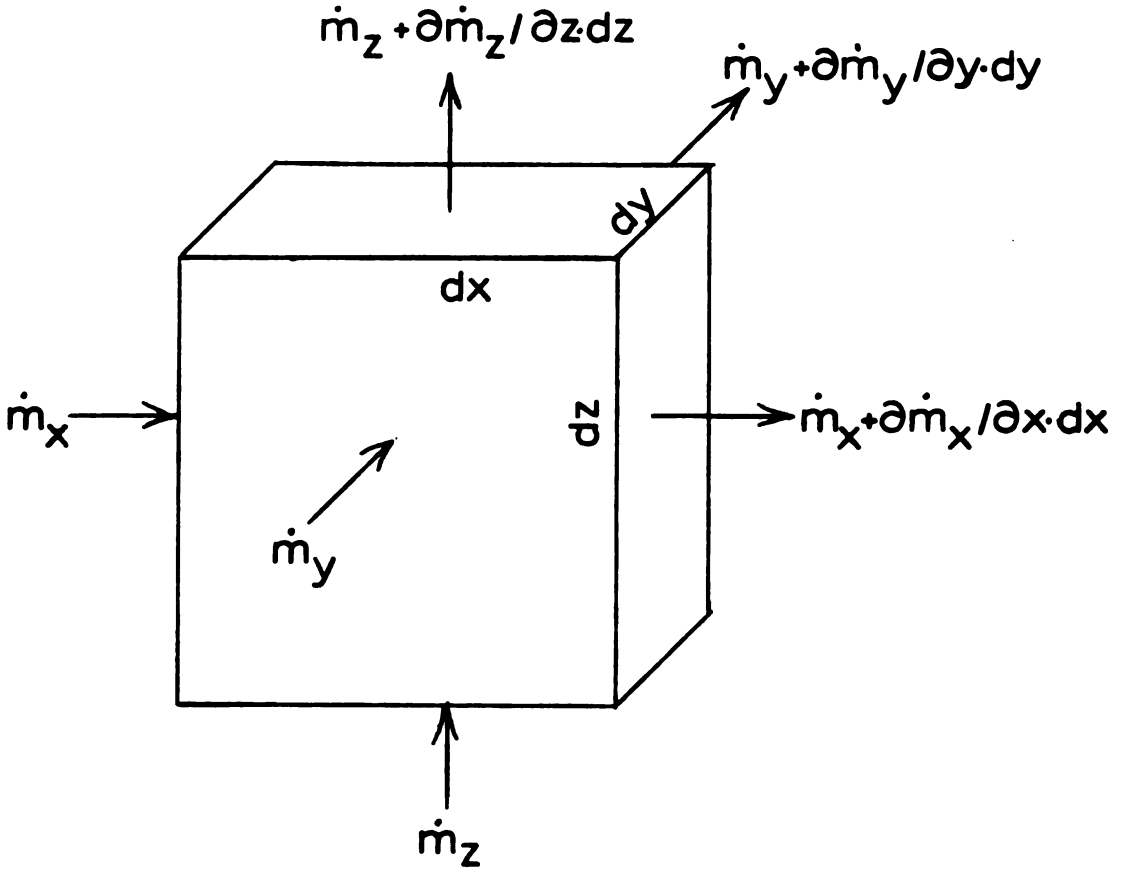


**Figure 2.2. Infinitesimal Element of Soil for Mass Flow**

$$\frac{\partial \dot{m}_x}{\partial x} dx\ (dydz) = \rho_\ell \frac{\partial}{\partial x}\left[D_{Tx} \frac{\partial T}{\partial x} + D_{\theta x} \frac{\partial \theta}{\partial x}\right] dx\ (dydz)$$

However, the introduction of air-vapor mass flow through the soil element due to air density and pressure gradients produces an additional term in the z direction for $\dot{m}_z$:

$$\rho_\ell \left[D_{Tz} \frac{\partial T}{\partial z} + D_{\theta z} \frac{\partial \theta}{\partial z}\right] + \rho_\ell\ (\theta_v V)$$

and the change in mass flow through the element in the z direction becomes:

$$\frac{\partial \dot{m}_z}{\partial z} dz\ (dxdy) = \rho_\ell \left\{\frac{\partial}{\partial z}\ [D_{Tz} \frac{\partial T}{\partial z} + D_{\theta z} \frac{\partial \theta}{\partial z} + \theta_v V]\right\} dz\ (dxdy)$$

The air mass flow term is:

$$\frac{\partial}{\partial z}\ (\theta_v V) = V \frac{\partial \theta v}{\partial z} + \theta_v \frac{\partial V}{\partial z}$$

If the moisture content is considered above the wilting point, the relative humidity of the air-filled pores remains constant at 100%, and

$$V \frac{\partial \theta v}{\partial z} = 0$$

Assuming an isotropic soil medium where diffusivities are constant in all directions, the total change in mass flow through the element is:

$$\rho_\ell \left[\frac{\partial}{\partial x}\ (D_\theta \frac{\partial \theta}{\partial x} + D_T \frac{\partial T}{\partial x}) + \frac{\partial}{\partial z}\ (D_\theta \frac{\partial \theta}{\partial z} + D_T \frac{\partial T}{\partial z}) + \theta_v \frac{\partial V}{\partial z}\right] dxdydz$$

The time rate of change of stored mass in the element is:

$$\frac{\partial}{\partial t}\left[\begin{matrix}\text{mass of water} \\ \text{in soil element}\end{matrix}\right] = \frac{\partial}{\partial t}\left[\rho_\ell \left(\begin{matrix}\text{volume of water} \\ \text{in element}\end{matrix}\right)\right]$$

$$= \frac{\partial}{\partial t}\left[\rho_\ell \left(\frac{\text{volume of water}}{\text{volume of soil element}}\right)\right] dxdydz = \rho_\ell \frac{\partial \theta}{\partial t} dxdydz$$

Finally, equating the time rate of change with the change in mass flow, we obtain the moisture equation:

$$\frac{\partial \theta}{\partial t} = \frac{\partial}{\partial x}\left(D_\theta \frac{\partial \theta}{\partial x} + D_T \frac{\partial T}{\partial x}\right) + \frac{\partial}{\partial z}\left(D_\theta \frac{\partial \theta}{\partial z} + D_T \frac{\partial T}{\partial z}\right) + \theta_v \frac{\partial V}{\partial z} \quad [11]$$

Mass flow adds a term on the right hand side of this equation very similar to that added to the heat equation.

2.5.5 Evaluation of the Velocity Gradient. Both equations (10) and (11) call for the gradient of the air mass velocity with respect to depth z, $\partial V/\partial z$. This gradient is now evaluated by differentiating equations (6) and (7) and adding.

For the top few centimeters of soil we can assume the air permeability and soil porosity changes with depth are relatively small, and $K^*$ and $\varepsilon$ are then constant. Letting $A = K^*\lambda^* a_o/\varepsilon$ and $\partial^* = (\omega t - \gamma^* z - 2\pi y/L^*)$, the partial derivative of equation [6] becomes:

$$\frac{\partial V_p}{\partial z} = A\exp(-\lambda^* z)\left(\gamma^*(r\cos\partial^* - \sin\partial^*) + \lambda^*(\cos\partial^* + r\sin\partial^*)\right) \quad [12]$$

For a similar treatment of equation [7],

$$\frac{V_{du} - V_{dl}}{\Delta z} = \frac{\left(\sqrt{2g\beta^*\Delta T\Delta z + V_{dl}^2} - V_{dl}\right)}{\Delta z} = \sqrt{2g\beta^*(\Delta T/\Delta z) + (V_{dl}/\Delta z)^2} - V_{dl}/\Delta z \quad [13]$$

The total velocity gradient is then:

$$\frac{\partial V}{\partial z} = A\exp(-\lambda^* z)\left(\gamma^*(r\cos\partial^* - \sin\partial^*) + \lambda^*(\cos\partial^* + r\sin\partial^*)\right) + i\left(\sqrt{2g\beta^*(\Delta T/\Delta z) + (V_{dl}/\Delta z)^2} - V_{dl}/\Delta z\right) \quad [14]$$

Equations [10] and [11], with equation [14], now form the governing equations for moisture-heat interactions in the seed zone of the soil, accounting for wind gusts and temperature reversals.

## 2.6 Summary

This chapter developed the two governing equations for heat and moisture movement in the soil. A separate term for vertical air mass movement through the soil was developed and incorporated into the equations. Chapter 3 further develops these equations into a set of algebraic equations suitable for modeling on a computer.

# 3. MODEL FOR NUMERICAL SOLUTION

## 3.1 Background of Finite Element Modeling

The governing equations [10] and [11] are nonlinear, coupled, second-order partial differential equations in space and time, and require solution by numerical methods. Zienkiewicz (1971), Segerlind (1976) and others have shown the application of the finite element method of solution to many types of engineering problems governed by equations of this type.

Typically the governing equation and boundary conditions are incorporated into a functional term. This functional possesses the property that any function which makes the functional a minimum also satisfies the governing differential equation and boundary conditions. Variational calculus is used for the development. This functional is given physical meaning in the theory of elasticity when it is the potential energy of the stressed system, but is less obvious physically in other engineering problems.

A number of investigators have applied the finite element method to moisture and/or heat flow in soils and biological materials. Comparisons with the finite difference method have been made recently by Gray and Pinder (1974), Cushman and Kirkham (1978) and Pall, et al. (1980). Pall, et al. found for a one-dimensional soil water case the finite element method was simple, flexible, conditionally stable but not economical for precision over a long time period. The finite difference method was found to be

unconditionally stable, complex, fast, efficient, a computer space economizer, but could not handle unequal grid sizes.

Treatment of time-dependent problems by the finite element-functional method reduces a partial differential equation in space and time to a set of ordinary differential equations with time as the only independent variable. The finite difference method is then used to reduce this set of ordinary differential equations in time to a set of algebraic equations readily programmed on the computer. This approach has been used by many investigators, and most recently by Haghighi and Segerlind (1978), Misra and Young (1979), Gustafson, et al. (1979), Haghighi (1979), Misra and Young (1980) and Misra, et al. (1981).

An alternate method has been used lately for solving finite element problems. The Galerkin weighted residual method has been used successfully as a more direct way than the functional method of formulating the governing numerical equations. This method has the advantage of being able to treat the time variable in time-dependent problems along with the dimension variables in the spatial domain within the same formulation, rather than two separate ones. Thus, the reduction to a set of algebraic equations for computer programming is obtained with one formulation, rather than with two in sequence with each other. This has been demonstrated by Gray and Pinder (1974), Judah et al. (1975), Cushman and Kirkham (1978), and Cushman (1979). Other advantages of the Galerkin method are it retains the solution

in the form of functions, retains closer contact with the physical problem, and provides greater flexibility in the trial functions.

Solving two or more coupled phenomena simultaneously has also been done recently. Haghighi and Segerlind (1978) and Haghighi (1979) studied moisture and heat diffusion and their effect on stresses in soybeans. Gustafson et al. (1979) studied temperature and stress interactions in corn kernels. Misra and Young (1980) and Misra et al. (1981) studied moisture, shrinkage and stress interactions in soybeans.

It is the objective of this research to develop a model of the heat-moisture interactions in the soil using the Galerkin method for a two-dimensional, time-dependent case.

## 3.2 Model Development

Since the air mass velocity has been determined as an explicit function of depth and time, equation [14] can be evaluated directly at every point in the soil for every time step using the temperature gradient at that point from the previous time step. Thus, the velocity gradient $\partial V/\partial z$ in the equations [10] and [11] can be evaluated independent of the moisture-heat interaction. With this approximation, the problem becomes that of evaluating two field variables, moisture content and temperature, simultaneously in two dimensions, x and z, over the time variable t.

Gray and Pinder (1974) demonstrated the Galerkin method

for a two-dimensional, time-dependent case. They used three-dimensional elements with a simple triangle representing the x and z coordinates in the spatial domain

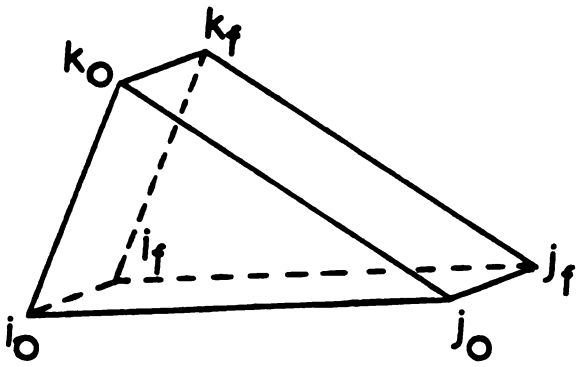


i,j,k = nodes in space domain

o,f = original, final nodes in time domain

Figure 3.1. Gray and Pinder Model

and a third dimension representing the time domain. This element is shown in Figure 3.1 as a prism of triangular cross section.

This element can be thought of as being composed of three spatial nodes with each node located at two different positions in time. The resulting three-dimensional space can be considered as sheets of three-dimensional elements that lie parallel to the x-z plane and extend over the x-z domain of the problem. Each sheet has a finite thickness determined by the time span covered by that sheet. The problem is then solved sequentially sheet by sheet. Initial time conditions for one sheet are determined by the solution generated on the previously considered sheet.

The Galerkin method can be applied to time-dependent problems in finite element analysis if the unknown field variable can be approximated by:

$$\bar{\phi}(x,z,t) = \sum_{i=1}^{nn} G_i(x,z,t)\ \Phi_i \qquad [15]$$

where $\bar{\phi}$ = approximation to unknown field variable in the space and time domain

$G_i$ = basis function at node i in the space domain, dependent on space and time

$\Phi_i$ = predetermined value of field variable at node i

nn = total nodes in the space-time domain

The basis function in equation [15] is composed of a spatial and a temporal part. The spatial part is the

well-known shape function for a triangular element in a finite element grid, designated $N_i$ at node i of that element. The temporal part is designated $\beta_i$. Thus the basis function becomes:

$$G_i(x,z,t) = N_i(x,z) \cdot \beta_i(t) \qquad [16]$$

The temporal functional can be expressed by a Lagrangian polynomial in one dimension, which at node i in the element has the form:

$$\beta_i = \prod_{\substack{r=1 \\ r \neq i}}^{m} \frac{(t_r - t)}{(t_r - t_i)}$$

where m = number of time locations for node i. For a linear time dimension with two time nodes for each spatial node in the element in Figure 3.1, m = 2, and the temporal function becomes:

$$\beta_i = \left[ \frac{t_2 - t}{t_2 - t_1} \text{ @ node } i_1, \frac{t_1 - t}{t_1 - t_2} \text{ @ node } i_2 \right] \qquad [17]$$

In Figure 3.1 the total number of nodes of the element geometrically is six. However, initial conditions are used in the time domain in such a way that the known field variable at each node at the end of the previous time period is assigned that same node at the beginning of the next time period. Thus, the actual number of unknown nodes to be determined at each time step for each element equals the number of spatial nodes per element times (m-1) time nodes. For the linear time dimension, (m = 2), the calculated nodes equal three.

Galerkin's method obtains an approximate solution to a differential equation by requiring that the error between the approximate solution and the true solution be orthogonal to the functions used in the approximation. Generally, if we start with a differential equation $L(\phi) = 0$ where L is a differential operator, and approximate the solution by $\bar{\phi}$ in equation [15], then the solution $L(\bar{\phi}) = \epsilon$ where $\epsilon$ is a residual or error due to the approximation. In order to minimize $\epsilon$ mathematically, we require:

$$\int\int_{tR} G_i \, \epsilon \, dRdt = 0$$

for each of the basis functions $G_i$. This integral requires that $G_i$ must be orthogonal to $\epsilon$ over the region R over the given time period t. Thus

$$\int\int_{tR} G_i L(\bar{\phi}) dRdt = 0 \text{ or } \int\int\int_{tzx} G_i L(\bar{\phi}) \, dxdzdt = 0 \qquad [18]$$

The expressions for $L(\bar{\phi})$ for both moisture and temperature for a single element are obtained by substituting the following expressions from equation [15]

$$\bar{\theta}(x,z,t) = \sum_{i=1}^{6} G_i(x,z,t) \, \theta_i$$

$$\bar{T}(x,z,t) = \sum_{i=1}^{6} G_i(x,z,t) \, T_i$$

into equations [10] and [11].

$$L(\bar{\theta}) = \left[\frac{\partial}{\partial x}(D_T\frac{\partial}{\partial x}) + \frac{\partial}{\partial z}(D_T\frac{\partial}{\partial z})\right] \sum_i^6 G_i T_i + \left[\frac{\partial}{\partial x}(D_\theta\frac{\partial}{\partial x}) + \frac{\partial}{\partial z}(D_\theta \frac{\partial}{\partial z})\right]$$

$$\sum_i^6 G_i\theta_i - \frac{\partial}{\partial t}\left(\sum_i^6 G_i\theta_i\right) + \theta_v \frac{\partial V}{\partial z}$$

$$L(\bar{T}) = \left[\frac{\partial}{\partial x}(\lambda\frac{\partial}{\partial x}) + \frac{\partial}{\partial z}(\lambda\frac{\partial}{\partial z})\right]\sum_i^6 G_i T_i + C_g \frac{\partial V}{\partial z} \sum_i^6 G_i T_i \qquad (19)$$

$$- C \frac{\partial}{\partial t}\left(\sum_i^6 G_i T_i\right)$$

The moisture expression above assumes the vapor content $\theta_v$ remains essentially constant over space and time.

A notation more convenient than summation terms is that of matrices. Thus, we equate for each element:

$$\sum_{i=1}^6 G_i\theta_i = \left[G_{io}G_{if}G_{jo}G_{jf}G_{ko}G_{kf}\right]\begin{Bmatrix}\theta_{io}\\ \theta_{if}\\ \theta_{jo}\\ \theta_{jf}\\ \theta_{ko}\\ \theta_{kf}\end{Bmatrix} = \left[G^e\right]\left\{\theta^e\right\}$$

$$\sum_{i=1}^6 G_i T_i = \left[G_{io}G_{if}G_{jo}G_{jf}G_{ko}G_{kf}\right]\begin{Bmatrix}T_{io}\\ T_{if}\\ T_{jo}\\ T_{jf}\\ T_{ko}\\ T_{kf}\end{Bmatrix} = \left[G^e\right]\left\{T^e\right\} \quad [20]$$

where the subscripts i, j, and k now represent the three nodes of the triangle in the space domain, subscripts o and

f represent the original and final values of the triangle moving through the time domain, and the superscript e denotes the matrix value for a single element in the grid of the space domain.

Substituting these expressions and those of [19] into equation [18] yields the Galerkin approximation to the soil heat-moisture interaction for a single element:

$$\iiint_{tzx} [G^e]^T \left\{ \left[ \frac{\partial}{\partial x}(D_T \frac{\partial}{\partial x}) + \frac{\partial}{\partial z}(D_T \frac{\partial}{\partial z}) \right] [G^e] \{T^e\} \right.$$

$$+ \left[ \frac{\partial}{\partial x}(D_\theta \frac{\partial}{\partial x}) + \frac{\partial}{\partial z}(D_\theta \frac{\partial}{\partial z}) \right] [G^e] \{\theta^e\} - \frac{\partial}{\partial t}([G^e] \{\theta^e\})$$

$$\left. + \theta_v \frac{\partial V}{\partial z} \right\} dxdzdt = 0$$

$$\text{and } \iiint_{tzx} [G^e]^T \left\{ \left[ \frac{\partial}{\partial x}(\lambda \frac{\partial}{\partial x}) + \frac{\partial}{\partial z}(\lambda \frac{\partial}{\partial z}) \right] [G^e] \{T^e\} \right.$$

$$\left. + C_g \frac{\partial V}{\partial z} [G^e] \{T^e\} - C \frac{\partial}{\partial t}([G^e] \{T^e\}) \right\} dxdzdt = 0 \qquad [21]$$

The second derivatives in the above equations impose unnecessary continuity restrictions between elements. These may be eliminated by the applications of Gauss' theorem. One of the special forms of Gauss' theorem listed in Potter and Foss (1975) is:

$$\iiint_V \vec{\nabla} \cdot \vec{W} \, dV = \iint_A \vec{W} \cdot \vec{n} \, dA \qquad [22]$$

Where $\vec{W}$ is a vector, A is the surface completely surrounding the volume V, and $\vec{n}$ is an outward-pointing unit vector normal to the elemental area dA. If we let the vector take on two dimensions with magnitudes as follows:

$$\vec{W} = M \frac{\partial P}{\partial x} \vec{i} + Q \frac{\partial P}{\partial z} \vec{k}$$

where $\vec{i}$ and $\vec{k}$ are unit vectors in the x and z directions, then equation [22] can be expanded and rearranged to obtain:

$$\iiint_V \left(M \frac{\partial^2 P}{\partial x^2} + Q \frac{\partial^2 P}{\partial z^2}\right) dV = - \iiint_V \left( \frac{\partial M}{\partial x} \cdot \frac{\partial P}{\partial x} + \frac{\partial Q}{\partial z} \cdot \frac{\partial P}{\partial z}\right) dV + \iint_A \left(M \frac{\partial P}{\partial x} \vec{i} + Q \frac{\partial P}{\partial z} \vec{k}\right) \cdot \vec{n} \, dA \qquad [23]$$

The left hand side of equation [23] now is of the same form as the three terms in equations [21] which contain the second derivatives. Using equation [23], these can now be reduced to first derivatives. For sufficiently small elements, we can also assume the diffusivities and conductivities are constant over each element.

Using the space-time domain $D^e$ for each element rather than volume V and $A^e$ to denote the elemental boundary-time domain, we can evaluate each of the three terms. For example, the first term becomes:

$$\iiint_{D^e} \left\{ [G^e]^T D_T \frac{\partial^2}{\partial x^2} \left([G^e] \left\{T^e\right\}\right) + [G^e]^T D_T \frac{\partial^2}{\partial z^2} \left([G^e] \left\{T^e\right\}\right) \right\} dx dz dt$$

$$= - \iiint_{D^e} D_T \left[ \frac{\partial}{\partial x} [G^e]^T \cdot \frac{\partial}{\partial x} [G^e] + \frac{\partial}{\partial z} [G^e]^T \cdot \frac{\partial}{\partial z} [G^e] \right] \left\{T^e\right\} dx dz dt$$

$$+ \iint_{A^e} [G^e]^T D_T \left[ \frac{\partial}{\partial x} [G^e] \vec{i} \cdot \vec{n} + \frac{\partial}{\partial z} [G^e] \vec{k} \cdot \vec{n} \right] \left\{T^e\right\} dA$$

Similar expressions can be obtained for the second and third terms.

If we further let:

$$[G_x] = \frac{\partial}{\partial x}[G],\ [G_z] = \frac{\partial}{\partial z}[G],\ [G_t] = \frac{\partial}{\partial t}[G]$$

then incorporating the above expressions into the equations [21] and summing over all nt elements in the domain yields the following:

**Moisture:**

$$\sum_{e=1}^{nt} \iiint_{D^e} \left[ D_T \left( [G_x^e]^T [G_x^e] + [G_z^e]^T [G_z^e] \right) \left\{ T^e \right\} + D_\theta \left( [G_x^e]^T [G_x^e] + [G_z^e]^T [G_z^e] \right) \left\{ \theta^e \right\} + [G^e]^T [G_t^e] \left\{ \theta^e \right\} - \theta_v \frac{\partial V}{\partial z} [G^e]^T \right] dxdzdt \qquad [24]$$

$$- \sum_{e=1}^{nt} \iint_{A^e} \left[ \left( [G^e]^T [G_x^e] \left( D_T \left\{ T^e \right\} + D_\theta \left\{ \theta^e \right\} \right) \right) \vec{i} \cdot \vec{n} + \left( [G^e]^T [G_z^e] \left( D_T \left\{ T^e \right\} + D_\theta \left\{ \theta^e \right\} \right) \right) \vec{k} \cdot \vec{n} \right] dA = 0$$

**Temperature:**

$$\sum_{e=1}^{nt} \iiint_{D^e} \left[ \lambda \left( [G_x^e]^T [G_x^e] + [G_z^e]^T [G_z^e] \right) + C [G^e]^T [G_t^e] - C_g \frac{\partial V}{\partial z} [G^e]^T [G^e] \right] \left\{ T^e \right\} dxdzdt \qquad [25]$$

$$- \sum_{e=1}^{nt} \iint_{A^e} \left[ \lambda [G^e]^T [G_x^e] \left\{ T^e \right\} \vec{i} \cdot \vec{n} + \lambda [G^e]^T [G_z^e] \left\{ T^e \right\} \vec{k} \cdot \vec{n} \right] dA = 0$$

The last summation term in each of the two equations above represents the boundary values around the x-z domain.

The dot products $\vec{i}\cdot\vec{n}$ and $\vec{k}\cdot\vec{n}$ are the x and z direction cosines and are unity when the $\vec{n}$ vector is considered along the x and z directions, respectively.

We now return to equations [16] and [20] and delineate the following:

$$[G_x] = \left[\frac{\partial G_{io}}{\partial x} \quad \frac{\partial G_{if}}{\partial x} \quad \frac{\partial G_{jo}}{\partial x} \quad \frac{\partial G_{jf}}{\partial x} \quad \frac{\partial G_{ko}}{\partial x} \quad \frac{\partial G_{kf}}{\partial x}\right]$$

$$= \left[\frac{\partial N_i}{\partial x}\cdot\beta_o \quad \frac{\partial N_i}{\partial x}\cdot\beta_f \quad \frac{\partial N_j}{\partial x}\cdot\beta_o \quad \frac{\partial N_j}{\partial x}\cdot\beta_f \quad \frac{\partial N_k}{\partial x}\cdot\beta_o \quad \frac{\partial N_k}{\partial x}\cdot\beta_f\right]$$

Similarly:

$$[G_z] = \left[\frac{\partial N_i}{\partial z}\cdot\beta_o \quad \frac{\partial N_i}{\partial z}\cdot\beta_f \quad \frac{\partial N_j}{\partial z}\cdot\beta_o \quad \frac{\partial N_j}{\partial z}\cdot\beta_f \quad \frac{\partial N_k}{\partial z}\cdot\beta_o \quad \frac{\partial N_k}{\partial z}\cdot\beta_f\right]$$

If we now identify two terms as found in Segerlind (1976), $b_\alpha = 2A\,\frac{\partial N_\alpha}{\partial x}$ and $c_\alpha = 2A\,\frac{\partial N_\alpha}{\partial z}$ for $\alpha = i,j,k$ and where A = the area of the triangular element, then:

$$[G_x] = \frac{1}{2A}\left[b_i\cdot\beta_o \quad b_i\cdot\beta_f \quad b_j\cdot\beta_o \quad b_j\cdot\beta_f \quad b_k\cdot\beta_o \quad b_k\cdot\beta_f\right] \qquad [26]$$

$$[G_z] = \frac{1}{2A}\left[c_i\cdot\beta_o \quad c_i\cdot\beta_f \quad c_j\cdot\beta_o \quad c_j\cdot\beta_f \quad c_k\cdot\beta_o \quad c_k\cdot\beta_f\right] \qquad [27]$$

To delineate the matrix $[G_t]$, we recognize that the polynomial governing the movement of the triangular element through the time domain is of the form:

$$\phi = \beta_o\phi_o + \beta_f\phi_f$$

where $\phi$ denotes the field variable at a particular node

passing from one time sheet to the next. From equation [17], and using local coordinates, the expression becomes:

$$\phi = \left[(1- \frac{t}{\Delta t}) \quad (\frac{t}{\Delta t})\right] \left\{ \begin{matrix} \Phi_o \\ \Phi_f \end{matrix} \right\} \qquad [28]$$

where $\Delta t$ is the time increment from one sheet to the next. Then:

$\frac{d\beta o}{dt} = - \frac{1}{\Delta t}$ and $\frac{d\beta f}{dt} = \frac{1}{\Delta t}$, and:

$$[G_t] = \frac{1}{\Delta t} \left[-N_i \quad N_i \quad -N_j \quad N_j \quad -N_k \quad N_k\right] \qquad [29]$$

Equations [24] and [25] can be further delineated by carrying out the matrix manipulations within the integrals using equations [20], [26], [27] and [29].

$$[G_x^e]^T \; [G_x^e] = \frac{1}{4A^2} \begin{bmatrix} b_i^2\beta_o^2 & b_i^2\beta_o\beta_f & b_ib_j\beta_o^2 & - & - \\ b_i^2\beta_o\beta_f & b_i^2\beta_f^2 & - & - & \\ b_jb_i\beta_o^2 & - & - & \text{(6X6 matrix)} & \\ - & & & & \end{bmatrix} \qquad [30]$$

$$[G_z^e]^T[G_z^e] = \frac{1}{4A^2}\begin{bmatrix} c_i^2\beta_o^2 & c_i^2\beta_o\beta_f & c_ic_j\beta_o^2 & --- \\ c_i^2\beta_o\beta_f & --- & & \\ c_jc_i\beta_o^2 & --- & \text{(6X6 matrix)} & \\ --- & & & \end{bmatrix} \quad [31]$$

$$[G^e]^T[G_t^e] = \frac{1}{\Delta t}\begin{bmatrix} -N_l^2\beta_o & N_i^2\beta_o & -N_iN_j\beta_o & --- \\ -N_i^2\beta_f & N_i^2\beta_f & -N_iN_j\beta_f & --- \\ -N_iN_j\beta_o & --- & \text{(6X6 matrix)} & \\ --- & & & \end{bmatrix} \quad [32]$$

$$[G^e]^T[G^e] = \begin{bmatrix} N_i^2\beta_o^2 & N_i^2\beta_o\beta_f & N_iN_j\beta_o^2 & --- \\ N_i^2\beta_o\beta_f & N_i^2\beta_f^2 & --- & \\ N_jN_i\beta_o^2 & --- & \text{(6X6 matrix)} & \\ --- & & & \end{bmatrix} \quad [33]$$

The line integral resulting from the boundary conditions term in each of the equations [24] and [25] can be simplified with the following substitutions:

$$\frac{\partial \theta}{\partial n} = [G_x] \{\theta\} \vec{i}\cdot\vec{n} + [G_z] \{\theta\} \vec{k}\cdot\vec{n}$$

$$\frac{\partial T}{\partial n} = [G_x] \{T\} \vec{i}\cdot\vec{n} + [G_z] \{T\} \vec{k}\cdot\vec{n} \qquad [34]$$

where n is the outward normal to the surface.

If we abbreviate the expressions [30] through [33] with the following:

$$[G_x^e]^T[G_x^e] = \frac{1}{4A^2} [b\beta], \quad [G_z^e]^T[G_z^e] = \frac{1}{4A^2} [c\beta]$$

$$[G^e]^T[G_t^e] = \frac{1}{\Delta t} [N\beta], \quad [G^e]^T[G^e] = [N\beta\beta] \qquad [35]$$

and sum over nb boundary elements, the governing equations finally assume the following integral form:

<u>Moisture</u>:

$$\sum_{e=1}^{nt} \left[ \frac{1}{4A^2} \iiint_{tzx} ([b\beta] + [c\beta])\, dxdzdt\, (D_\theta \{\theta^e\} + D_T \{T^e\}) \right.$$

$$\left. + \frac{1}{\Delta t} \iiint_{tzx} [N\beta]\, dxdzdt \{\theta^e\} - \theta_v \frac{\partial V}{\partial z} \iiint_{tzx} [G^e]^T\, dxdzdt \right]$$

$$- \sum_{b=1}^{nb} \left[ \iint_{tL} [G^e]^T\, dLdt\, (D_\theta \frac{\partial \theta^b}{\partial n} + D_T \frac{\partial T^b}{\partial n}) \right] = 0 \qquad [36]$$

<u>Temperature</u>:

$$\sum_{e=1}^{nt} \left[ \frac{\lambda}{4A^2} \iiint_{tzx} ([b\beta] + [c\beta])\, dxdzdt \{T^e\} \right.$$

$$+ \frac{C}{\Delta t} \iiint_{tzx} [N\beta]\, dxdzdt \left\{T^e\right\} - C_g \frac{\partial V}{\partial z} \iiint_{tzx} [N\beta\beta]\, dxdzdt \left\{T^e\right\}\Bigg] \qquad [37]$$

$$- \sum_{b=1}^{nb} \left[ \lambda \iint_{tL} [G^e]^T\, dLdt \left( \frac{\partial T^b}{\partial n} \right) \right] = 0$$

where $L$ = length of the boundary. It is important to note here that the parameters $D_T$, $D_\theta$ and $\lambda$ in the line integral representing boundary conditions are not necessarily the same as those in the surface integral representing conditions within the element.

## 3.3 Integration of Terms in the Model

**3.3.1 Area Integrals.** The space domain integrations in equations [36] and [37] can be carried out using techniques found in Segerlind (1976). Since the b and c terms in the first integration are constants and the $\beta$ terms are only functions of time, then:

$$\frac{1}{4A^2} \iiint_{tzx} ([b\beta] + [c\beta])\, dxdzdt = \frac{1}{4A} \int_t ([b\beta] + [c\beta])\, dt$$

Using the area coordinate system,

$$\frac{1}{\Delta t} \iiint_{tzx} [N\beta]\, dxdzdt = \frac{A}{12\Delta t} \int_t \begin{bmatrix} -2\beta_o & 2\beta_o & -\beta_o & \beta_o & --- \\ -2\beta_f & 2\beta_f & -\beta_f & --- & \\ -\beta_o & \beta_o & -2\beta_o & --- & \\ -\beta_f & \beta_f & \text{(6X6 matrix)} & & \\ --- & & & & \end{bmatrix} dt$$

and

$$\int\int\int_{tzx} [G^e]^T \, dxdzdt = \int\int\int_{tzx} \begin{bmatrix} N_i\beta_o \\ N_i\beta_f \\ N_j\beta_o \\ N_j\beta_f \\ N_k\beta_o \\ N_k\beta_f \end{bmatrix} dxdzdt = \frac{A}{3} \int_t \begin{bmatrix} \beta_o \\ \beta_f \\ \beta_o \\ \beta_f \\ \beta_o \\ \beta_f \end{bmatrix} dt$$

and $\int\int\int_{tzx} [N\beta\beta] \, dxdzdt =$

$$\frac{A}{12} \int_t \begin{bmatrix} 2\beta_o^2 & 2\beta_o\beta_f & \beta_o^2 & \beta_o\beta_f & \beta_o^2 & \beta_o\beta_f \\ & 2\beta_f^2 & \beta_o\beta_f & \beta_f^2 & \beta_o\beta_f & \beta_f^2 \\ & & 2\beta_o^2 & 2\beta_o\beta_f & \beta_o^2 & \beta_o\beta_f \\ & & & 2\beta_f^2 & \beta_o\beta_f & \beta_f^2 \\ \text{(symmetrical)} & & & & 2\beta_o^2 & 2\beta_o\beta_f \\ & & & & & 2\beta_f^2 \end{bmatrix} dt$$

3.3.2. Line Integrals.

$$\int\int_{tL} [G^e]T \, dLdt = \int\int_{tL} \begin{bmatrix} N_i\beta_o \\ N_i\beta_f \\ N_j\beta_o \\ N_j\beta_f \\ N_k\beta_o \\ N_k\beta_f \end{bmatrix} dLdt = \frac{Lxx}{2} \int_t \begin{Bmatrix} 01\cdot\beta_o \\ 01\cdot\beta_f \\ 02\cdot\beta_o \\ 02\cdot\beta_f \\ 03\cdot\beta_o \\ 03\cdot\beta_f \end{Bmatrix} dt$$

where $L_{xx} = \{Lij, Ljk, Lki\}$ .

In the line integral above, the boundary element is assumed small in space and time so that the heat and moisture flux terms

$\frac{\partial T}{\partial n}$ and $\frac{\partial \theta}{\partial n}$ can be assumed constant. The final, generalized form above will assume specific values of 0 or 1 for the terms 01, 02 and 03 depending on which of the three sides of the triangular element is on the boundary.

3.3.3 Time Integrals. Returning to equation [28],

$$\beta_o = 1 - \frac{t}{\Delta t} \text{ and } \beta_f = \frac{t}{\Delta t}$$

Then, integrating from 0 to $\Delta t$, the length of one time increment, the integrals become:

$$\int_o^{\Delta t} \beta_o dt = \int_o^{\Delta t} \beta_f dt = \frac{\Delta t}{2}$$

$$\int_o^{\Delta t} \beta_o^2 dt = \int_o^{\Delta t} \beta_f^2 dt = \frac{\Delta t}{3} \qquad \int_o^{\Delta t} \beta_o \beta_f dt = \frac{\Delta t}{6}$$

Thus, the first term in Section 3.3.1, $\frac{1}{4A} \int_t ([b\beta] + [c\beta])\, dt$ $= \frac{\Delta t}{24A} \begin{bmatrix} 2 & 1 \\ 1 & 2 \end{bmatrix} \cdot [BC]$, where the 2X2 matrix is multiplied by every element in the BC matrix, and:

$$[BC] = \begin{bmatrix} b_i^2 & b_i b_j & b_i b_k \\ & b_j^2 & b_j b_k \\ \text{(symmetric)} & & b_k^2 \end{bmatrix} + \begin{bmatrix} c_i^2 & c_i c_j & c_i c_k \\ & c_j^2 & c_j c_k \\ \text{(symmetric)} & & c_k^2 \end{bmatrix}$$

The second term becomes:

$$\frac{A}{24} \begin{bmatrix} -1 & 1 \\ -1 & 1 \end{bmatrix} \cdot \begin{bmatrix} 2 & 1 & 1 \\ 1 & 2 & 1 \\ 1 & 1 & 2 \end{bmatrix}$$

The third term becomes:

$$\frac{A\Delta t}{6} \cdot \begin{Bmatrix} 1 \\ 1 \\ 1 \\ 1 \\ 1 \\ 1 \end{Bmatrix}$$

The fourth term becomes:

$$\frac{A\Delta t}{72} \begin{bmatrix} 2 & 1 \\ 1 & 2 \end{bmatrix} \cdot \begin{bmatrix} 2 & 1 & 1 \\ 1 & 2 & 1 \\ 1 & 1 & 2 \end{bmatrix}$$

The boundary term in Section 3.3.2 becomes:

$$\frac{\Delta t \cdot Lxx}{4} \begin{Bmatrix} 01 \\ 01 \\ 02 \\ 02 \\ 03 \\ 03 \end{Bmatrix}$$

## 3.4 Set of Algebraic Equations

Substituting the above matrices into equations [36] and [37], the governing equations for a single element assume the following algebraic form:*

*It should be noted here that the individual element equations are not equalities in the true sense of the word. The conductance matrix of the temperature term for each element is a contribution to the construction of the global conductance matrix for the entire grid of elements. The same is true for the diffusivity matrices and the force vectors. Thus the pseudo equality symbol * will be used for the element expressions.

**Moisture:**

$$\frac{\Delta t}{24A}\begin{bmatrix}2 & 1\\ 1 & 2\end{bmatrix}\cdot[BC]\,(D_\theta\{\theta\}+D_T\{T\})+\frac{A}{24}\begin{bmatrix}-1 & 1\\ -1 & 1\end{bmatrix}\cdot\begin{bmatrix}2 & 1 & 1\\ 1 & 2 & 1\\ 1 & 1 & 2\end{bmatrix}\{\theta\}$$

$$-\theta_v\frac{\partial V}{\partial z}\frac{A\Delta t}{6}\begin{Bmatrix}1\\1\\1\\1\\1\\1\end{Bmatrix}-\frac{L_{xx}\Delta t}{4}\begin{Bmatrix}01\\01\\02\\02\\03\\03\end{Bmatrix}\left(D_\theta\frac{\partial\theta}{\partial n}+D_T\frac{\partial T}{\partial n}\right)\overset{*}{=}\{0\}\qquad[38]$$

**Temperature:**

$$\frac{\lambda\Delta t}{24A}\begin{bmatrix}2 & 1\\ 1 & 2\end{bmatrix}\cdot[BC]\{T\}+\frac{CA}{24}\begin{bmatrix}-1 & 1\\ -1 & 1\end{bmatrix}\cdot\begin{bmatrix}2 & 1 & 1\\ 1 & 2 & 1\\ 1 & 1 & 2\end{bmatrix}\{T\}$$

$$-C_g\frac{\partial V}{\partial z}\frac{A\Delta t}{72}\begin{bmatrix}2 & 1\\ 1 & 2\end{bmatrix}\cdot\begin{bmatrix}2 & 1 & 1\\ 1 & 2 & 1\\ 1 & 1 & 2\end{bmatrix}\{T\}\qquad[39]$$

$$-\frac{\lambda\Delta t L_{xx}}{4}\begin{Bmatrix}01\\01\\02\\02\\03\\03\end{Bmatrix}\frac{\partial T}{\partial n}\overset{*}{=}\{0\}$$

These represent a set of six algebraic equations per element for each of the two field variables, a total system of twelve coupled equations for moisture and temperature on three nodes, each at two different times.

The above equations can be rearranged to the following form:

<u>Moisture</u>:

$$\frac{D_T \Delta t}{24A}\,[BC]\cdot\begin{bmatrix}\begin{bmatrix}2&1\\1&2\end{bmatrix}&0&0\\0&\begin{bmatrix}2&1\\1&2\end{bmatrix}&0\\0&0&\begin{bmatrix}2&1\\1&2\end{bmatrix}\end{bmatrix}\begin{Bmatrix}T_{io}\\T_{if}\\T_{jo}\\T_{jf}\\T_{ko}\\T_{kf}\end{Bmatrix}+\frac{D_\theta \Delta t}{24A}\,[BC]\cdot$$

$$\begin{bmatrix}\begin{bmatrix}2&1\\1&2\end{bmatrix}&0&0\\0&\begin{bmatrix}2&1\\1&2\end{bmatrix}&0\\0&0&\begin{bmatrix}2&1\\1&2\end{bmatrix}\end{bmatrix}\begin{Bmatrix}\theta_{io}\\\theta_{if}\\\theta_{jo}\\\theta_{jf}\\\theta_{ko}\\\theta_{kf}\end{Bmatrix}+\frac{A}{24}\begin{bmatrix}-2&2&-1&1&-1&1\\-2&2&-1&1&-1&1\\-1&1&-2&2&-1&1\\-1&1&-2&2&-1&1\\-1&1&-1&1&-2&2\\-1&1&-1&1&-2&2\end{bmatrix}\begin{Bmatrix}\theta_{io}\\\theta_{if}\\\theta_{jo}\\\theta_{jf}\\\theta_{ko}\\\theta_{kf}\end{Bmatrix}$$

$$-\theta_v\frac{\partial V}{\partial z}\frac{A\Delta t}{6}\begin{Bmatrix}1\\1\\1\\1\\1\\1\end{Bmatrix}-D_T\frac{L_{xx}\Delta t}{4}\frac{\partial T}{\partial n}\begin{Bmatrix}01\\01\\02\\02\\03\\03\end{Bmatrix}-D_\theta\frac{L_{xx}\Delta t}{4}\frac{\partial \theta}{\partial n}\begin{Bmatrix}01\\01\\02\\02\\03\\03\end{Bmatrix}$$

$$\overset{*}{=}\{0\}$$

**Temperature:**

$$\frac{\lambda\Delta t}{24A}[BC]\cdot\begin{bmatrix}\begin{bmatrix}2&1\\1&2\end{bmatrix}&0&0\\0&\begin{bmatrix}2&1\\1&2\end{bmatrix}&0\\0&0&\begin{bmatrix}2&1\\1&2\end{bmatrix}\end{bmatrix}\begin{Bmatrix}T_{io}\\T_{if}\\T_{jo}\\T_{jf}\\T_{ko}\\T_{kf}\end{Bmatrix}+\frac{CA}{24}\begin{bmatrix}-2&2&-1&1&-1&1\\-2&2&-1&1&-1&1\\-1&1&-2&2&-1&1\\-1&1&-2&2&-1&1\\-1&1&-1&1&-2&2\\-1&1&-1&1&-2&2\end{bmatrix}\begin{Bmatrix}T_{io}\\T_{if}\\T_{jo}\\T_{jf}\\T_{ko}\\T_{kf}\end{Bmatrix}$$

$$-C_g\frac{\partial V}{\partial z}\frac{A\Delta t}{72}\begin{bmatrix}4&2&2&1&2&1\\2&4&1&2&1&2\\2&1&4&2&2&1\\1&2&2&4&1&2\\2&1&2&1&4&2\\1&2&1&2&2&4\end{bmatrix}\begin{Bmatrix}T_{io}\\T_{if}\\T_{jo}\\T_{jf}\\T_{ko}\\T_{kf}\end{Bmatrix}-\frac{\lambda\Delta tL_{xx}}{4}\frac{\partial T}{\partial n}\begin{Bmatrix}01\\01\\02\\02\\03\\03\end{Bmatrix}\stackrel{*}{=}\{0\}$$

These matrices can be combined to produce the governing equations in the following form:

**Moisture:**

$$\begin{bmatrix}Y\text{ matrix}\\(6\times 6)\end{bmatrix}\{T_{io}\ \ T_{if}\ \ T_{jo}\ \ T_{jf}\ \ T_{ko}\ \ T_{kf}\}^T+$$

$$\begin{bmatrix}U\text{ matrix}\\(6\times 6)\end{bmatrix}\{\theta_{io}\ \ \theta_{if}\ \ \theta_{jo}\ \ \theta_{jf}\ \ \theta_{ko}\ \ \theta_{kf}\}^T-\theta_v\frac{\partial V}{\partial z}\frac{A\Delta t}{6}\cdot \qquad [40]$$

$$\{1\ \ 1\ \ 1\ \ 1\ \ 1\ \ 1\}^T\stackrel{*}{=}\frac{L_{xx}\Delta t}{4}\left(D_T\frac{\partial T}{\partial n}+D_\theta\frac{\partial\theta}{\partial n}\right)\{01\ 01\ 02\ 02\ 03\ 03\}^T$$

**Temperature:**

$$\left[\begin{matrix}\text{W matrix}\\(6\ X\ 6)\end{matrix}\right]\left\{T_{io}\quad T_{if}\quad T_{jo}\quad T_{jf}\quad T_{ko}\quad T_{kf}\right\}^{T} \qquad [41]$$
$$\overset{*}{=} \frac{L_{xx}\Delta t}{4}\left(\lambda\frac{\partial T}{\partial n}\right)\left\{01\quad 01\quad 02\quad 02\quad 03\quad 03\right\}^{T}$$

This set of twelve equations has now been given physical meaning through delineazation in space and time. At each calculation, six of the field variables are known, having been solved from the previous time step. Further, temperature and moisture are now decoupled. Thus, the temperature is solved first, then the moisture can be solved. This set can be reduced to six equations in six unknowns by combining pairs of equations. The first pair of the temperature subset will take on the form:

$$W_1T_{io}+W_2T_{if}+W_3T_{jo}+W_4T_{jf}+W_5T_{ko}+W_6T_{kf}+W_7T_{io}+W_8T_{if}$$
$$+\ W_9T_{jo}+W_{10}T_{jf}+W_{11}T_{ko}+W_{12}T_{kf} \overset{*}{=} \frac{\lambda L_{xx}\Delta t}{2}\frac{\partial T}{\partial n}\ (01)$$

where $W_i$ are the elements of the W matrix in equation [41]. The other five pairs of equations assume a similar form.

Rearranging the matrix elements and variables as a temperature contribution $R_T^{(e)}$ and moisture contribution $R_M^{(e)}$ from each element, the governing equations finally assume the following form:

**Temperature:**

$$\begin{bmatrix} \text{S1 matrix} \\ (3 \times 3) \end{bmatrix} \begin{Bmatrix} T_{if} \\ T_{jf} \\ T_{kf} \end{Bmatrix} - \frac{L_{xx}\Delta t}{2} \left(\lambda \frac{\partial T}{\partial n}\right) \begin{Bmatrix} 01 \\ 02 \\ 03 \end{Bmatrix} + \begin{bmatrix} \text{S2 matrix} \\ (3 \times 3) \end{bmatrix} \begin{Bmatrix} T_{io} \\ T_{jo} \\ T_{ko} \end{Bmatrix} = R_T(e) \qquad [42]$$

**Moisture:**

$$\begin{bmatrix} \text{R1 matrix} \\ (3 \times 3) \end{bmatrix} \begin{Bmatrix} \theta_{if} \\ \theta_{jf} \\ \theta_{kf} \end{Bmatrix} - \frac{L_{xx}\Delta t}{2} \left(D_T \frac{\partial T}{\partial n} + D_\theta \frac{\partial \theta}{\partial n}\right) \begin{Bmatrix} 01 \\ 02 \\ 03 \end{Bmatrix}$$

$$- \theta_v \frac{\partial V}{\partial z} \cdot \frac{A\Delta t}{3} \begin{Bmatrix} 1 \\ 1 \\ 1 \end{Bmatrix} + \begin{bmatrix} \text{R2 matrix} \\ (3 \times 3) \end{bmatrix} \begin{Bmatrix} \theta_{io} \\ \theta_{jo} \\ \theta_{ko} \end{Bmatrix}$$

$$+ \begin{bmatrix} \text{Q matrix} \\ (3 \times 3) \end{bmatrix} \begin{Bmatrix} (T_{io} + T_{if}) \\ (T_{jo} + T_{jf}) \\ (T_{ko} + T_{kf}) \end{Bmatrix} = R_M(e) \qquad [43]$$

The elements of the S temperature matrices each contain a soil conduction, soil bulk capacitance, and a soil air convection term characterized by the following example:

$$S_1 = \frac{\lambda \Delta t (BC_{11})}{8A} + \frac{CA}{6} - C_g \frac{\partial V}{\partial z} \frac{A\Delta t}{12}$$

The elements of the R moisture matrices include a liquid diffusivity and a moisture capacitance term of the

form:

$$R_1 = D_\theta \frac{\Delta t(BC_{11})}{8A} + \frac{A}{6}$$

The elements of the Q moisture matrix contain a thermal diffusivity term of the form:

$$Q_1 = D_T \frac{\Delta t(BC_{11})}{8A}$$

Equations [42] and [43] now comprise the six equations needed for moisture and temperature at the three nodes of any given element for a given time.

## 3.5 Summary

This chapter brought the governing equations of Chapter 2 to the algebraic form necessary for modeling on a computer. These equations require the soil parameters $\lambda$, $D_\theta$, $D_T$, C, $C_g$, $\Theta_v$ and $\partial V/\partial z$. These parameters are now delineated in Chapter 4.

# 4. SOIL PARAMETERS

The soil properties needed for solution of the model comprised of equations [42] and [43] are $D_\theta$, $D_T$, $\lambda$, $\theta_v$, $\partial V/\partial z$, C, and $C_g$, all identified earlier. These properties, as they relate generally to all soils or to average temperature and moisture conditions, are now developed in more detail.

## 4.1 Moisture Diffusivity $D_\theta$

Philip and DeVries (1957) showed that $D_\theta = D_{\theta l} + D_{\theta v}$. However, DeVries (1958) and Jackson, et al. (1975) showed that $D_{\theta v}$ is significant with respect to $D_{\theta l}$ only at extremely dry soil conditions (see Table 7.2). Thus, $D_\theta$ can be set equal to $D_{\theta l} = K\,(\partial\psi/\partial\theta_l)$ with no loss of generality in the moisture range above the wilting point.

**4.1.1 Moisture Characteristic Slope $\partial\psi/\partial\theta_l$.** Ghosh (1980) proposed a method of calculating soil moisture characteristics from mechanical properties. The method is applicable for those soils for which the $\psi - \theta$ relation can be expressed as

$$\psi = \psi_e \left(\frac{\theta}{\theta_o}\right)^{-\beta} \qquad [44]$$

where $\psi_e$ = air entry value of matric potential, $mH_2O$

$\theta_o$ = saturation moisture content = S

$\beta$ = dimensionless empirical constant

Ghosh fitted actual data from eight soils ranging from sand to clay, and the empirical versus published $\psi$ values

gave correlation coefficients ranging from 0.88 to 0.99. The following relations or values were determined.

$\theta_e$ (air entry water content) $\tilde{=}$ 0.9S, according to Ghosh.

S = total porosity = $1 - \rho_B/(2.65 \times 10^3)$

and

$$\beta = 2.619(\lambda_2/\lambda_1)^{0.2822}(\lambda_4+0.7)^{0.0625}\lambda_4^{0.125} \cdot (5.91\lambda_3/(\lambda_1+\lambda_3) + 1.1)^{0.0625}$$

where $\lambda_{1,2,3}$ = % sand, silt, and clay, respectively

$$\lambda_4 = 6.2\sqrt{\lambda_2/\lambda_1} - 5.91\lambda_3/(\lambda_1 + \lambda_3)$$

The value of $\psi_e$ was published for the soils considered. For any unknown soil, a single $\psi$-$\theta$ reading is sufficient to establish the relation [44]. Once the relation is established, the slope can be obtained mathematically.

$$\frac{\partial\psi}{\partial\theta} = \frac{-\beta\psi_e S^\beta}{\theta^{\beta+1}} = \frac{-\beta\psi_e(1-\rho_B/2650)^\beta}{\theta^{\beta+1}} \qquad [45]$$

4.1.2 Hydraulic Conductivity K. Recent work by Mualem (1978) and Hirschi and Moore (1980) has established a mathematical relation to obtain K from easily measured soil properties. The basic relation from Mualem is:

$$K_r = S_e^n$$

where: $K_r = K/K_s$

$K_s$ = K at saturation

$S_e = \theta/\theta_o$

n = .015w + 3.0 from Mualem (1978)

w = energy required to drain a unit bulk volume of soil from saturation condition

$$= \int_{\theta_H}^{\theta_o} \gamma_w \psi d\theta$$

$\psi$ = matric potential, cm $H_2O$

$\gamma_w$ = weight density of water, $g/cm^3$

$\theta_H$ = moisture content where soil is considered dry, or where $\psi$-$\theta$ curve reaches the assymptotic level

Using the expression [44] and integrating:

$$w = \int_{\theta_H}^{\theta_o} \gamma_w \psi_e \left(\frac{\theta}{\theta_o}\right)^{-\beta} d\theta = \frac{\psi_e}{-\beta+1}(S - S^{\beta}\ \theta_H^{-\beta+1}) \qquad [46]$$

and:

$$K = K_s \left(\frac{\theta}{S}\right)^{.015w+3.0} \qquad [47]$$

4.1.3 Hysteresis Effects. Hillel (1977) stated the following:

"After its strong daytime desiccation, the surface zone of the soil draws moisture from below during the night, so that the top layer is in a process of sorption while the underlying donor layer is in a process of desorption. In principle, the hysteresis phenomenon makes it possible for a sorbing zone of soil to approach potential equilibrium with a desorbing zone of the same soil while the former is at a lower moisture content, and hence at a lower value of hydraulic conductivity. It would seem to follow that the hysteresis effect can contribute to the self-arresting tendency of the evaporation process by causing it to fall below the potential rate earlier than it would if hysteresis were nonexistent."

Hillel, in a computer simulation, demonstrated that hysteresis has a marked effect on the overall evaporation in a diurnal cycle, and thus cannot be ignored. Bresler et al. (1969) and others have determined that K is essentially a unique function of $\theta$, and the hysteretic effects are present in the $\psi$-$\theta$ relationship. Therefore, a separate relation, similar to equation [44] but with different parameters, needs to be defined and stored for the sorption curve of the soil in question. Since sorption curves have not received much attention, are difficult to measure, and transition is still not well understood, transition between the two curves when used in the computer simulation will be delayed by one time step. Further, only the two primary curves will be used.

## 4.2 Moisture Diffusivity $D_T$

Philip and DeVries (1957) showed that $D_T = D_{Tl} + D_{Tv}$. These diffusivities are further delineated to:

$$D_{Tl} = K\gamma\psi$$
$$D_{Tv} = fD_{atm}\nu\beta h(\nabla T)_a/\rho_l\nabla T$$

The following parameters were either evaluated by Philip and DeVries or cited by them from earlier works:

$h = 1.00$ for $\psi$ above the wilting point

$\nu = 1.024$ for $T = 20°C$

$\rho_o = 1.73 \times 10^{-2}$ kg $m^{-3}$ for $T = 20°C$

$\beta = 1.05 \times 10^{-3}$ kg $m^{-3}{}^{\circ} C^{-1}$ for $10°C \leq T \leq 30°C$

4.2.1 Flow Factor f. This factor was equated to:

$$f = S = \theta_o \qquad \text{for } \theta_1 \leq \theta_{1k}$$

$$f = a + a\theta_1/(S-\theta_{1k}) = (S-\theta_1)(1+\theta_1/(S-\theta_{1k})) \qquad \text{for } \theta_1 > \theta_{1k}$$

since $a = S - \theta_1$.

4.2.2 Moisture Content $\theta_{1k}$. This has been defined as the point where liquid continuity fails. It is somewhat arbitrary, but may be extracted from a K-$\theta$ performance curve where K falls to some percentage (perhaps 1/1000) of its saturated value.

Philip and DeVries (1957) cited from Moore's work a $\theta_{1k} = 0.20$ for Yolo light clay. DeVries (1958) used $\theta_{1k} = 0.10$ for a medium sand. If the point where $K = K_s/1000$ is used, the corresponding $\theta$ from several actual soil K-$\theta$ curves published in Mualem (1978) are tabularized below. The values in parentheses correspond to $\theta = 40\%$ saturation.

Table 4.1. Moisture contents at $K = K_S/1000$ for several soils (Mualem (1978))

| | | | |
|---|---|---|---|
| Grenville silt loam | .34 (.20) | Volcanic sand | .11 |
| Adelanto loam | .22 (.17) | Plainfield sand | .10 |
| Loamy coarse sand | .20 (.16) | River sand | .08 (.16) |
| Fine sand | .12 (.14) | Sand fraction | .07 (.14) |
| Silt Mont Cenis | .20 (.18) | | |

Table 4.1 demonstrates clearly the wide variability of moisture parameters in natural soils. Because of this and the arbitrary nature of liquid continuity, a $\theta_{lk}$ = 40% of $\theta_o$, as suggested by Jury and Letey (1979), will be adopted.

4.2.3 Atmospheric Diffusion $D_{atm}$. Using P = 762 mm Hg (standard total pressure for air) and converting T to °C, the term becomes:

$$D_{atm} = 5.80 \times 10^{-7} (T + 273)^{2.3} \text{ cm}^2 \text{ sec}^{-1}$$

or

$$D_{atm} = 5.80 \times 10^{-11} (T + 273)^{2.3} \text{ m}^2 \text{ sec}^{-1} \qquad [48]$$

4.2.4 Air Pore Temperature Gradient Ratio $(\nabla T)_a / (\nabla T)$. Philip and DeVries listed temperature gradient ratios for different $\theta$ and S values. A linear regression analysis of their results calculated by the author produced the following expression:

$$\frac{(\nabla T)_a}{(\nabla T)} = 0.24\theta - 1.53S + 2.46 \qquad [49]$$

This is good for $10°C \leq T \leq 30°C$ and $0.1 \leq \theta \leq 0.5$. Their theory produced values for temperature gradient ratios between 1 and 2.07. However, it should be noted that Hadas (1968) reported values up to 3.2, Cary (1965) reported up to 5, and Woodside and Kuzmak (1958) reported values up to 20.

4.2.5 Theory Modification. Although some investigators have tested the Philip-DeVries theory under field conditions and have proposed correction factors to make the purely diffusion mechanism better fit convection phenomena, Jury and Letey (1979) actually studied the theory itself. They compared the mechanistic theory with that of the thermodynamic approach by Cary and Taylor (1962a, b) to explain vapor diffusion through porous media under the influence of temperature gradients. These two theories were compared with experimental data from five investigations.

They explained that discrepancies between the Philip-DeVries theory and experimental data arise from the "liquid island" effect, accounted for by the factor f. Whereas Philip and DeVries considered liquid islands as equivalent to vapor flow paths and assumed tortuosity was included in the $(\nabla T)_a/(\nabla T)$ calculation, Jury and Letey argued that liquid islands are actually shorter paths as seen by diffusing vapor, and the tortuosity needs to be adjusted. They proposed the following path correction factor:

$$\xi = \left[ \frac{a + \theta_l g(a)}{a + \frac{\theta_l}{g(a)} \left(\frac{\lambda_v}{\lambda_l}\right)} \right]^2 \qquad [50]$$

where $g(a) = 1$ for $\theta < \theta_{lk}$

$= a/(S-\theta_{lk})$ for $\theta \geq \theta_{lk}$

$\lambda_v/\lambda_l = 0.124$

If the above factor is multiplied with the other factors in the expression $D_{Tv} = f\, D_{atm}\, \nu\beta h\, (\nabla T)_a/\rho_l \nabla T$, the theory more closely predicts vapor flow under temperature gradients.

## 4.3 Thermal Conductivity $\lambda$.

The thermal conductivity of the soil has been presented in the literature as a weighted average of the several soil constituents. A fundamental study spanning many years has been published by DeVries (1963). The soil conductivity has been equated to:

$$\lambda = \frac{\Sigma x_i k_i \lambda_i}{\Sigma x_i k_i}$$

where $x_i$, $k_i$, and $\lambda_i$ are volume fraction, ratio of constituent temperature gradient to overall gradient, and thermal conductivity, respectively, of the ith constituent.

When $\theta < \theta_{lk}$, then air in the soil pores is considered the continuous medium. For $\theta \geq \theta_{lk}$, the water is considered the continuous medium. Whichever medium is used as the basis for $\lambda$, the k for that constituent is taken as unity. Thus:

$$\lambda = \frac{x_{av}\lambda_{av} + k_l x_l \lambda_l + k_s x_s \lambda_s}{x_{av} + k_l x_l + k_s x_s} \qquad \text{for } \theta < \theta_{lk} \qquad [51]$$

and

$$\lambda = \frac{x_l \lambda_l + k_{av} x_{av} \lambda_{av} + k_s x_s \lambda_s}{x_l + k_{av} x_{av} + k_s x_s} \qquad \text{for } \theta \geq \theta_{lk} \qquad [52]$$

where subscripts s, l, and av designate soil, liquid water and air-vapor mixture in the soil pores.

4.3.1 Soil Temperature Gradient Ratios $k_s$. The expression for $k_i$ is given in DeVries (1963) as:

$$k_i = \frac{1}{3} \sum_{N=a,b,c} \left[1 + \left(\frac{\lambda_i}{\lambda_o} - 1\right) g_N\right]^{-1} \qquad [53]$$

where a,b,c are the dimensions of the three axes of the constituent particle and $\lambda_o$ the thermal conductivity of the continuous medium. The quantity $g_N$ depends on the ratio of the three axes. For soil particles, the dimensions can be assumed closest to an ellipsoid of revolution where a = b = nc. The constant of proportionality n can be assumed to be around 5. From a graphical relation between $g_a$ and n shown

by DeVries for ellipsoids, $g_a = g_b = 0.125$. And, since $g_a + g_b + g_c = 1$, $g_c = 0.75$.

The thermal conductivities of several natural elements are tabularized below from DeVries (1963) and Hadas (1969a, 1977a).

Table 4.2 Thermal conductivities of several elements, J/m sec°C

| | | | |
|---|---|---|---|
| quartz sand | 8.799 | dry air at 20°C | .02577 |
| silt | 2.179 | water at 20°C | .595 |
| clay | 2.975 | saturated air at 20°C | .0997 |

Using the above values in equation [53], and using saturated air as the continuous medium for $\theta < \theta_{1k}$, the resulting $k_s$ values are tabularized below.

Table 4.3 Soil temperature gradient ratios

| Element | $\theta \geq \theta_{1k}$ | $\theta < \theta_{1k}$ |
|---|---|---|
| quartz sand | .274 | .061 |
| clay | .527 | .159 |
| silt | .611 | .205 |

### 4.3.2 Temperature Gradient Ratio of the Dispersed Fluid $k_{av}$ or $k_l$.

When $\theta \geq \theta_{1k}$, water is the continuous medium, air is considered a dispersed particle. DeVries showed that as $\theta$ approaches saturation, the shape of air pockets will become

spherical, where $g_a = g_b = g_c = 1/3$. When $\theta < \theta_{1k}$, air is the continuous medium, and the water is the dispersed fluid. As $\theta$ approaches zero, the $g_a$ for water becomes approximately 0.013. The actual shape in each case depends on the water content as:

$$g_a \text{ air voids} = 0.035 + 0.298\ (\theta/S) \qquad \text{for } \theta \geq \theta_{1k}$$

Since $g_b = g_a$ and $g_c = 1 - g_a - g_b$, then from equation [53],

$$k_{av} = 0.333\left[\frac{2}{0.971 - 0.248(\theta/S)} + \frac{1}{0.226 + 0.496\ (\theta/S)}\right]$$

$$\text{for } \theta \geq \theta_{1k} \qquad [54]$$

Similarly:

$$g_a \text{ water} = 0.013 + 0.085(\theta/\theta_{1k})$$

and:

$$k_1 = 0.333\left[\frac{2}{1.287 + 1.878(\theta/\theta_{1k})} + \frac{1}{22.514 - 3.755(\theta/\theta_{1k})}\right] \qquad [55]$$

$$\text{for } \theta < \theta_{1k}$$

**4.3.3 Thermal Conductivity of Air-filled Pores $\lambda_{av}$.** Philip and DeVries (1957) proposed:

$$\lambda_{av} = \lambda_a + \lambda_v$$

The vapor term takes into account the vapor distillation due to temperature gradients in the air-filled pores. And

$$\lambda_v = h\nu\beta LD_{atm} \qquad [56]$$

All terms on the right hand side have been identified except the latent heat of vaporization, which is $L = 2.451 \times 10^6$ J/kg at 20°C.

Recent investigators have found this expression under predicts actual heat flow. Although temperature reversals and wind gusts under actual field conditions may account for heat and vapor flow beyond that accountable by the Philip-DeVries theory, an adjustment to the theory has been proposed by Hadas (1977) and Sepaskhah and Boersma (1979) to improve predictions of the diffusion mechanism itself. This adjustment is the incorporation of a "mass enhancement factor" § in:

$$\lambda_{av} = \lambda_a + \S\lambda_v \qquad [57]$$

Sepaskhah and Boersma suggested § = 1.3 for loam and silty clay loam soils.

## 4.4 Heat Capacities C and $C_g$

DeVries (1963) showed the expression for heat capacity of soils to be:

$$C = (1 - S)C_s + \theta C_l + aC_g \qquad [58]$$

where C, $C_s$, $C_l$, $C_g$ are the volumetric heat capacity of the total soil medium, soil particle constituent, liquid and air-vapor gas mixture constituents, respectively. The constituent values are tabularized below.

Table 4.4 Heat capacities, $Jm^{-3}{}^{\circ}C^{-1}$

| | |
|---|---|
| Quartz and clay minerals | $2.011 \times 10^{6}$ |
| Organic matter | $2.514 \times 10^{6}$ |
| Water | $4.190 \times 10^{6}$ |
| Air | $1.257 \times 10^{3}$ |

According to the properties of saturated water vapor listed by VanWijk (1963) and DeVries, the density of vapor can be expressed as

$$\rho_o = (0.90T^{1.015}) \times 10^{-3} \ kgm^{-3} \qquad [59]$$

for $10°C \leq T \leq 30°C$. Since we can assume the soil air is saturated over most of the moisture range, and $\rho_l = 1000 \ kgm^{-3}$, then the ratio $\rho_o/\rho_l$ = the ratio of liquid volume to total volume of the mixture.

Then:

$$C_g = (0.90 \times 10^{-6} \ T^{1.015})(4.190 \times 10^{6}) + (1 - 0.90 \times 10^{-6} \ T^{1.015})(1.257 \times 10^{3}) \qquad [60]$$

At 20°C, $C_g = 1.332 \times 10^{3} \ Jm^{-3}{}^{\circ}C^{-1}$.

## 4.5 Vapor Content $\theta_v$.

The volumetric vapor content $\theta_v$ can be obtained directly from the expression [59].

$$\theta_v = (0.90 \times 10^{-6} \ T^{1.015}) a \qquad [61]$$

for $10°C \leq T \leq 30°C$.

## 4.6 Velocity Gradient $\partial V/\partial z$.

4.6.1 Pressure Changes Component $\partial V_p / \partial z$. Equation [6] expresses the velocity component due to pressure fluctuations proposed by Farrell et al. (1966). Both the works of Farrell and Fukuda (1955) were supported by experimental data, but both admitted there was insufficient data to go beyond a qualitative conclusion. For this reason we can assume a soil of infinite depth with the wavelength of the air pressure fluctuations of the same magnitude as the soil thickness. These were assumptions made by Fukuda which make the analysis simpler than the model by Farrell et al. According to Fukuda for equation [6]:

$$L^* = \infty, \quad \lambda^* = \gamma^* = \sqrt{\omega\varepsilon/2K^* p_o},$$

where $\omega = 2\pi/t_p$ ($t_p$ = period, sec.)

$$\varepsilon = a \qquad [62]$$

$$p_o = 10.35 \text{ m } H_2O$$

Air permeability $K^*$ is highly variable with porosity, soil particle size, and moisture content, as shown in the table below.

**Table 4.5 Air permeabilities, $K^*$, m $sec^{-1}$**

| Material | Particle diameter (mm) | Air content a | Permeability | Reference |
|---|---|---|---|---|
| Oder River sand | 0.5-1.0 | .36 | 0.1487 | Fukuda |
| | 0.25-0.5 | .36 | 0.0575 | " |
| Main sand | 0.5-1.0 | .36 | 0.0603 | " |
| " | " | .40 | 0.0671 | " |
| Spheres | 2.0 | .40 | 0.75 | Farrell |
| " | 10.0 | .40 | 18.85 | " |

For unstructured soil, the air permeability is much more sensitive to the smaller particle sizes. With appreciable clay and silt, $K^*$ can be expected to be quite small. However, for drier, tilled surface layers with the desired degree of aggregation of 1 to 5 mm, $K^*$ can vary significantly.

Pall and Mohsenin (1980) showed data to match a relationship between permeability and functions of particle diameter and air porosity. Using this relationship and the permeability values tabularized above, the following equation is developed:

$$K^* = D_{vs}^2 \frac{(1.111 \times 10^6) a^3}{(1-a)^2} \qquad [63]$$

where $D_{vs}$ = volume surface mean diameter (m), delineated in Table 4.6 for sand, silt and clay.

Table 4.6 Volume surface mean diameters, mm

| Constituent | Particle Size Range | Representative Size |
|---|---|---|
| Sand | 2.0-.05 | 1.025 |
| Silt | .05-.002 | .026 |
| Clay | <.002 | .001 |

Thus, for an unstructured soil:

$$D_{vs} = \frac{\left[(1.025)^3\lambda_1 + (.026)^3\lambda_2 + (.001)^3\lambda_3\right] x10^{-3}}{(1.025)^2\lambda_1 + (.026)^2\lambda_2 + (.001)^2\lambda_3} \qquad [64]$$

Allmaras et al. (1977), in their study of tillage effects on soil structure, found tilled layers with a total porosity greater than 60% (bulk density < 1033 kg/m $^3$) exhibited significant air mass turbulent effects in the soil pores. Ojeniyi and Dexter (1979) studied the size and distribution of soil aggregates and pores produced by various tillage treatments. They stated that much of the drying of tilled soil in the field occurs as a result of convective transport of air through pores larger than 8 mm. They found that, for a sandy loam after one pass of a set of tines, the portion of the total porosity greater than 8 mm in the 10-20 cm. depth may range from 39 to 48%.

Since tillage greatly affects the porosity and air permeability, $K^*$ must be corrected for this condition. Ojeniyi and Dexter proposed an empirical expression for the aggregation:

$$\bar{D} = 25.2\ e^{-0.192N}$$

where: $\bar{D}$ = mean aggregate size, mm

N = number of implement passes

For lack of other quantitative expressions, this will be incorporated into the model for structured soil as:

$$D_{vs} = 0.0252\ e^{-0.192N} \qquad [65]$$

where: $D_{vs}$ = mean aggregate size, meters, for the tilled layers.

Making use of the simplifying expressions [62];

$$\frac{\partial V_p}{\partial z} = \frac{2K^*\lambda^{*2}a_o}{a} \exp(-\lambda^* z)\ \mathrm{Cos}(\omega t - \lambda^* z) \qquad [66]$$

Farrell et al. made several field measurements of pressure fluctuations at the surface of a grassed field. Probes were placed at spacings of .05, .15 and .60 m on the surface and differences in pressure between them recorded for wind speeds of 4.20 to 6.60 m/sec, measured at a 2-meter height. Table 4.7 shows several pressure wave values produced by that study.

Table 4.7 Air pressure wave measurements (Farrell, et al.)

| Wavelength $L^*$ (m) | Period $t_p$ (sec) | Amplitude $a_o$ (m) | Frequency $\omega$ ($sec^{-1}$) |
|---|---|---|---|
| $\infty$ | 10.0 | .00100 | 0.628 |
| .60 | 2.5 | .00025 | 2.513 |
| .30 | 1.5 | .00015 | 4.189 |
| .15 | 1.0 | .00010 | 6.283 |
| .05 | 0.5 | .00005 | 12.566 |

The term $\partial V_p/\partial z$ in the moisture and temperature models is evaluated at different depths z and time increments. The time increments chosen are to conveniently characterize the germination period and in no way attempt to lock into the sinusoidal times of surface pressure waves. The velocity gradient is therefore evaluated at the same point in the pressure wave sinusoidal train at every time increment throughout the germination period. If this point is chosen to be where the sinusoidal component is maximum at 1.0, then equation [66] reduces to:

$$\frac{\partial V_p}{\partial z} = \frac{\omega a_o}{10.35} \exp\left(-\sqrt{\frac{\omega a}{20.70K^*}} \cdot z\right) \qquad [67]$$

4.6.2 Density Changes Component $\partial V_d/\partial z$. According to Hollman (1976), $\beta^*$ in equation [13] for ideal gases in the range between 10 °C and 30 °C, can be equated to:

$$\beta^* = \frac{1}{(°K)} = .0034\ °C^{-1}$$

Equation [13] becomes:

$$\frac{\partial V_d}{\partial z} = i\left[\sqrt{.0667(\Delta T/\Delta z) + (V_{dl}/\Delta z)^2} - V_{dl}/\Delta z\right] \qquad [68]$$

Finally equations [67] and [68] are combined:

$$\frac{\partial V}{\partial z} = \frac{\omega a_o}{10.35}\exp\left(-\sqrt{\frac{\omega a}{20.70K^*}}\cdot z\right) + i\left[\sqrt{.0667(\Delta T/\Delta z) + (V_{dl}/\Delta z)^2} - V_{dl}/\Delta z\right] \qquad [69]$$

## 4.7 Summary

Equations [44] through [69] characterize the general soil parameters needed for the model. These parameters, in turn, have been developed to now require the following specific parameters as inputs:

| | |
|---|---|
| $\lambda_1$, $\lambda_2$, $\lambda_3$ | % sand, silt, and clay |
| $\rho_B$ | bulk density |
| $\psi_e$ | air-entry soil moisture matric potential during desorption |
| $\psi_{ea}$ | air-entry soil moisture matric potential during adsorption |
| $K_s$ | hydraulic conductivity at saturation |
| $\theta_H$ | immobile moisture content |
| $\omega$ | frequency of surface air pressure waves |
| $a_o$ | amplitude of surface air pressure waves |

In Chapter 5 the meteorological model and the soil surface interface will be developed.

## 5. SURFACE CONDITIONS

The soil heat-moisture flow model equations [42] and [43] include a time-dependent driving force for $\theta$ and T at the surface throughout the period of study. Providing realistic surface conditions rather than imposing artificial conditions will allow the model to be verified with actual data, thus lending it considerable strength and applicability.

The governing equations can be revised to a form better suited for analysis at the soil surface. The terms containing the boundary or surface conditions are:

a. $\lambda\frac{\partial T}{\partial n}$ = heat flow to or from the surface of the soil

b. $(D_T \frac{\partial T}{\partial n} + D_\theta \frac{\partial \theta}{\partial n})$= evaporation rate E from the surface, considered negative when the flux is from the surface into the air. It is the volume of water per surface area per time.

### 5.1 Evaporation at the Surface

Equation [43] calls for the evaporation rate E at the surface. Van Bavel and Hillel (1976) and Hillel (1977) have developed computer models incorporating a straightforward calculation of the evaporation:

$$E_m = \frac{H_s - H_a}{R_c} \qquad [70]$$

where: $E_m$ = mass evaporation rate, kg $m^{-2}$ $sec^{-1}$, (If we divide $E_m$ by the density $\rho_1$ = 1000 kg $m^{-3}$, the result is E, m $sec^{-1}$, the form called for in equation [43].)

$H_s$ = absolute humidity of air at the soil surface, kg $m^{-3}$

$H_a$ = absolute humidity of air, kg $m^{-3}$

$R_c$ = aerodynamic coefficient between surface and reference elevation

According to Hillel, the absolute humidity of air at the surface is obtained from the expression:

$$H_s = H_o \exp [\psi_s/46.97(T_s + 273.16)] \quad [71]$$

where $H_o$ = saturation absolute humidity at the surface temperature $T_s$,

and $\psi_s$ = soil matric potential at the surface, m $H_2O$. Also:

$$H_o = \frac{1.323 \exp (17.27T_s/(237.3 + T_s))}{273.16 + T_s} \quad [72]$$

The air humidity $H_a$ can be obtained from the relative humidity h and the air temperature $T_a$, or from a direct measurement of the vapor pressure. If we define the relative humidity $h = p_v/p_s$, where $p_v$ = vapor pressure and $p_s$ = saturated vapor pressure, both in mbar and at temperature $T_a$, then:

$$p_v = hp_s \quad [73]$$

Using regression analysis, the author formulated an expression for $p_s$ from a table of values in Mark's Mechanical Engineer's Handbook.

$$p_s = 2.039 (1.0365)^{(1.8T_a + 32)} \text{ mbar} \quad [74]$$

The value of $p_v$ can then be calculated and substituted into the following expression for absolute humidity

$$H_a = \frac{0.2175 p_v}{(T_a + 273.16)} \qquad [75]$$

The aerodynamic resistance $R_c$ is obtained from:

$$R_c = R_a(St) \qquad [76]$$

where $R_a$ = adiabatic or neutral value of $R_c$, sec $m^{-1}$

St = stability correction

The neutral value is given by:

$$R_a = \frac{\left[\ln_e(2.0/z_o)\right]^2}{0.16 S_a} \qquad [77]$$

where $z_o$ = surface roughness, m

$S_a$ = wind speed measured at 2m, m $sec^{-1}$

Both $z_o$ and $S_a$ are inputs to the model. Hillel (1977) chose a $z_o$ value of .01 m for his model of natural soil. VanWijk (1963) presented a table of values for a number of different surface conditions, both bare and grassed, and Allmaras, et al. (1977) gave values before and after several tillage treatments, as did Cruse, et al. (1980). Table 5.1 presents several recent $z_o$ studies.

Table 5.1 Surface roughness $z_o$, cm.

| Soil | Condition | $z_o$ | Researchers |
|---|---|---|---|
| Nicollet clay loam | Undisturbed | .47 - .68 | Allmaras, et al. (1977) |
| | Plowed | 2.92 - 3.47 | |
| | Plow - disk - harrow | 1.56 - 2.01 | |
| Input to model | Bare, undisturbed | 0 | Cruse, et al. (1980) |
| | Plowed | 2.44 | |

The stability correction St is obtained from:

$$St = \frac{1}{(1 - 10.Ri)} \qquad [78]$$

where Ri = Richardson Number. This dimensionless number is obtained from:

$$Ri = \frac{9.81(2.0-z_o)(T_a-T_s)}{(T_a + 273.16)S_a^2} \qquad [79]$$

where $T_a$ = air temperature, °C, an input.

It should be noted in equation [78] that if Ri $\geq$ + 0.1, an absurd answer would result. This condition would be indicative of an extreme inversion at very low wind speed.

To prevent this, the value of Ri was limited in Hillel's program to +0.08.

## 5.2 Heat Flux at the Surface

The soil model includes an expression for surface heat flux, $\lambda \partial T/\partial n$. Heat flows mostly by conduction in the soil, and by convection and radiation through the air above the surface. This expression in the model represents sensible heat loss (or gain) by the soil through the surface, and can be calculated from a surface energy balance analysis. This is stipulated in VanBavel and Hillel (1976) by:

$$Q_{RN} = LE_m + Q_A + Q_s \qquad [80]$$

where $Q_{RN}$ = net irradiance, L = latent heat of vaporization, $Q_A$ = sensible heat flux to the air, and $Q_s$ = sensible heat flux into the soil.

Equation [80] represents the total heat flow to and from the surface, and can be used to calculate $Q_s$ at each time increment of the model. The value $Q_s$ will then be the surface heat flux appearing as $(\lambda \partial T/\partial n)$ in the model, a positive value when heat flux is from the surface into the soil.

The net irradiance can be obtained from VanBavel and Hillel (1976) and Hillel (1977):

$$Q_{RN} = (1 - al)Q_{RG} + Q_{RL} - \varepsilon\sigma(T_s + 273.16)^4 \qquad [81]$$

where $Q_{RG}$ = total global short-wave irradiance from the sun and atmosphere, W $m^{-2}$. This can be obtained from meteorological measurements. Further, $Q_{RL}$ = incoming long-wave

radiation from the sky, $W\ m^{-2}$, al = albedo or reflectivity coefficient of the surface, $\varepsilon$ = emissivity of soil surface, and $\sigma$ = Stefan-Boltzmann constant, $5.67 \times 10^{-8}\ W\ m^{-2} {}^{\circ}K^{-4}$.

The albedo of the surface varies with the surface cover, its color, roughness and moisture content, as shown in Table 5.2. Van Bavel and Hillel proposed the following expression for al based on $\theta_s$ of the surface layer:

$$\begin{aligned} al &= 0.10 \quad \text{for } \theta_s > 0.25 \\ &= 0.25 \quad \text{for } \theta_s < 0.10 \\ &= 0.10 + (0.25 - \theta_s) \quad \text{for } 0.10 \leq \theta_s \leq 0.25 \end{aligned} \qquad [82]$$

Table 5.2. Soil surface albedo

| Condition | Albedo | Reference |
|---|---|---|
| Dark clay, wet | .02-.08 | VanWijk (1963) |
| Dark clay, dry | .16 | " |
| Sand, wet | .09 | " |
| Sand, dry | .18 | " |
| Bare fields | .12-.25 | " |
| Wet plowed fields | .05-.14 | " |
| Heavy clay, 4 natural tillage conditions during wheat germination, Manitoba | .06-.09 | Townsend and Migchels (1981) |

Based on the Van Wijk values in Table 5.2, expressions [82] will adequately represent al for $\theta$'s considered in the model.

VanWijk further proposed that the earth can be assumed to be close to a black body in regards to its emission characteristics of long wave radiation. VanBavel and Hillel proposed the following:

$$\varepsilon = 0.90 + 0.18\theta_s \qquad [83]$$

where $\theta_s$ = moisture content of surface layer

The long-wave radiation from the sky, as developed by VanBavel and Hillel from a literature search, is:

$$Q_{RL} = \sigma(T_a + 273.16)^4(0.605 + 0.048\sqrt{1370 \cdot H_a}) \qquad [84]$$

The sensible heat flux to the air is:

$$Q_A = \frac{(T_s - T_a)C_a}{R_c}$$

where $C_a$ = volumetric heat capacity of air. If we substitute $C_a = 1.257 \times 10^3$ J $m^{-3} {}^{\circ}C^{-1}$, then:

$$Q_A = 1257\ (T_s - T_a)/R_c \qquad [85]$$

## 5.3 Summary

Equations [70] through [85] represent the general relations of a soil-atmosphere model. These equations have been delineated to require the following specific inputs:

- $h$ air relative humidity
- $T_a$ air temperature
- $S_a$ air wind speed
- $Q_{RG}$ total global short wave irradiance
- $z_o$ surface roughness

Albedo was incorporated into the model as a function of the moisture content of the soil surface.

Chapter 6 explains the computer model and the incorporation of equations [42] through [85] into the model.

# 6. COMPUTER IMPLEMENTATION

## 6.1 Finite Element Grid of Soil Furrow Profile.

The furrow profile modeled was assumed to characterize a field of soybeans planted in rows of 70 cm (28 inches) spacing and at a depth of 5 cm (2 inches). The study of moisture and heat flow had to be extended below the seed depth to a depth where changes are no longer significant due to diurnal surface fluctuations throughout the germination/ emergence period. Based on the investigations tabularized below and on the model verification study, this depth of influence was set at 30 cm. This provided a compromise between increasing programming complexity for larger grids and decreasing accuracy with a grid too shallow.

Table 6.1. Depth of influence

| Investigator | Comment on depth of influence |
|---|---|
| Hadas (1968) | 6 to 7 cm. from source of change. Considered a 20 cm soil column semi-infinite. |
| Rose (1968a) | 10 cm for $\theta$ variations, but greater than 15 cm for T variations. States that daily T fluctuations go to 30 cm in a bare soil. |
| Hadas (1969a) | 6 cm from heat source in lab study. |
| Kimball, et al. (1976) | at 5 cm, diurnal amplitude of T and $\theta$ = 73% of surface. At 20 cm, it was 20%. |
| Bruce, et al. (1977) | 13 cm for $\theta$ in tilled soil. 12 cm for T in tilled soil. Some water coming from below 15 cm to supply evaporation. Appreciable change in T and $\theta$ at 14 cm within 2 days. |
| Hadas (1977a) | 20 cm for $\theta$, greater than 18 cm for T. |
| Merva (1975) | from 5 to 17 cm for daily T fluctuations. |

The finite element domain and grid are shown in Figures 6.1 through 6.3. The validation and simulation grids were similar. The simulation grid was designed for more detail and accuracy in the vicinity of the seed near the upper right hand corner, whereas the validation grid was used exclusively for one-dimensional flow.

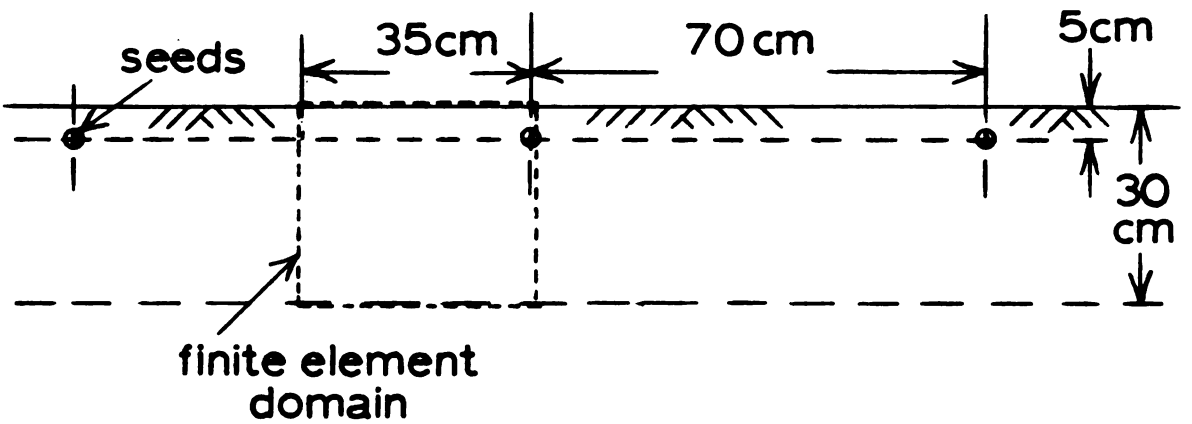


Figure 6.1. Finite Element Domain of Soil Profile

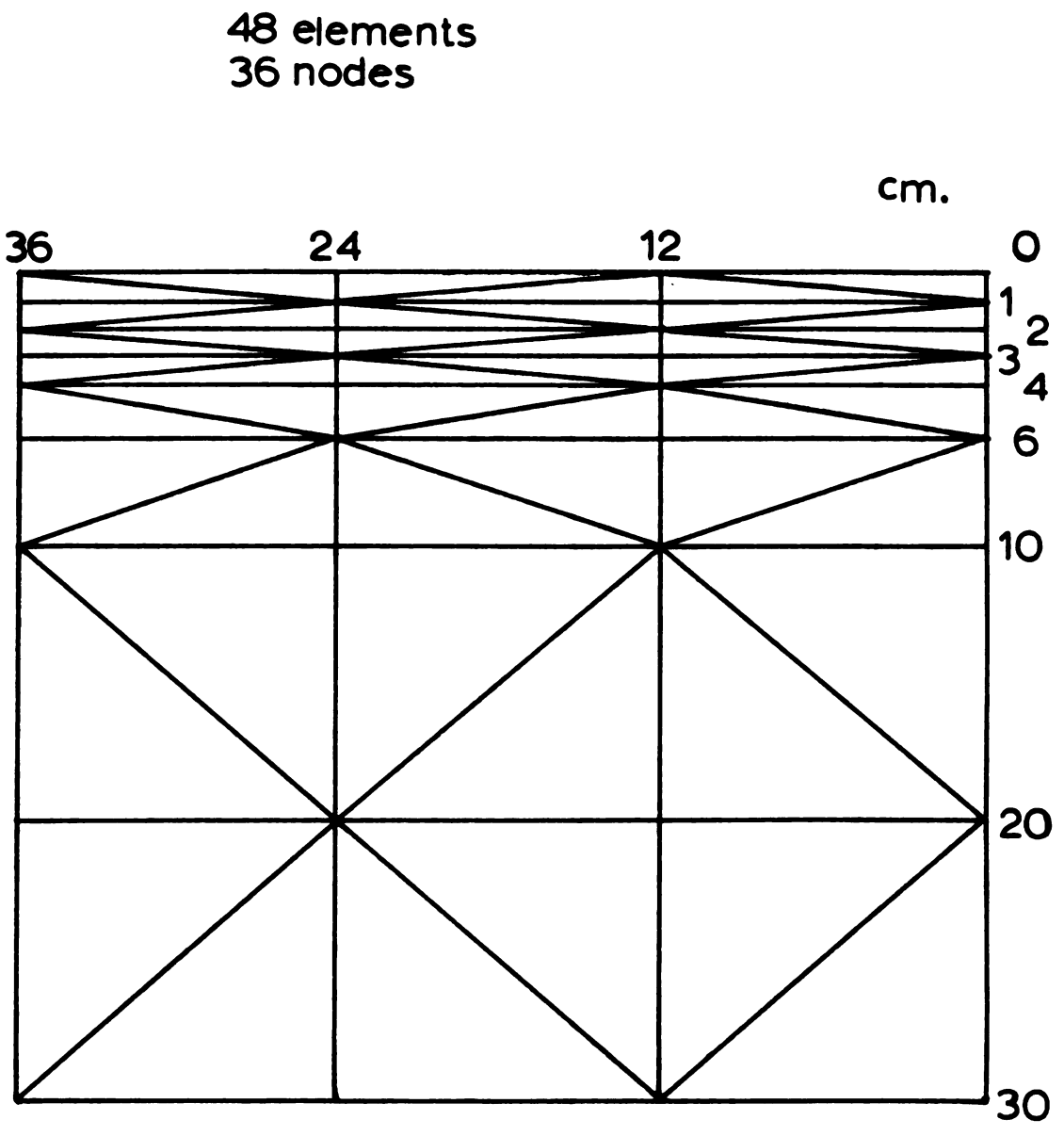


Figure 6.2. Finite Element Grid for Validation

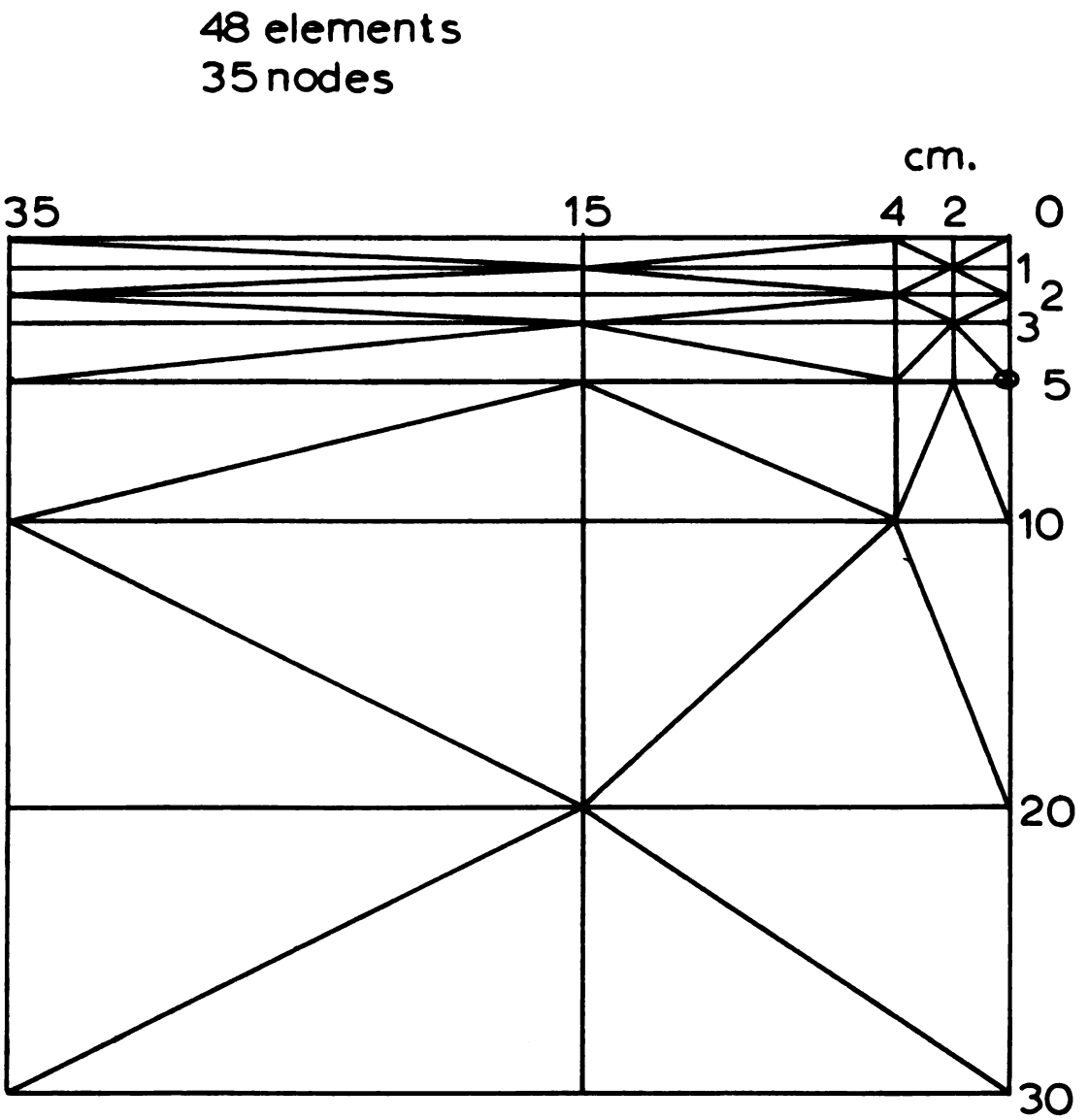


Figure 6.3. Finite Element Grid for Simulation

## 6.2 Boundary and Initial Conditions

Boundary and initial conditions for the finite element domain are listed in Table 6.2

Table 6.2. Boundary and initial conditions for the model.

| Location | Condition | Application |
|---|---|---|
| Each tilled node in grid | $\theta = \theta_i$, $T = T_i$ | for t = 0 |
| Each untilled node in grid | assumed gradient* | for t = 0 |
| Both side and bottom boundaries | $\partial\theta/\partial n = 0$<br>$\partial T/\partial n = 0$ | for all t |
| Top boundary | time-varying heat flux and evaporation (Chap. 5) | for all t |

*Gradient based on Bruce, et al. (1977) and trial solutions of the computer model.

There will normally be a gradient of both $\theta$ and T throughout the soil profile prior to planting. The model assumes that the planting/tillage operation thoroughly mixes the soil so that the tilled soil profile immediately after the planter has passed has a uniform $\theta$ and T. Untilled soil in a no-till pass retains its original gradient. The values $\theta_i$ and $T_i$ for all tilled nodes in the grid, including surface nodes, assume a value equal to the average between that at the surface and bottom boundaries of the grid prior to planting. This provides a surface temperature as an initial

condition used in the heat balance analysis of the surface-atmosphere interface.

## 6.3 Specific Inputs to the Model.

The summary sections 4.7 and 5.3 list the specific inputs to the computer model. The time-varying parameters h, $T_a$, $S_a$ and $Q_{RG}$ are modeled as sinusoidal expressions to represent a diurnal cycle. Refer to Appendix D for these expressions. Although the computer model makes rather complex and intricate calculations at each step, the inputs as listed above are generally easily measured in the field or lab, and are supported by an abundance of published data.

## 6.4 Computer Flow Diagram.

The computer flow diagram used to develop the program is listed in Appendix A. Briefly, the program follows this sequence:

a. Reads in constant soil properties and administrative limits.

b. Establishes nodes and elements in the grid.

c. For first time step, and using initial conditions at each node and time-varying conditions at the surface, calculates temperatures at each node in the grid, solving total matrix.

d. For first time step, using initial conditions, surface conditions, and temperatures calculated in c., calculates moistures at each node in the grid, solving total matrix.

e. Repeats c. and d. for each successive time step, using calculated T's and θ's of previous step as initial conditions of succeeding step, and using surface conditions programmed for that particular step.

## 6.5 Computer Program Listing

The computer program and its documentation are listed in Appendix B. It was written in the FORTRAN IV language for the IBM 360/40 system at Delta College. Although this system was readily accessible by the author, it did pose limitations. Memory capability did not allow a grid finer than about 40 nodes, and length of runs, because of other demands of computer usage, were limited mostly to 3-day simulations.

Six subroutines are used to calculate soil parameters or surface conditions. These are:

| | | |
|---|---|---|
| DIFFM | produces | $K$, $D_\theta$ and $\psi$ |
| DIFFT | " | $D_T$ |
| EVAP | " | $E$, $Q_s$ |
| VEL | " | $\partial V/\partial z$ |
| THCON | " | $\lambda$ |
| CAP | " | $C$, $\theta_v$ |

Two other subroutines, DCMPBD and SLVBD, earlier developed by Segerlind (1976), were used to decompose and solve the simultaneous equations in the global matrix.

A special feature of the program is the incorporation of a hysteresis effect. An adsorption moisture curve is entered as an adsorption $\psi_e$ in a DATA statement. Then in DIFFM a decision is made on which $\psi_e$ to use, depending on whether that element is losing or gaining moisture.

## 6.6 Summary.

This chapter explained the development of the computer program to solve soil water and temperature interactions. Special programs, separate from the main program, were developed to study the sensitivity of key parameters. Results of these studies are given in Chapter 7.

# 7. PARAMETER SENSITIVITY ANALYSIS

The soil parameters and surface conditions were analyzed individually using their respective subroutines. Computer values were compared with published experimental values.

## 7.1 Soil Moisture Diffusivity $D_\theta$, Matric Potential $\psi$, and Hydraulic Conductivity K.

Figures 7.1 through 7.3 compare the output from DIFFM with the experimental values of Adelanto loam from Jackson (1973). This soil did not exhibit a sharp break in the moisture curve, thus the air-entry matric potential $\psi_e$ had to be estimated. This estimate was made over a relatively wide range between -.05 to -.40 m $H_2O$.

Several computer runs were made at different $\psi_e$ values. Three examples are plotted. The plots clearly show how sensitive $D_\theta$, $\psi$ and K are to the $\psi_e$ value, and further indicate an optimum $\psi_e$ exists for the adequate modeling of all three parameters. That optimum for Adelanto loam appeared to be around $\psi_e$ = -.1017 m $H_2O$. Higher magnitudes would improve the $\psi$-$\theta$ model but reduce the $D_\theta$ model accuracy, and vice versa.

The relationships depicted in Figures 7.1 through 7.3 are consistent with the state of the art of soil modeling as reported by Mualem (1978). He proposed the K-$\theta$ relationship which improved predictions over two earlier models by several orders of magnitude. Yet it deviated from experimental curves of some soils by as much as two orders of

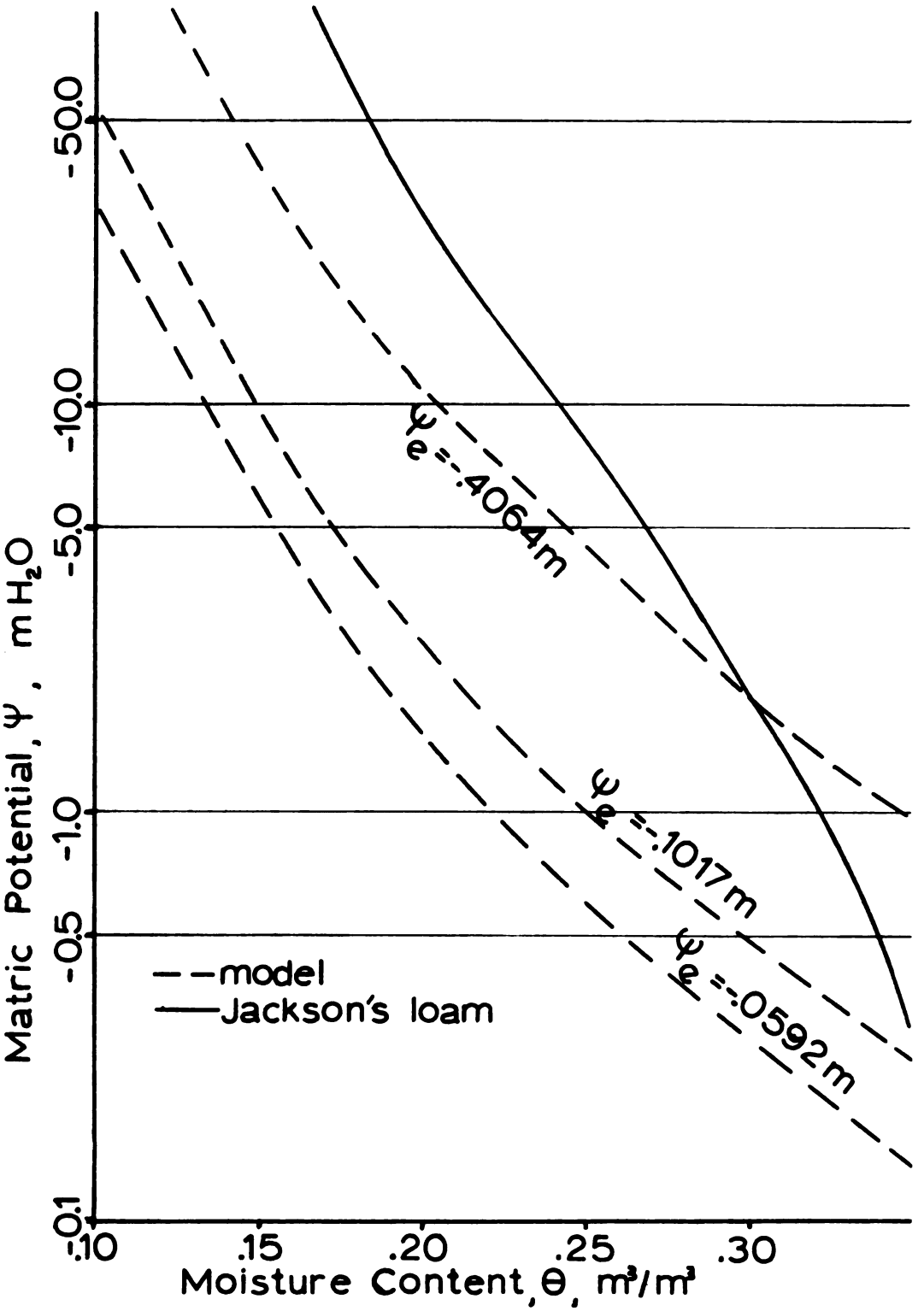


Figure 7.1. Moisture Characteristics Curve for Adelanto Loam

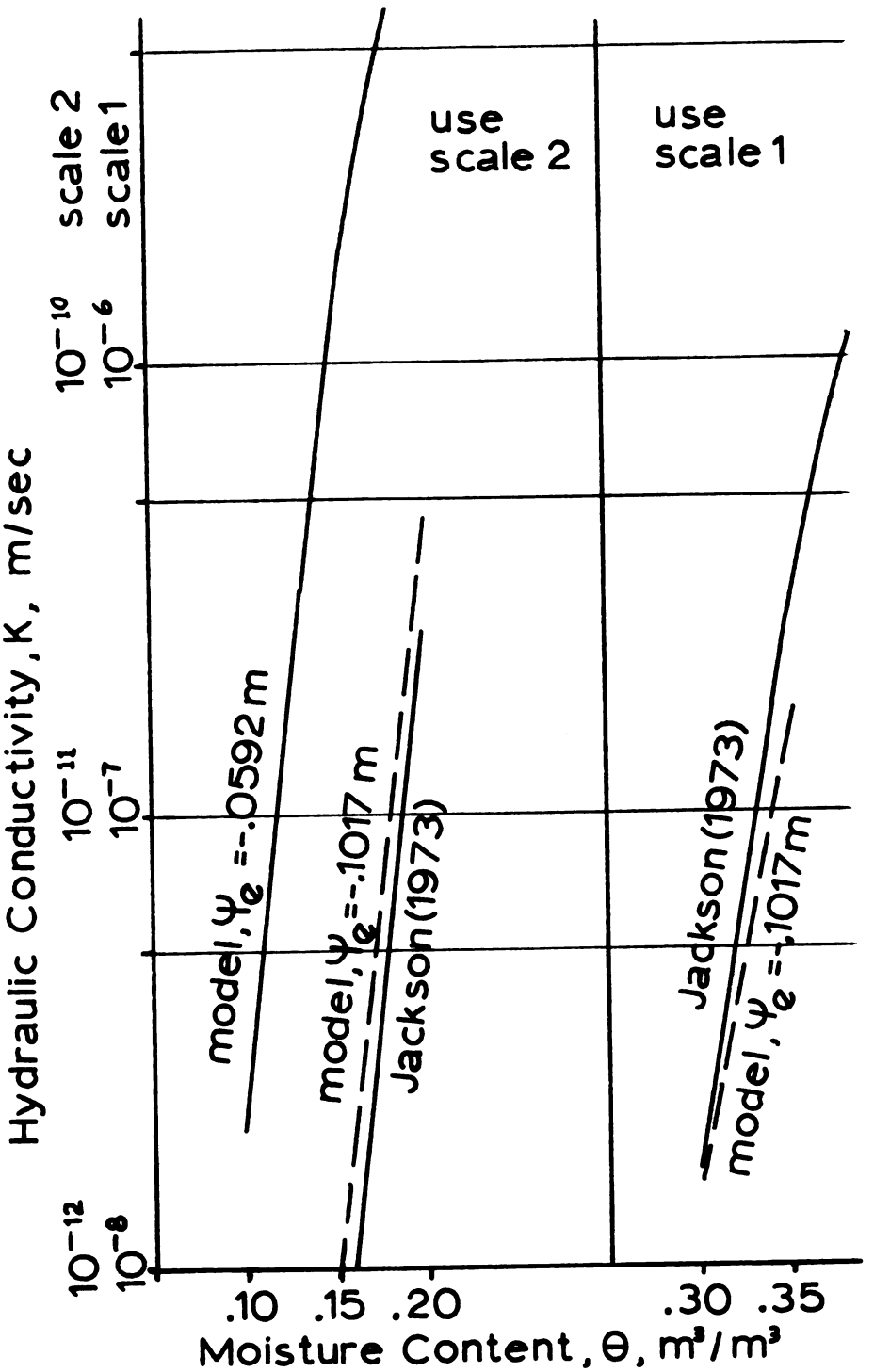


Figure 7.2. Hydraulic Conductivity for Adelanto Loam

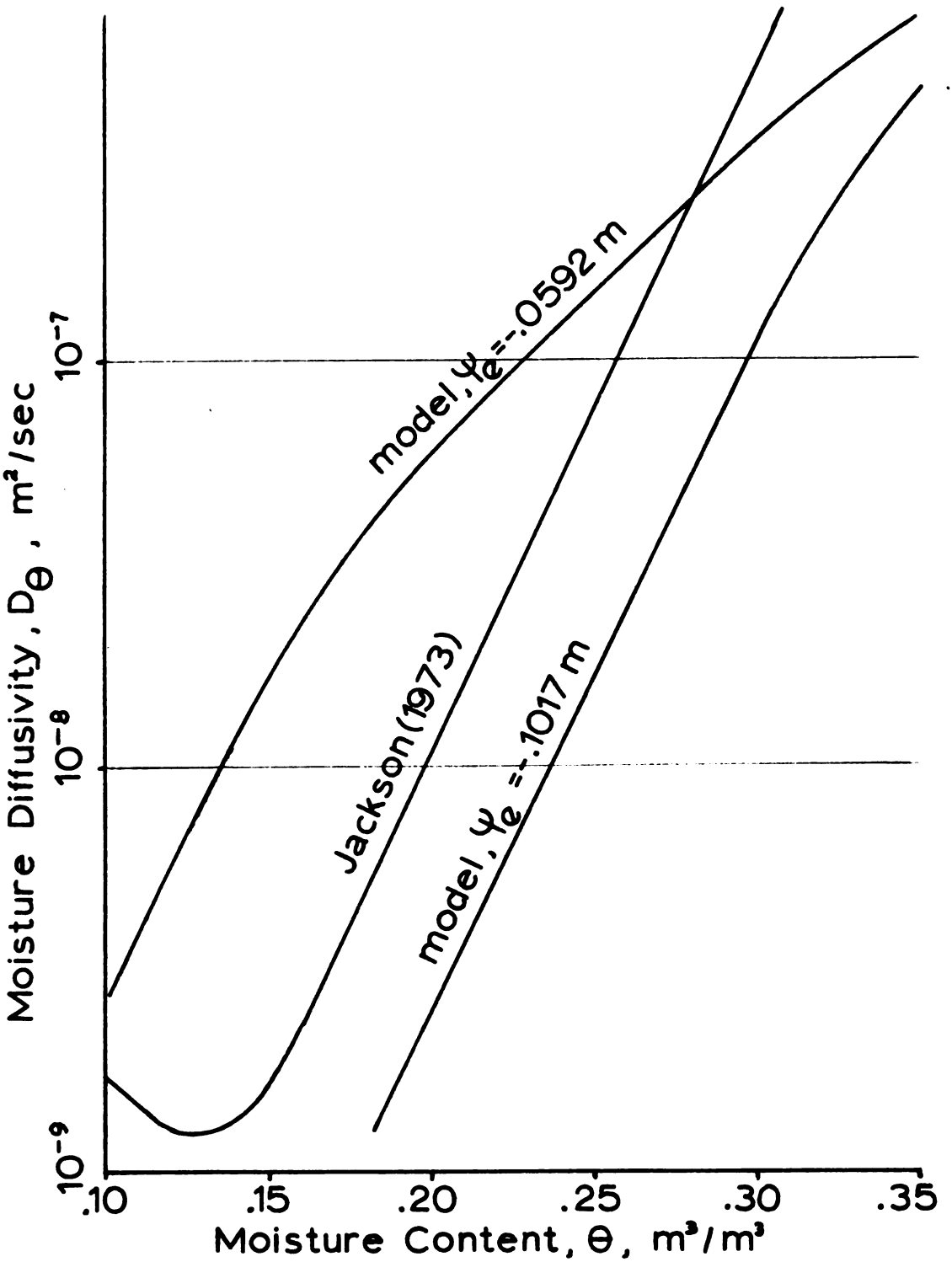


Figure 7.3. Moisture Diffusivity Dθ for Adelanto Loam

magnitude. The relation in expression [44] itself is not universal and is an inadequate model for some soils, according to Ghosh (1980).

It must be further emphasized that $D_\theta$ is very sensitive to several properties which are either difficult to measure accurately or vary considerably with even minute changes in moisture content.

The hydraulic conductivity changes by perhaps six to eight orders of magnitude from saturation to wilting point. It is very sensitive to the exponent in expression [47]. This exponent, in turn, is primarily dependent on w, the energy required to completely drain the soil. This "dried" condition and the corresponding $\theta_H$ itself is nebulous. Mualem calls this point the immobile or residual moisture content. A check with Jackson's Adelanto loam indicates this points falls midway between the wilting point and the point where the soil specific surface is covered by a one-molecule layer of water. The values for $\psi$ change by two orders of magnitude within this range.

Since K is strongly dependent on the $\psi$-$\theta$ curve, and $d\psi/d\theta$ is directly related, $D_\theta$ is very sensitive to the assumed relation between $\psi$ and $\theta$. This relation depends on $\beta$ and $\psi_e$. The variable $\beta$ is a function only of soil texture, which can be measured accurately in the lab.

Soil moisture properties are also very sensitive to the bulk density. For example, according to the model for

Adelanto loam at 15% moisture, increasing the bulk density from 1100 to 1600 kg/m$^3$ increased the $\left(\frac{\theta}{s}\right)^n$ expression in equation [47] by 5 orders of magnitude.

Table 7.1 displays the sensitivity of the soil moisture properties using soil #4005 of Mualem (1978) which is apparently the soil used by Bruce, et al. (1977). Calculations are based on the expressions used in the computer model.

Table 7.1. Soil moisture properties.

| $\psi_e$ (m) | $\theta_H$ | Bulk Density (kg/m$^3$) | Exponent n (Mualem) | K(m/sec) @ $\theta$ =.02 | $D_\theta$ ($m^2 sec^{-1}$) |
|---|---|---|---|---|---|
| -.1017 | .025 | 1200 | 8.1 | 4.6E-17 | 1.9E-12 |
| " | .020 | " | 10.0 | 8.6E-20 | |
| -.2000 | .025 | " | 13.1 | 3.0E-24 | |
| " | .040 | " | 8.0 | 6.4E-17 | 5.3E-12 |
| " | " | 1100 | 8.9 | 1.8E-18 | 1.8E-13 |

At low moisture contents, Table 7.1 demonstrates the keen sensitivity of K and $D_\theta$ with $\psi_e$ and $\theta_H$, both of which are subjective observations obtained from the $\psi$-$\theta$ curve.

## 7.2. Soil Moisture Diffusivity $D_T$.

Table 7.2 shows the individual diffusivity components for two different soils found in the literature. The numbers are rounded off for convenient gross comparisons. Both

soils demonstrate that $D_{Tv}$ is significant compared to $D_{Tl}$ only at low moistures, generally at or below the wilting point for those soils (14% for Jackson's loam). Otherwise, throughout the useful range of moisture content, its contribution is negligible.

The computer model for $D_T$ for Adelanto loam remained relatively constant throughout the moisture range studied. Also, comparing $D_T$ values in Table 7.2 with $D_\theta$ values in Figure 7.3 for the same soil modeled on the computer, the model demonstrates that $D_\theta$ is three to four orders of magnitude smaller than $D_\theta$. This conforms with published statements that the moisture diffusivity contribution due to a temperature gradient will be small in soils with adequate moisture and moderate temperatures.

Table 7.2. Moisture diffusivities, $m^2\ sec^{-1}/(°C \text{ or } \theta)$

| | DeVries "Medium sand" @ 20°C | | | Jackson loam @ 25°C | | | | |
|---|---|---|---|---|---|---|---|---|
| $\theta$ | $D_{\theta l}$ | $D_{Tl}$ | $D_{Tv}$ | $D_{\theta l}$ | $D_{\theta v}$ | $D_{Tl}$ | $D_{Tv}$ | $D_T$ |
| .05 | 1E-5 | 3E-10 | 2E-11 | 6E-10 | 2E-9 | | 7E-11 | 7E-11 |
| .10 | " | 8E-9 | " | 1E-9 | 5E-10 | | 8E-11 | 8E-11 |
| .15 | 2E-5 | 2E-8 | " | 2E-8 | 1E-10 | 2E-12 | 5E-11 | 5E-11 |
| .20 | 3E-5 | 6E-8 | 1E-11 | 2E-7 | | 2E-10 | 1E-11 | 2E-10 |
| .25 | | | | 1E-6 | | 1E-10 | 3E-12 | 1E-10 |
| .30 | 6E-5 | 2E-7 | 1E-11 | | | | | |
| .35 | 16E-5 | " | " | | | | | |

## 7.3. Soil Thermal Conductivity $\lambda$.

Figures 7.4 and 7.5 display $\lambda$ vs. $\theta$ at two different temperatures. DeVries (1963) plotted experimental and calculated values for a quartz sand, and these are replotted. With some refinements of his expressions (equations [73] to [75]), the model based on water medium came close to his calculated at 40°C, and in fact improved on his at 20°C.

DeVries gave a convincing argument that at very low moisture contents saturated air rather than water becomes the continuous medium for thermal conductivity. At extremely low moisture dry air can be considered the medium. Which medium is considered makes a significant difference in $\lambda$. Further, at what moisture content this should occur is not clear and is somewhat arbitrary.

The plots show model studies with saturated air as the medium at $\theta < \theta_{1k}$. These values, based on expressions [51] and [55], were considerably lower. DeVries also experienced difficulty with modeling dry soils, and resorted to a multiplier of 1.25 to bring theory in line with experimental values. However, when basing the calculations on water medium throughout the useful moisture range, the author produced a better model, which was then adopted for the final computer simulations.

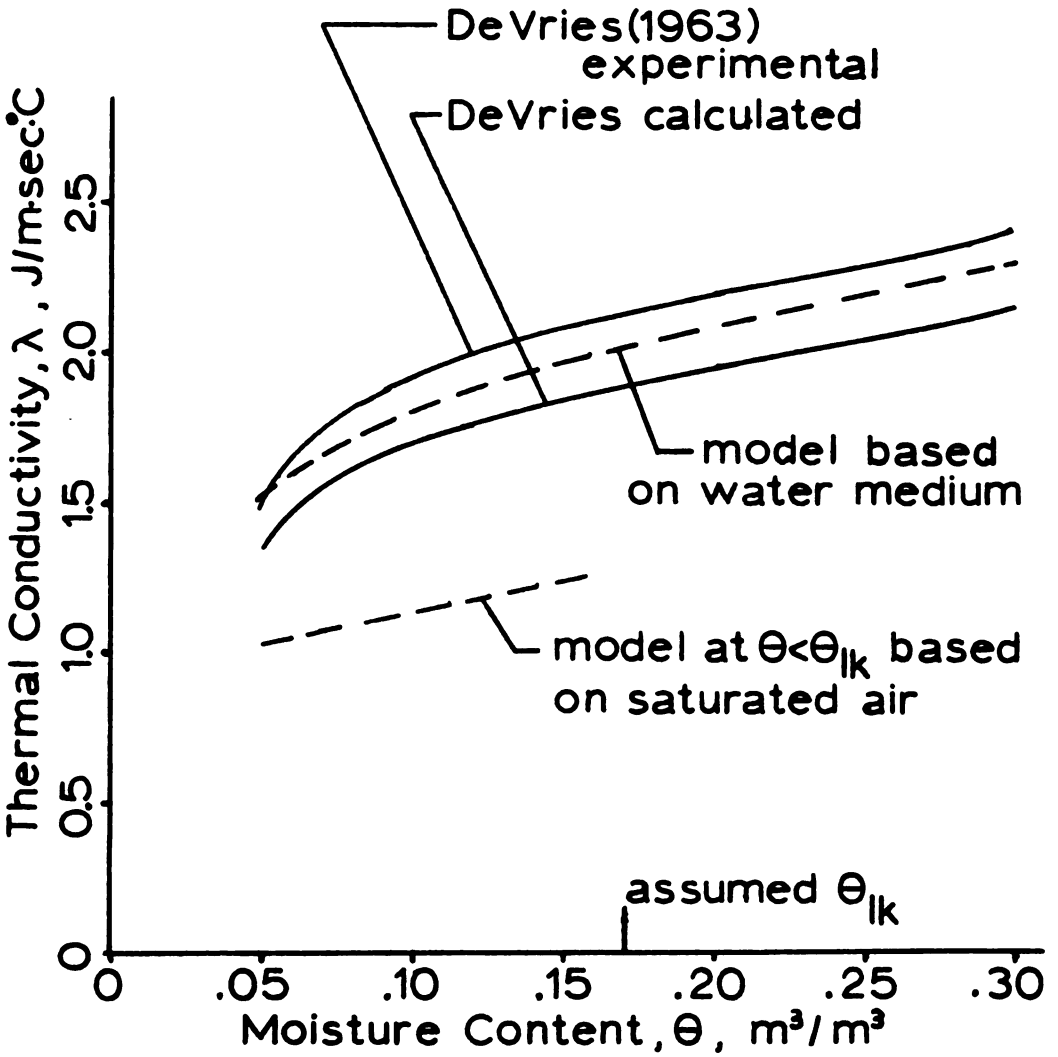


Figure 7.4. Thermal Conductivity of Quartz Sand @ 20°C

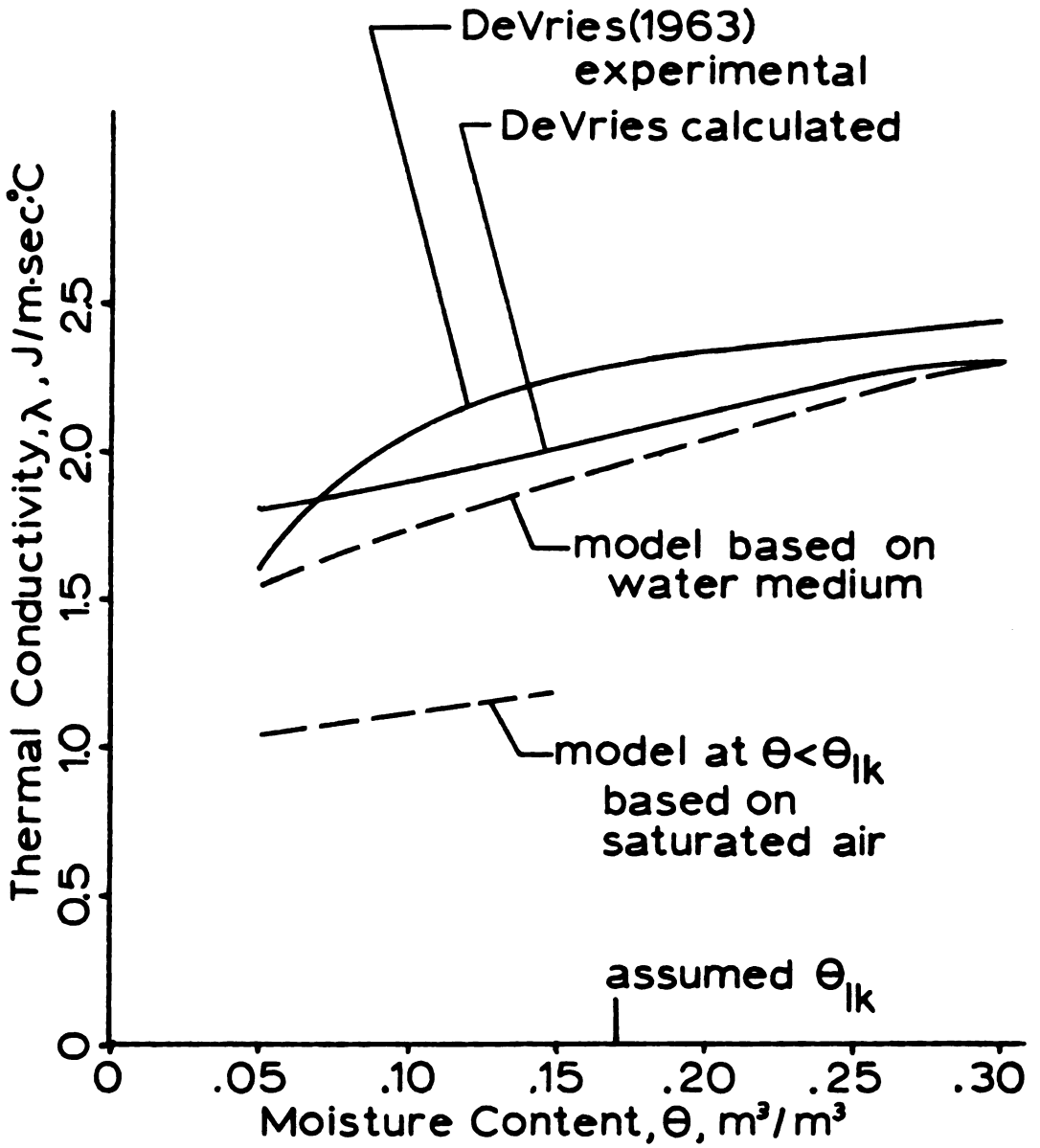


Figure 7.5. Thermal Conductivity of Quartz Sand @ 40°C

## 7.4. Soil Heat Capacity C.

Modeling DeVries' "medium sand" produced C values from 1.36E6 to 2.83E6 $J/m^3°C$. for $\theta$ between .05 and .40. This compares favorably with the following DeVries values:

| | | |
|---|---|---|
| Graded Ottawa sand | 1.82E6 | $J/m^3°C$ |
| Crushed quartz | 2.11E6 | $J/m^3°C$ |
| Northway fine sand | 2.28E6 | $J/m^3°C$ |
| Quartz and clay minerals | 2.01E6 | $J/m^3°C$ |

## 7.5. Velocity Gradients $\partial V_p/\partial z$ and $\partial V_d/\partial z$ of Soil Air.

Velocity gradients due to pressure gradients were modeled for a fictitious soil approximating the air porosity used by Farrell (1966). Comparisons are made in Table 7.3, showing very close agreement.

Velocity gradients due to positive density gradients were modeled and proved to be consistently larger than those due to pressure gradients by several orders of magnitude. Table 7.3 compares the two at several depths, maintaining a constant porosity, and using the temperature gradient reported by Bruce et al. (1977).

Pressure gradients prevail during the day when density gradients in the soil are negative, but density gradients prevail at night when the wind has quieted down. Nevertheless, moisture vapor movement due to pressure gradients is expected to be small compared to that due to positive density gradients.

Table 7.3. Velocity gradients, m/sec·m

| $\partial V_p/\partial z$ comparisons at z=5 cm. | | | |
|---|---|---|---|
| Amp. | Freq. | $\partial V_p/\partial z$ model | $\partial V_p/\partial z$ Farrell |
| 1.0E-3 | .628 | 5.98E-5 | 5.94E-5 |
| 2.5E-4 | 2.513 | 5.89E-5 | 5.80E-5 |
| 1.0E-4 | 6.283 | 5.79E-5 | 5.65E-5 |

| Depth comparisons | | | |
|---|---|---|---|
| z(cm) | $\Delta T$ | $\partial V_d/\partial z$ | $\partial V_p/\partial z$ |
| 0 - 1 | 2 | 3.85 | 6.05E-5 |
| 1 - 2 | 0 | 0 | 6.04E-5 |
| 2 - 3 | .5 | 1.93 | 6.02E-5 |
| 3 - 4 | .5 | 1.93 | 6.01E-5 |
| 4 - 6 | 1 | 1.93 | 5.98E-5 |

## 7.6. Evaporation and Soil Heat Gain at the Surface.

Computer simulations were made using the published atmospheric and soil data of VanBavel and Hillel (1976) for a loam soil in Binghamton, NY. Total global irradiance, air temperature and relative humidity were entered as sinusoidal functions of time throughout the day* using, in some cases, only daily or even monthly averages found in the publication for experimental verification. Figure 7.6 shows the evaporation model peaked at the same level as the simulation published by VanBavel and Hillel, but was delayed by about 2

*Refer to Appendix D

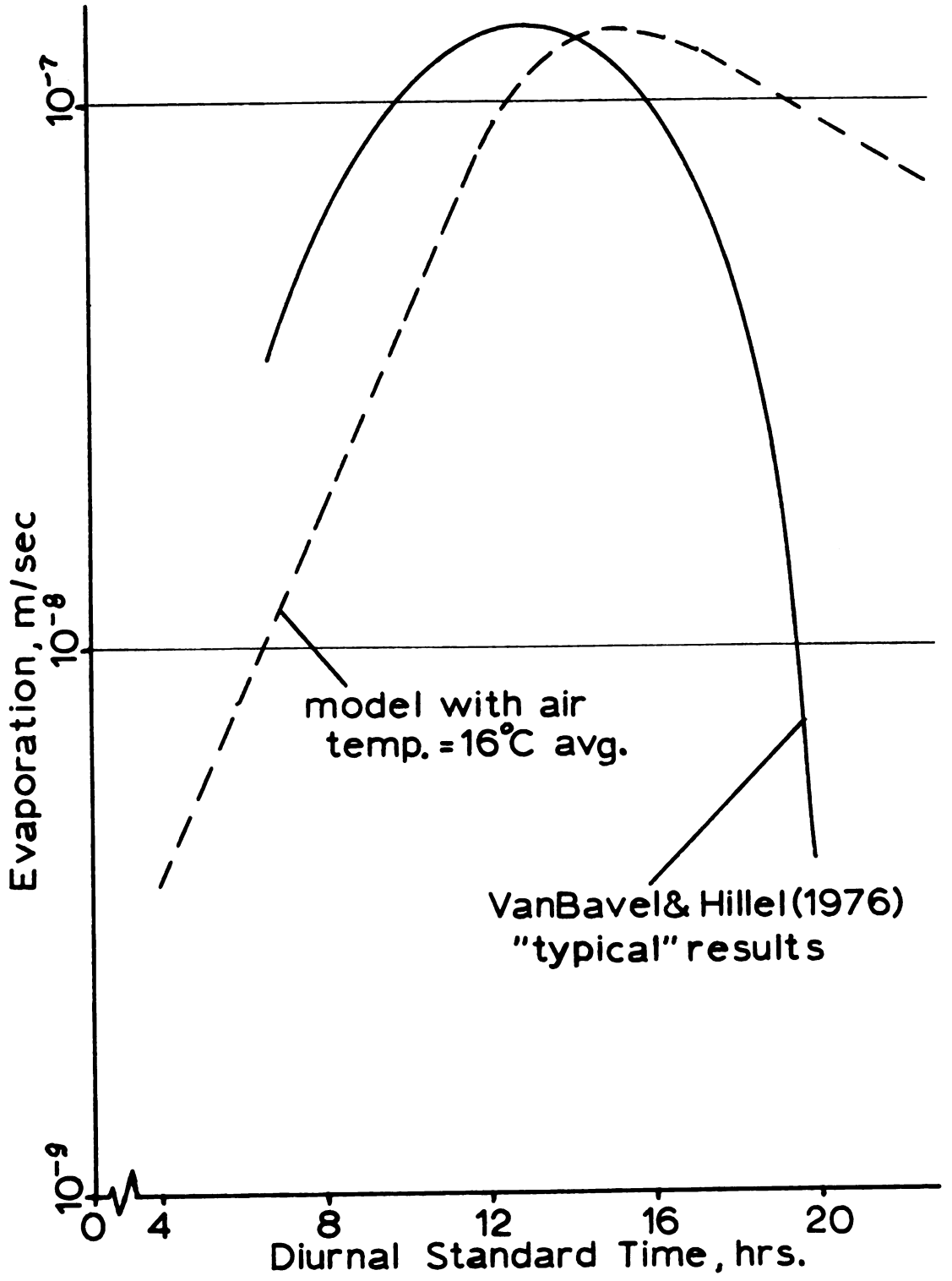


Figure 7.6. Daily Evaporation for a Loam in Binghamton, NY in June

hours. In the afternoon, evaporation in the model declined more slowly. This cannot be discounted as error in the model, however, since a direct cause-effect comparison was impossible.

It must also be emphasized that certain soil parameters were held artificially constant during this initial verification check. These were the soil surface moisture and matric potential, and the wind speed. The combination of air and soil surface temperatures used provided no inversion. Had the air temperature been allowed to exceed the surface temperature, an inversion would have resulted, making Ri positive. If the wind speed would be decreased, as at night, Ri would increase more positively, increasing St and consequently $R_c$, and finally reducing E throughout the nighttime.

A check of surface roughness and wind speed effects on the aerodynamic resistance $R_c$, using $T_s-T_a$ = 4°C, a moderate differential, produced the values in Table 7.4. For this combination, wind speed had negligible effect.

Table 7.4 Aerodynamic resistance for $\Delta T$ = 4°C.

| $z_o$ (m) | $S_a$ (m·sec$^{-1}$) | Ri | $R_c$ (sec·m$^{-1}$) |
|---|---|---|---|
| .010 | 1.22 | -.173 | 52.7 |
| .025 | " | -.172 | 36.2 |
| .035 | " | -.171 | 30.9 |
| .025 | 2.00 | -.064 | 36.6 |

# 8. MODEL VALIDATION

The computer model was validated using the field data published by Bruce, et al. (1977). Additional information on the soil used by Bruce was obtained from Harper, et al. (1976).

## 8.1 The Bruce Study

The Bruce study involved one of the most detailed and complete works found in the literature on actual soil moisture and temperature measurements. The study spanned eight days, from June 16 to June 23, measuring moisture hourly at ten depth intervals to a maximum of 15 cm., and temperature every 15 minutes at eight depth intervals, also to a maximum of 15 centimeters.

Soil conditions published were:

1. texture and particle size distribution measured to 15 cm.
2. bulk density vs. depth to 15 cm.
3. moisture characteristic curve
4. saturated hydraulic conductivity

This provided all the soil inputs required by the model except the adsorption curve for hysteresis. For the validation, hysteresis was assumed negligible. The author felt this to be the better option rather than assuming some unsubstantiated relation.

Above-surface conditions published in the Bruce study were:

1. air vapor pressure
2. air temperature
3. incoming solar radiation
4. wind speed

Relative humidity for the model had to be calculated from the vapor pressure using Equation [73], and surface roughness had to be estimated. This fulfilled the surface condition inputs to the model.

A particular day in the Bruce study, June 18, was selected for validation. This day followed several uneventful days of drying and preceeded a heavy rain by one day. A copy of the raw data for that day was obtained from Bruce for better accuracy.

## 8.2 Model Refinements

The modeled 24-hour histories of temperature and moisture for June 18 are shown in Figures 8.1 and 8.2. The model accepted the initial conditions shown on the 0000 hr (midnight) curve, used the finite element grid shown in Figure 6.2, was exposed to the sinusoidal surface conditions and stepped through the day in 30-minute increments.

Validation of the model with the Bruce data required some refinements of the model. These refinements concentrated mainly on five areas, although all elements were eventually scrutinized before being accepted for the model. These five area were:

1. oscillations of the finite element formulation
2. the air mass flow in the soil
3. the surface conditions submodel
4. filling in where the Bruce data was spotty
5. moisture diffusivity due to vapor

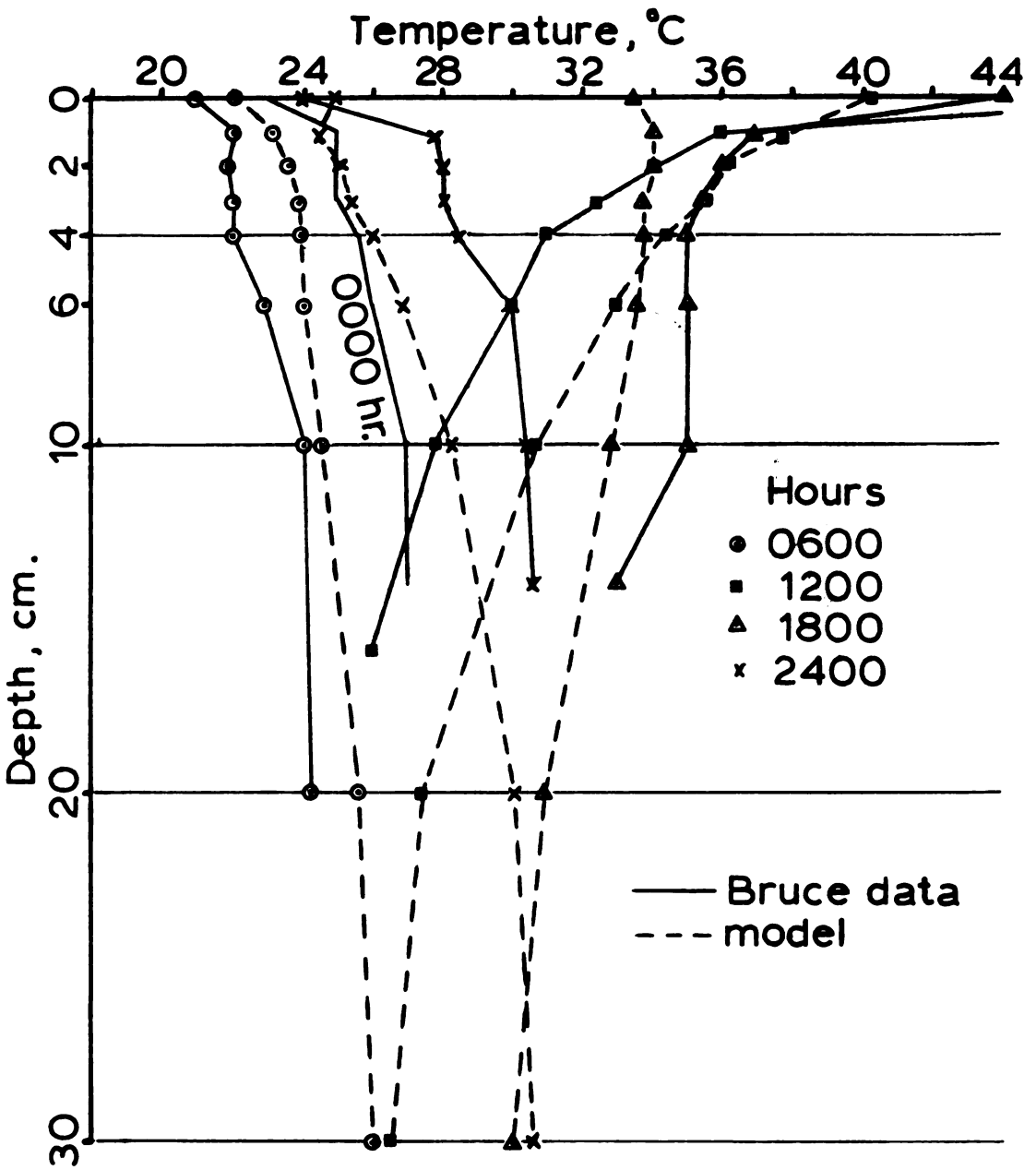


Figure 8.1. June 18 Temperatures Comparing Model with Bruce Data

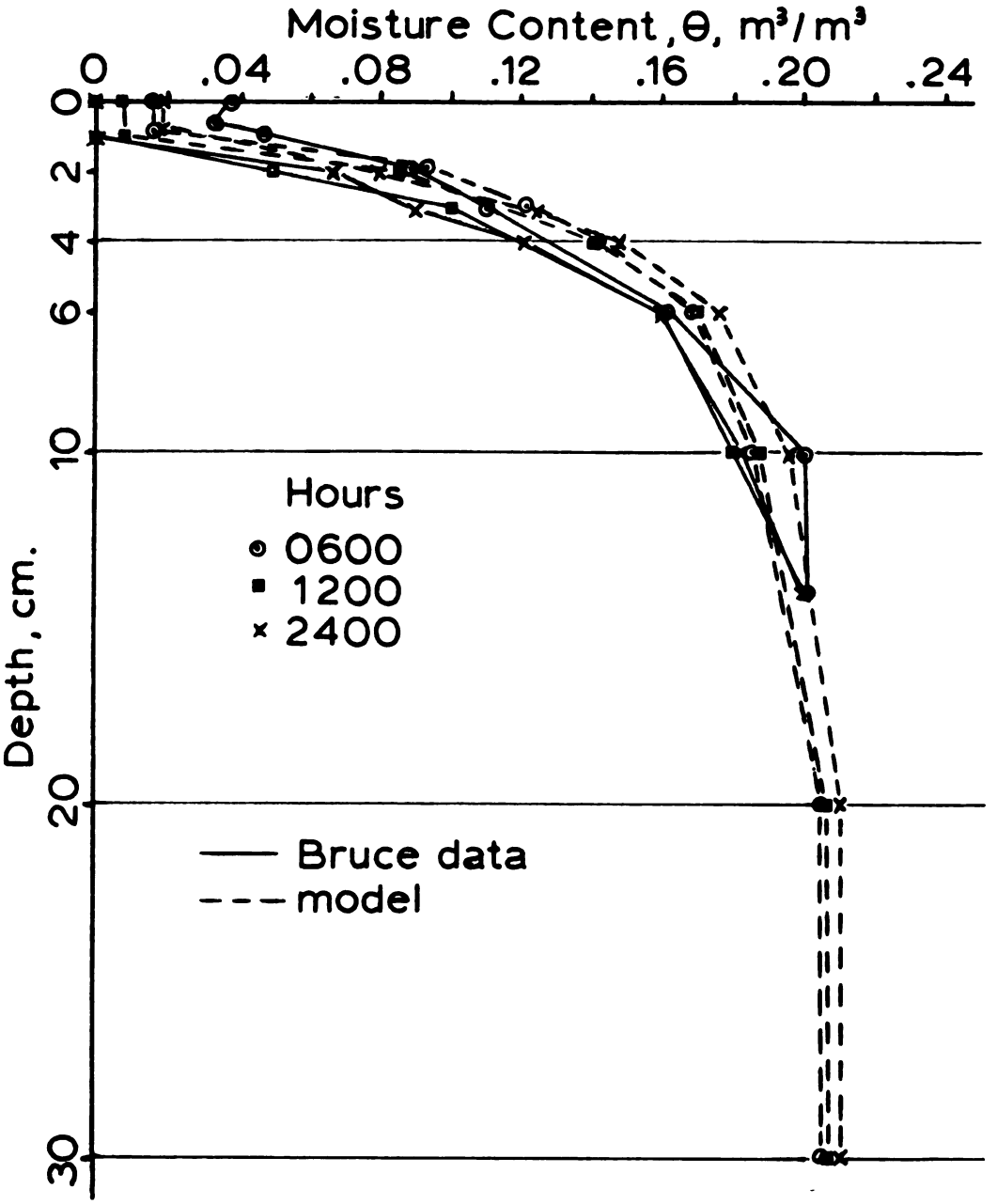


Figure 8.2. June 18 Moistures Comparing Model with Bruce Data

8.2.1 Finite Element Formulation. The surface conditions (soil-air interface) model imposed upon the soil model produced unacceptable swings in the surface temperatures and moistures. Several different grid and time step combinations were employed, as well as changing the element capacitance matrix to the non-consistent (lumped) form. Oscillations were virtually eliminated when the time increment was reduced to 10 minutes, but this would require too much computer time for a 7- to 10-day simulation. A compromise was reached by using a 30-minute time increment and limiting the temperature change at any node to 4°C for each time increment. This produced sufficient stability for the model with a reasonable physical constraint, based on field data of soil surface temperatures.

8.2.2 Soil Air Mass Flow. Vertical air mass movement in the soil was incorporated into the mathematical equations for both temperature and moisture. This term, including $\partial V/\partial z$, represented moisture movement towards the surface during the evening and early morning hours due to density gradients, and a much smaller component due to pressure gradients. The comparable temperature term represented the corresponding thermal convection due to this air mass movement.

Use of these terms in the model produced moistures and temperatures higher than those published by Bruce. Comparisons with field data indicated that the "mass enhancement

factor" already added to the soil thermal conductivity term apparently fully accounted for any thermal convection. Thus, the extra $\partial V/\partial z$ term was deleted for temperature. The density gradient component of the term in the moisture equation was adjusted to coincide with field data. The pressure gradient component was left unchanged.

8.2.3 Surface Conditions Model. Because of the lower inertia of the properties of the air above the soil and the greater sensitivity of those properties to temperature, this model experienced greater oscillations than the soil model. Although these were substantially attenuated by controlling the surface temperature (see Section 8.2.1), additional controls were necessary. Limits were placed on the sensible heat flux to the air and on the evaporation consistent with maximum and minimum measured values for similar regions published by VanBavel and Hillel (1976).

8.2.4 Bruce Data. Although the Bruce study was the most complete available, some information was either missing or sketchy. Data on the soil moisture characteristics, bulk density, and soil texture in the sublayer, as well as the presentation of the temperature and moisture values themselves still posed cause-effect uncertainties and required clarification.

a. Soil moisture characteristics. The published $\psi$-$\theta$ curve, measured from -.01 to -15 bar, did not exhibit a clearly defined $\psi_e$ value, thus one had to be estimated.

Extrapolation of the curve for $\theta_H$ was virtually impossible, thus a computed value for other sandy loam soils published by Mualem (1978) was used.

The saturated hydraulic conductivity $K_s$ supplied by Bruce seemed to produce simulated moisture in the upper soil layers higher than published. Comparisons with the texture triangle and with $K_s$ values published by Rawls, et al. (1982) showed that the texture and wilting point moisture content of Bruce's Cecil sandy loam indeed placed it squarely in the realm of a sandy loam, but the $K_s$ value was far too high, characteristic more of a loamy sand. The $K_s$ characterizing a sandy loam published by Rawls was then used for the computer model.

Although the data used were that of June 18 in the Bruce study, the $\psi$-$\theta$ relationship was not measured until October 30. Bulk densities in the top soil layers had increased during that time period.

b. Bulk density. The bulk density of the Bruce study exhibited the high degree of variability in the top several centimeters of soil and the probable difficulty of sampling near the surface, especially in tilled soil. At a 1.5 cm depth, the bulk density, $\pm$ one standard deviation, ranged from 1060 to 1280 $kg/m^3$ . According to Table 7.1, this would correspond to a change in $D_\theta$ of the order of one magnitude.

c. The $B_1$ horizon. Soil texture of Bruce's Cecil loam was sampled at several different depths to a total depth

of 15 cm The texture was constant down to 9 cm , and became slightly sandier at the 15 cm. depth. Initially, the texture published for the top nine cm was used for the entire 30 cm. profile simulated on the computer. Computed moistures were typically higher than published values.

However, an earlier study, Bruce (1972), showed a $B_1$ horizon at 18 to 33 cm. depth to be a sandy clay loam underlying an $A_p$ horizon of loamy coarse sand, all typified by a Cecil loamy sand profile. Although the $B_1$ texture of the site in the study may not have been the same as the 1977 study, incorporation of it into the model substantially improved the moisture values.

d. Moisture and temperature measurements. Soil water content was averaged by Bruce over five sampling sites and temperature over two sites. Thus, a direct cause-effect relation using one site and its corresponding bulk density, etc. was not established. Difficulty in sampling moisture near the surface required extracting samples above 2 cm. with a spoon. Further, the plotted moisture data had been Fourier transform smoothed, thus the published plot might appear smoother than actual conditions.

### 8.2.5 Moisture Diffusivity Due to Vapor.

In section 4.1 the assumption was made that since moisture flow due to vapor was insignificant compared to liquid flow at soil moistures above the wilting point, then $D_\theta$ was set equal to $D_{\theta l}$. With this diffusivity, the model

exhibited moistures in the upper soil layers higher than actual field data from Bruce. Moistures in the top one centimeter, according to Bruce, were reduced to below $\theta_H$ . In these top layers, then, liquid movement essentially stopped, and the model accumulated moisture just below the surface from moisture movement from lower layers. Reconsideration of the basis of the original assumption indicated that in the top layers vapor movement is apparently a significant component when the surface dries, and cannot be ignored.

A comparison between $D_\theta$ based on liquid movement only and that with vapor movement added is shown in Figure 8.3. Ignoring vapor flow, the model deviated from the Bruce data by about 3% at the 5-cm. depth, but was within 1 1/2% when vapor was included.

Thus, the moisture diffusivity $D_\theta$ was reinstated in the model as

$$D_\theta = D_{\theta l} + D_{\theta v}$$

where $D_{\theta v} = \alpha\, a D_{atm}\, \nu g \rho_v \quad (\partial\psi/\partial\theta)/\rho_l RT$

With this addition of the vapor component, the model came into close agreement with the Bruce data as shown in Figure 8.2.

## 8.3 Comparisons Between the Model and Published Data.

After incorporating the refinements discussed in the previous section, the model followed actual data reasonably well. Some probable reasons for the discrepancies between the model and actual data have already been discussed.

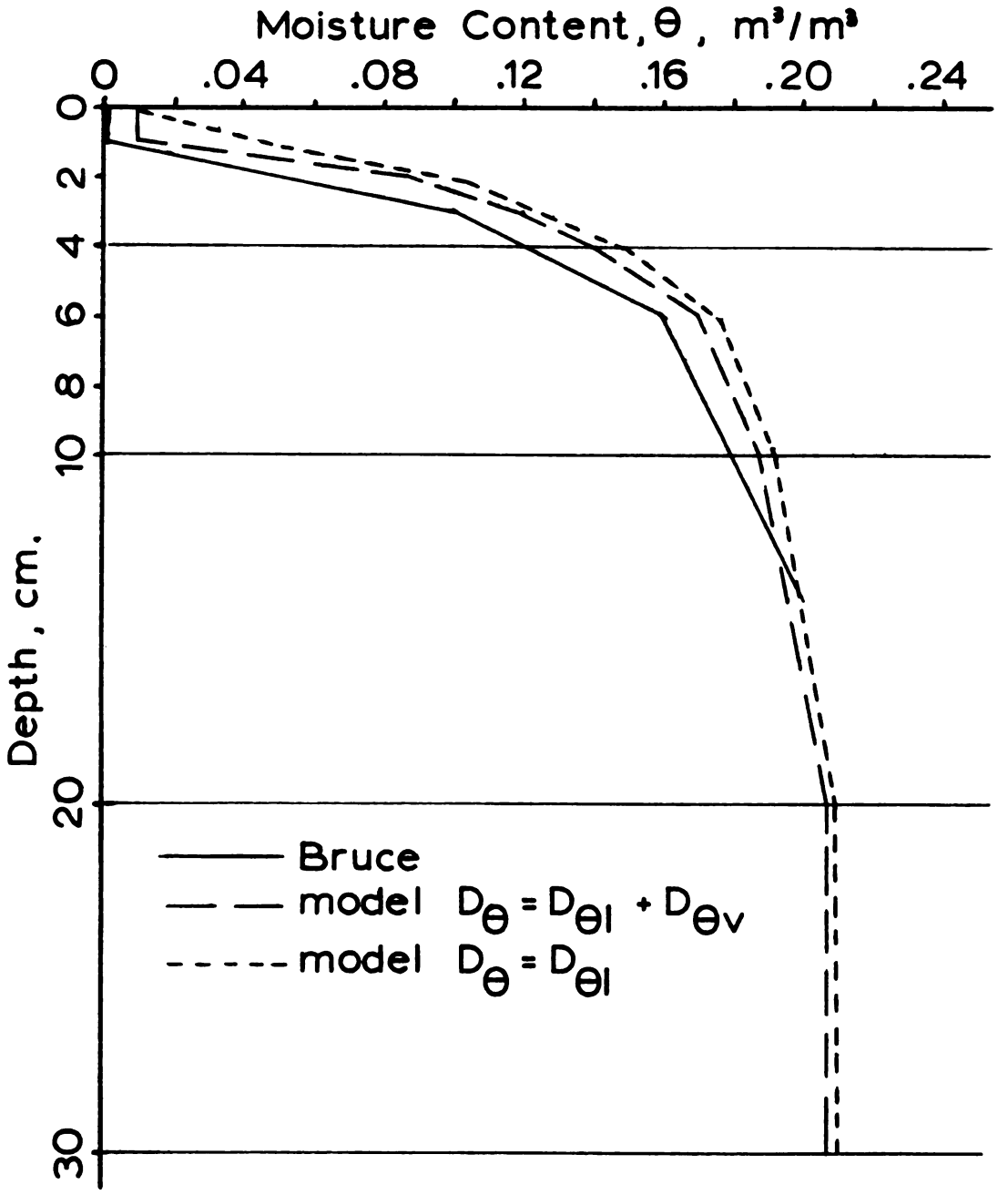


Figure 8.3. June 18 Noon Moistures Comparing Liquid and Vapor Diffusivities

In Figure 8.1 the modeled temperature at the surface did not reach the daytime levels of Bruce, but in the 1- to 6-cm. depth the modeled noon temperature was 2 to 3° C higher. Generally, the total range throughout the day was within 3° of the Bruce range throughout most of the soil profile compared. This model accuracy is consistent with the objective sought by Cruse, et al. (1980) which was to develop a soil temperature model with an accuracy of $\pm$ 2° C at the 5-cm depth.

The moisture comparisons in Figure 8.2 indicate agreement between the model and the Bruce data. The Bruce data exhibited a greater moisture rise due to density gradients at the surface between midnight and 6 a.m., whereas the model exhibited a greater rise from 6 p.m. to midnight. Model moistures were within 1% of Bruce moistures at the 10-cm and 6-cm depths, and within 2% at the 3-cm depth.

## 8.4 Summary

This chapter compared the model with field data reported by Bruce, et al. (1977). With some refinements, the model demonstrated good agreement with the data, as evidence by Figures 8.1 and 8.2. Versatility of the model will be demonstrated in Chapter 9 through simulations of different conditions.

# 9. SIMULATIONS

One of the principle uses of a model is simulation. Chapter 1 lists several potential applications of a simulation tool such as this. This chapter demonstrates the utility and versatility of the model for Michigan soils and conditions.

## 9.1 Model Parameters

### 9.1.1 Soil Profile

The soil profile used in the simulations reported here was previously explained in Chapter 6. The finite element grid shown in Figure 6.3, is a slice through the furrow extending from the furrow centerline out to the midpoint between rows, and down to a 30-cm. depth. The time increment for successive calculations of moisture and temperature was set for 30 minutes, for a total span of three days. All simulations were started at 8 a.m. with initial conditions as outlined in Chapter 6.

### 9.1.2 Undisturbed Soil

a. Metea sandy loam. The Michigan soil for which the author was provided the most complete information and which was modeled the most extensively was Metea sandy loam (Figure 9.1)*. This soil exhibits the following characteristics:

---

*Data compliments of Dr. Ray Kunze, Soil Science, Michigan State University

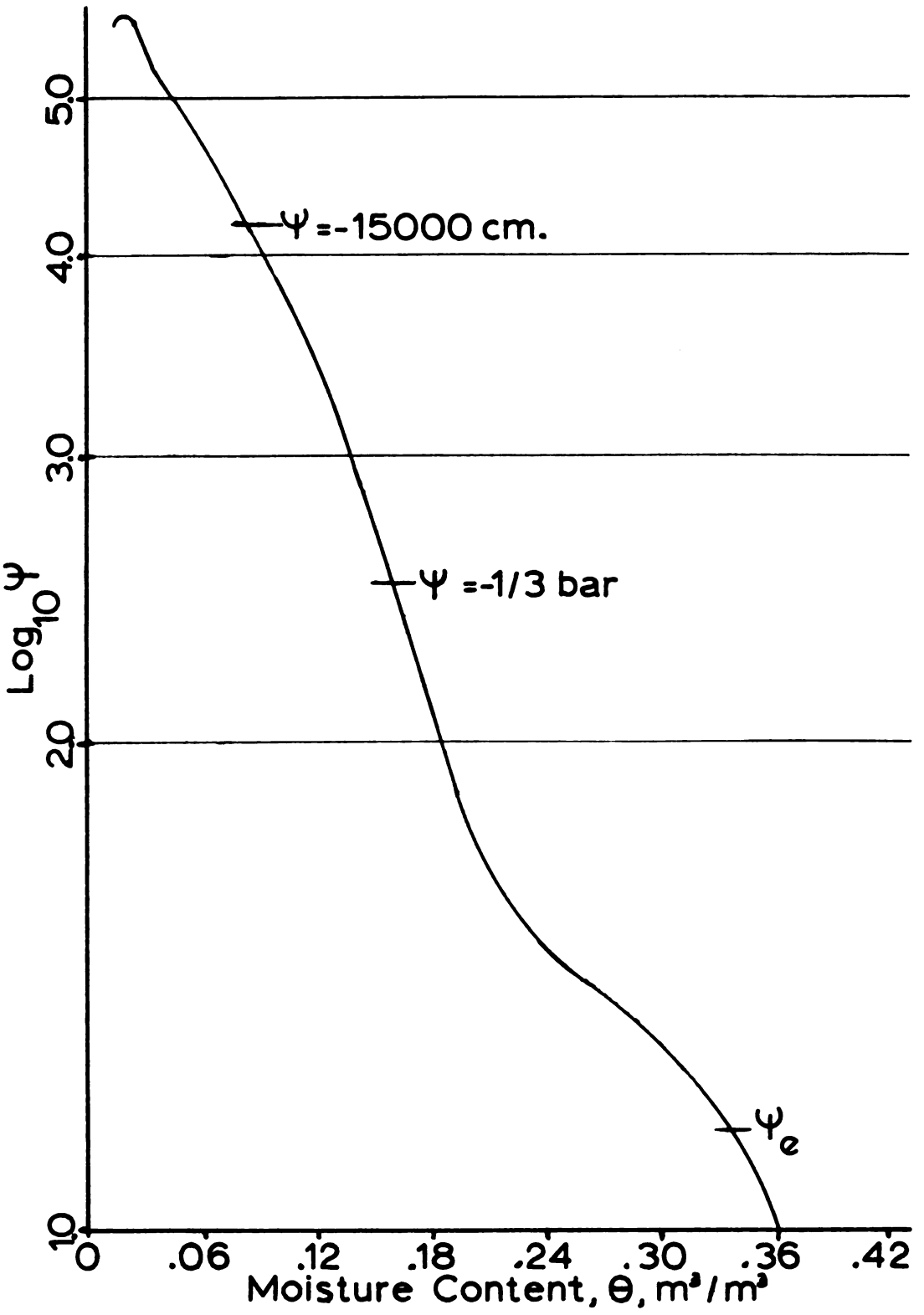


Figure 9.1. Moisture Characteristic Curve for Metea Sandy Loam

$\theta$ at saturation = 37.5%

$\theta$ at 1/3 atm. = 16.0%

$\theta$ at 15 atm. = 8.5%

$\theta_H$ (immobile) = 2.0%

$K_s$ = 1.32E-6 m/sec.

In addition, if the air-entry moisture content is taken as 90% of saturation, then

$$\theta_e = 33.8\%$$

and, from Figure 9.1, $\psi_e$ = -.1405 m $H_2O$.

There was not enough data available to develop a moisture adsorption curve. Hirschi and Moore (1980) stated that, to obtain adsorption data, reasonable results are derived by dividing the desorption data by 1.6. Using this factor, simulations were based on $\psi_e$ for adsorption = -.1000 m $H_2O$.

The texture of Metea sandy loam was not available. The author was advised to use the textural triangle, and the following soil analysis was chosen:

55% sand

30% silt

15% clay

Further, a $B_1$ horizon, starting at the 20-cm. depth, was chosen as:

45% sand

30% silt

25% clay

The bulk density for undisturbed, unstructured Metea loam was set equal to 1650 $Kg/m^3$, based on the saturation moisture content of 37.5% provided in the data.

The surface roughness $z_o$ was based on the values presented in Table 5.1, and was equated to 0.005 m for undisturbed soil.

The initial temperature at 8 a.m. was assumed a constant value throughout the soil profile. An initial moisture gradient was assumed for undisturbed soil. These initial conditions were based on values in Table 9.1, Figure 9.1, and several trial runs of the model.

b. Brookston clay loam. In order to study the effects of soil texture, a Michigan clay loam was also modeled using the characteristic curve in Figure 9.2*. This soil exhibits the following properties:

| | |
|---|---|
| 31.1% sand | $\theta$ at saturation = 33.6% |
| 45.9% silt | $\theta$ at 1/3 bar = 22.1% |
| 23.0% clay | $\theta$ at 15 bar = 13.0% |
| | $\theta_{pwp}$ = 11.3% |

$K_s$ = 1.26E-5 m/sec

Bulk density at test = 1390 $Kg/m^3$

At 90% of saturation, $\theta_e$ = 30.2% and $\psi_e$ = -.2690 m $H_2O$. Dividing $\psi_e$ by 1.6, $\psi_{ea}$ = -.1680 m $H_2O$. The residual

---

*Data compliments of Dr. Ray Kunze, Soil Science, Michigan State University

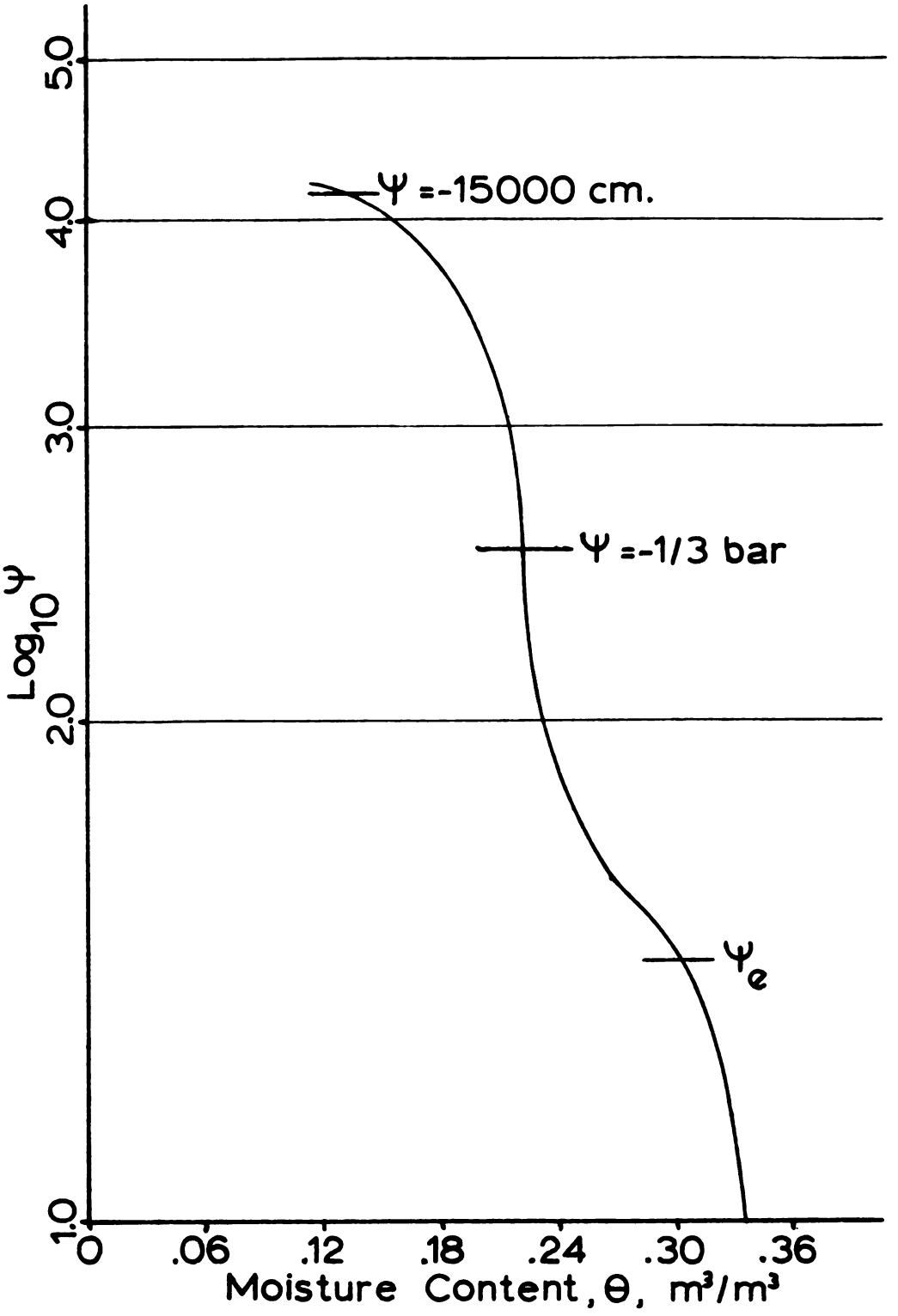


Figure 9.2. Moisture Characteristic Curve for Brookston Clay Loam

(immobile) moisture content $\theta_H$ was set equal to 11%. This was based on a tested $\theta_{pwp}$ = 11.3% and values for clay loams and silty clay loams recorded by Mualem (1978) ranging from 9% to 28%.

The $B_1$ horizon, starting at the 20-cm. depth, was chosen as:

21% sand

44% silt

32% clay

Initial conditions and the surface roughness were chosen as the same for the Metea loam.

Table 9.1. Soil conditions in northern locations pertinent to model.

| Soil | Date | T(°C) | θ(%) | Depth(cm) | Researchers |
|---|---|---|---|---|---|
| Nicollete loam | End of May | 18 | | 5 | Cruse, et al. (1980) |
| | Spring | 12.8 to 24.0 | | surface | VanBavel and Hillel (1976) |
| Nicollete loam | time of tillage 1965 | | 26<br>36<br>38 | 10<br>22<br>Below 22 | Allmaras, et al. (1977) |
| | time of tillage 1966 | | 22<br>26 | 20<br>30 | |
| Sandy loam #1 | at F.C. | | 22 | 5 | Ojeniyi and Dexter (1979) |
| Sandy loam #2 | at F.C. | | 12.6<br>25.2 | 5<br>5 | |

9.1.3 Tilled Soil. Tillage operations during planting substantially alter the structure of the soil. The model already incorporates an expression for mean aggregate size as a function of tillage passes (equation [65]) used in the calculation of air permeability. But the greater effect on the model is the reduction in the bulk density $\rho_B$, which in turn affects other key parameters. Bruce, et al. (1977) recorded an average $\rho_B$ = 1200 Kg/m$^3$ in the top ten centimeters for a single pass of the tillage implement. Since their Cecil sandy loam was similar to the Metea sandy loam, this value was adopted for a single pass tilled zone in the model. For two tillage passes through Metea, a $\rho_B$ = 1350 Kg/m$^3$ was assumed.

Tillage also alters the moisture properties of the soil. Hillel (1971) presented a qualitative discussion that soil structure affects the $\psi$-$\theta$ relation, especially at low suctions (see Figure 9.3).

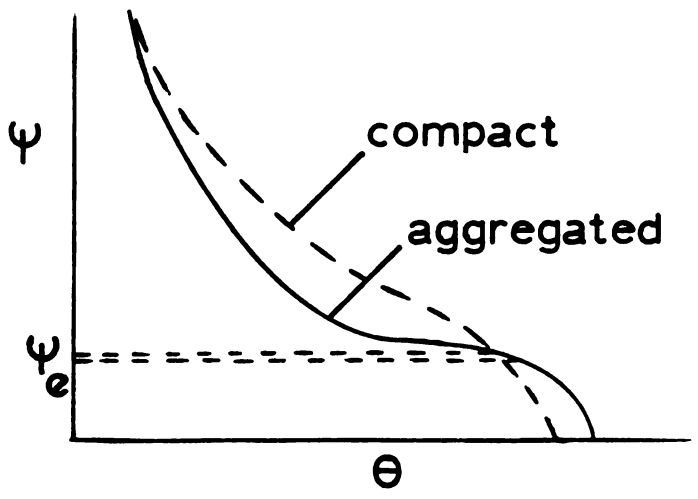


Figure 9.3. Effect of Soil Structure on Moisture Characteristics

For a given $\psi$ near saturation, there is wide disparity in $\theta$. However, above $\psi_e$, and throughout most of the range, the difference is generally diminished, and the two curves converge at high suction. We can deduce from Ghosh (1980) that the difference in $\psi_e$ between the two curves in Figure 9.3 would be small. He argued that, if $\theta_e = .90$ , then $\theta_o - \theta_e$ is small, and $\psi_e$ may be approximated as the intercept on the line $\psi = \psi_e \ (\theta/\theta_o)^{-\beta}$ at $\theta/\theta_o = 1$. Therefore only one $\psi_e$ is needed for a particular soil, independent of $\rho_B$ and $\theta_o$ (see Figure 9.4).

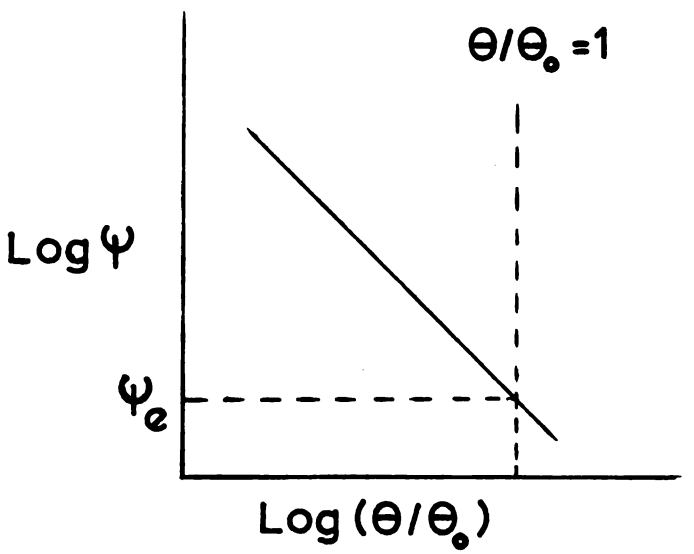


Figure 9.4. Ghosh Argument for One $\psi_e$

The $\psi_e$ and $\psi_{ea}$ for the undisturbed soil were assumed for all tilled conditions as well.

The saturated hydraulic conductivity $K_s$ is typically given in the literature as a single value, even for studies extending over variable bulk densities. Rawls, et al. (1982) reported that $K_s$, although dependent on $\rho_B$ and other factors, is much more dependent on texture, so investigators typically ignore other factors, and record one $K_s$ for each soil type.

However, to reflect a more accurate interdependence, the $\rho_B$ factor should be included.* Rawls, et al. cited an expression of the form:

$$K_s = f(S^2)$$

Using this form, the following equation was used to calculate $K_{st}$ of the tilled zone, knowing $K_{su}$ of the undisturbed soil:

$$K_{st} = K_{su}\left[\frac{2650 - \rho_{Bt}}{2650 - \rho_{Bu}}\right]^2 \qquad [86]$$

9.1.4 Meteorological Inputs. In order to simulate weather conditions for central Lower Michigan, thirty-year statistics were obtained from Bishop Airport in Flint, and are shown in Tables 9.2 and 9.3.

---

*Dr. Ray Kunze of Michigan State University indicated tillage could change $K_s$ by a factor of ten, but very little consistent data is presently available.

**Table 9.2. Meteorological statistics from Bishop Airport (1941-1970)**

| Month | Temp. (°F) | | | % Rel. Hum. | | | |
|---|---|---|---|---|---|---|---|
| | Daily Max. | Daily Min. | Monthly Avg. | 0100 | 0700 | 1300 | 1900 |
| May | 67.0 | 44.5 | 55.8 | 75 | 77 | 54 | 56 |
| June | 77.0 | 54.6 | 65.8 | 79 | 80 | 57 | 58 |

**Table 9.3. Diurnal meteorological statistics for 1981 from Bishop Airport**

| Hour | May Monthly Summary | | | June Monthly Summary | | |
|---|---|---|---|---|---|---|
| | Temp(°F) | %Rel.Hum. | Wind(mph) | Temp(°F) | %Rel.Hum. | Wind(mph) |
| 0100 | 49 | 73 | 6.7 | 61 | 79 | 6.4 |
| 0400 | 46 | 78 | 6.4 | 59 | 84 | 6.6 |
| 0700 | 48 | 76 | 7.0 | 62 | 80 | 8.2 |
| 1000 | 58 | 57 | 10.7 | 69 | 64 | 11.6 |
| 1300 | 62 | 50 | 11.8 | 74 | 57 | 12.5 |
| 1600 | 63 | 48 | 12.0 | 75 | 53 | 12.5 |
| 1900 | 60 | 52 | 9.2 | 72 | 56 | 9.8 |
| 2200 | 53 | 67 | 7.6 | 64 | 74 | 6.6 |

Global radiation data for the simulations were obtained from Baker and Haines (1969) and Baker and Klink (1975). For simulating conditions in central Lower Michigan, statistics for East Lansing were gleaned from these reports and are presented in Table 9.4.

Table 9.4. Mean weekly solar radiation over East Lansing, langley/day.

| Month | Week | 1953-1966 Avg. | 1952-1970 Avg. | | |
|---|---|---|---|---|---|
| | | | Clear sky | 100% cloud | Mean |
| May | 1 | 490 | 725 | 265 | 487 |
| | 2 | 469 | 740 | 150 | 465 |
| | 3 | 504 | 680 | 200 | 501 |
| | 4 | 544 | 700 | 260 | 539 |
| June | 1 | 550 | 735 | 160 | 544 |
| | 2 | 532 | 760 | 250 | 529 |
| | 3 | 565 | 750 | 240 | 555 |
| | 4 | 580 | 760 | 235 | 552 |
| | 5 | 548 | | | |

Using the procedures outlined in Appendix D, meteorological inputs were calculated to simulate average May weather conditions and hot, dry June conditions for Michigan. These are shown in Table 9.5.

Table 9.5. Meteorological inputs used in the simulations

| Parameter | Average | | Amplitude | |
|---|---|---|---|---|
| | Avg. May | June | Avg. May | June |
| % Rel. Humidity | 63 | 56 | 15 | 16 |
| Air temp (°C) | 12.5 | 19.0 | 4.7 | 4.0 |
| Windspeed (m/sec) | 4.1 | 4.1 | 1.3 | 1.3 |
| Global Radiation ($W/m^2$) | 50.0 | 50.0 | 685.0 | 774.0 |

The same diurnal cycle was imposed onto the model each day for the duration of the simulation run.

## 9.2 Simulation Results

9.2.1 Temperature and Moisture in Undisturbed Metea Sandy Loam. Figure 9.5 shows the daily fluctuation in soil temperature in undisturbed Metea loam. Successive noon temperatures are cooling down, indicating sustained meteorological inputs during simulation are insufficient to maintain the temperature level dictated by the 8 a.m. start condition. Temperatures seem to be approaching equilibrium by the third day. Figure 9.6 exhibits the corresponding moisture conditions. The entire profile is reduced in moisture content, producing a steeper gradient by the third day. Although moisture depletion in the sublayers is

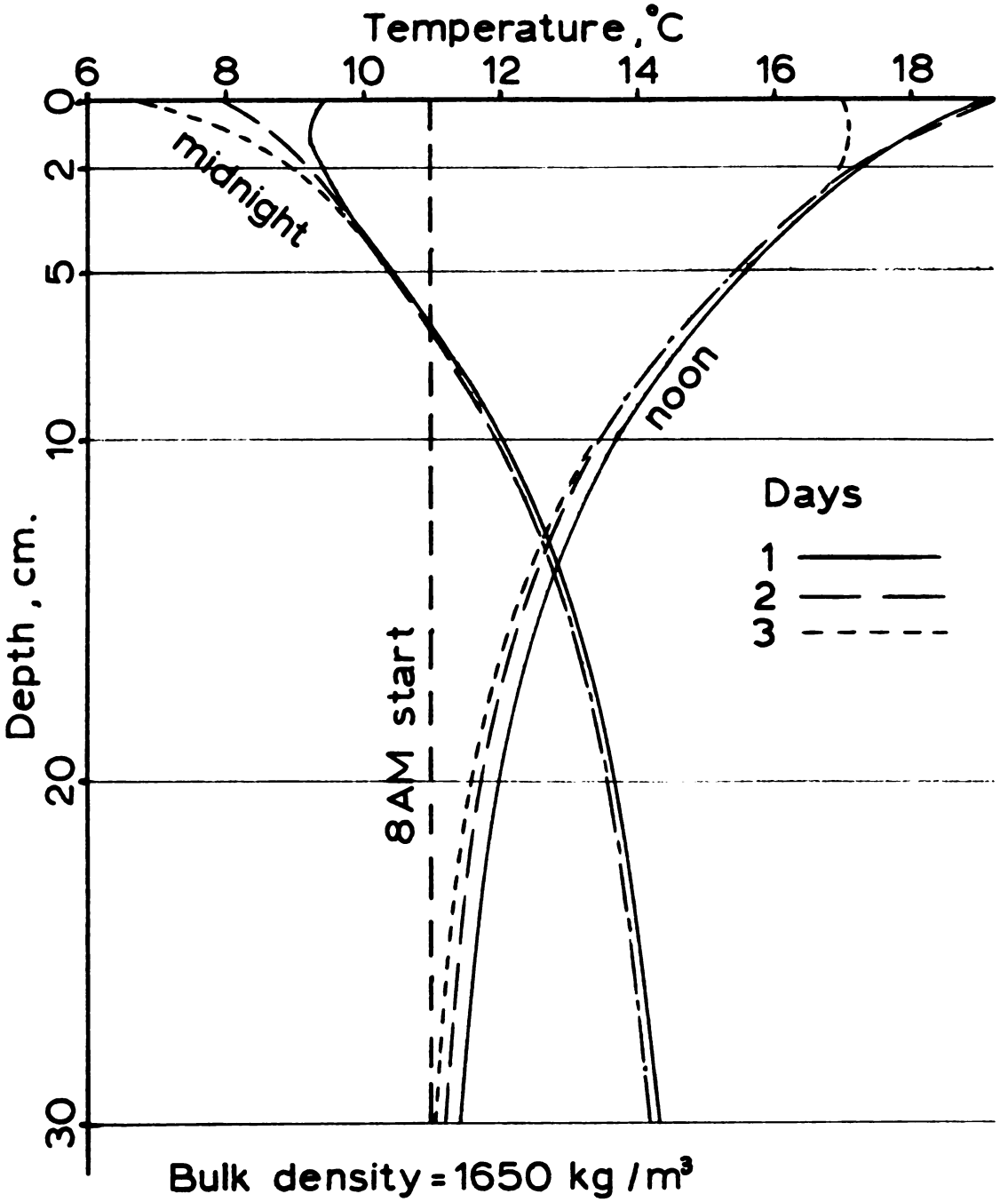


Figure 9.5. Temperatures in Undisturbed Metea Sandy Loam for Average Michigan May Climate

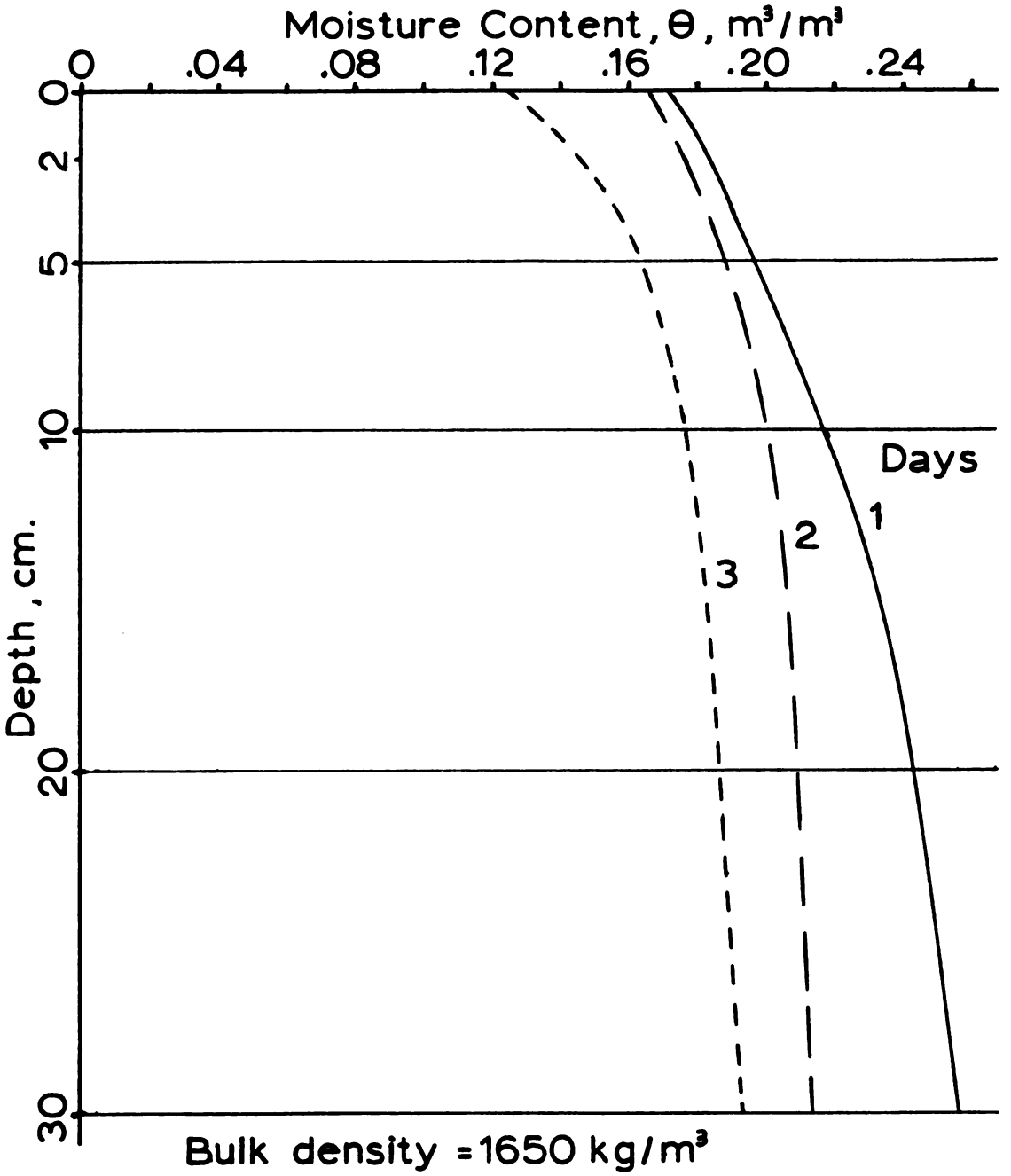


Figure 9.6. Noon Moistures in Undisturbed Metea Sandy Loam for Average Michigan May Climate

slowing down, drying of the top layers is accelerating. The drying toplayers have less thermal inertia, thereby cooling down further at night.

9.2.2 Temperature and Moisture in Undisturbed Brookston Clay Loam. Figures 9.7 and 9.8, showing temperature and moisture profiles in Brookston clay loam, can be compared to Figures 9.5 and 9.6, the counterparts for Metea sandy loam. The sandy loam has a higher thermal conductivity than the clay loam, but its higher bulk density creates a higher thermal inertia with fewer air pockets. Thus, the two appear to cancel each other in the temperature regime.

The clay soil retains more moisture in the top layers during the first day, but at the expense of deeper layers. By the third day, although the surface in the clay soil has dried out further, moistures below the surface are approximately the same for both soils. This surface condition probably can be attributed to a larger vapor flow component present near the surface for the lower bulk density.

The $B_1$ horizon of the clay soil restricted moisture movement, as evidenced by the moisture plot distortions in Figure 9.8. The evaporative demand thus drew more moisture from the 10- to 20-cm depth in the clay soil than from the sandy soil since moisture at deeper layers was not as available here as it was in the sandy soil.

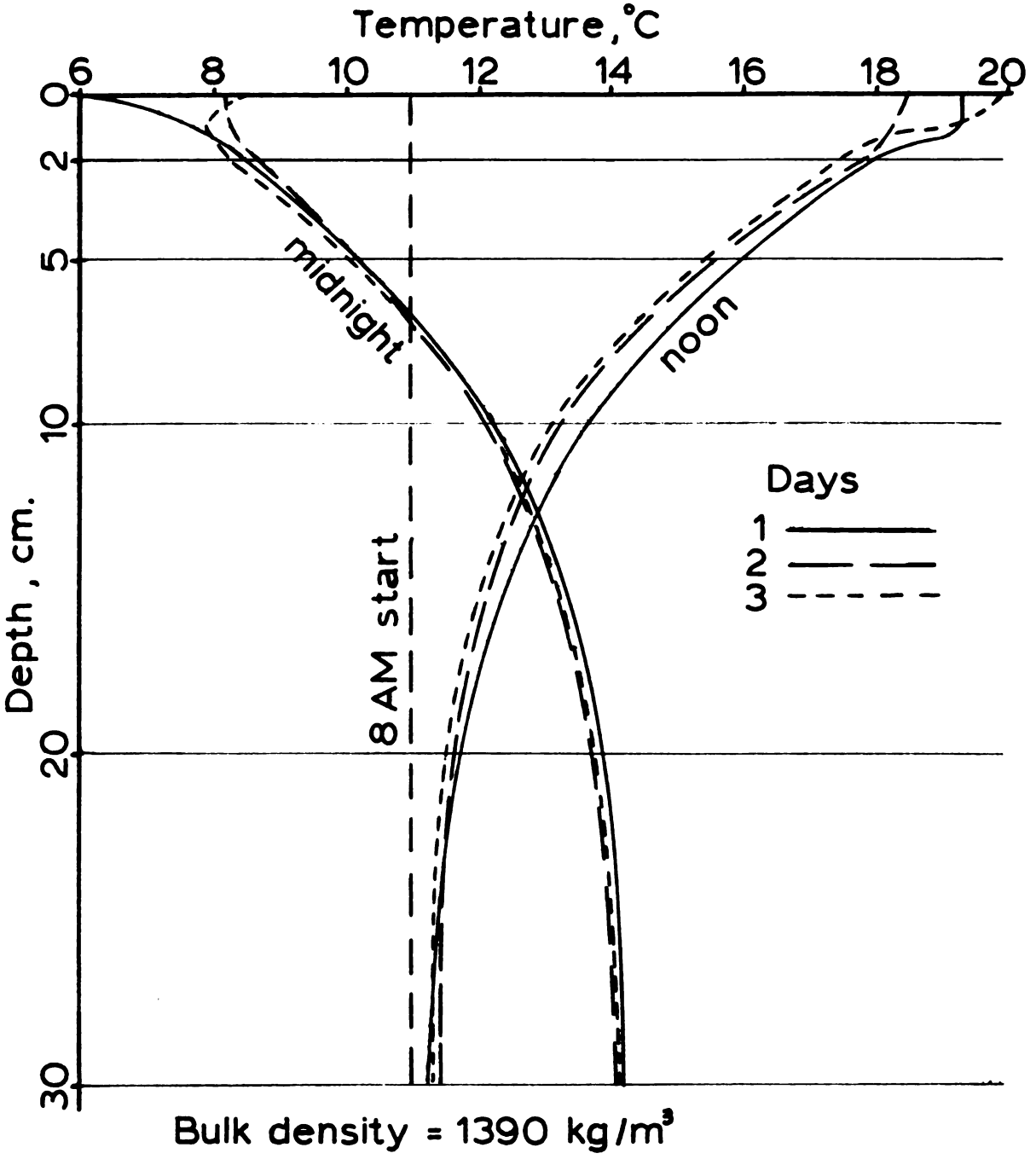


Figure 9.7. Temperatures in Undisturbed Brookston Clay Loam for May

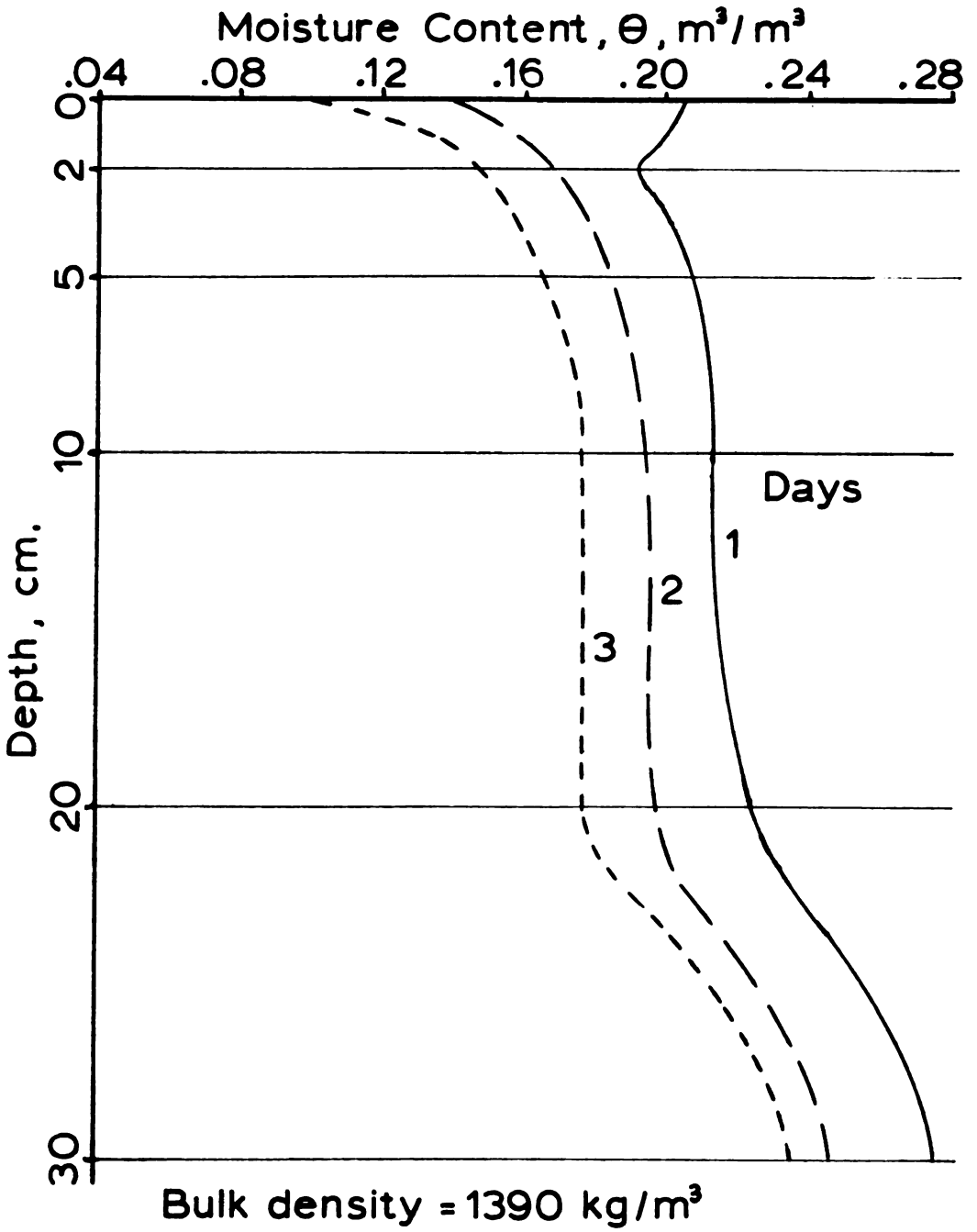


Figure 9.8. Noon Moistures in Undisturbed Brookston Clay Loam for May

9.2.3 Comparisons Between Undisturbed and Tilled Metea Loam. Figure 9.9 compares moistures at several depths for undisturbed Metea loam and after a single tillage pass creating a 10-cm surface layer at 1200 $Kg/m^3$. The diurnal moisture cycle is obvious with undisturbed soil, showing fluctuations highest at the surface and decreasing with depth. Peak-to-peak fluctuations these first three days ranged from 2% to 6% at the surface, and from 1% to 2% at five centimeters. Bruce, et al. (1977) reported identical fluctuations at these depths for their sandy loam. Hillel (1977), in his computer model of a fine sandy loam, exhibited a 10% fluctuation at the five millimeter depth.

Tilling the soil to a bulk density of 1200 $Kg/m^3$ appears to significantly alter these diurnal cycles. The surface moisture dries quickly to virtually zero (artificially held to 1% by the model), and increases only 2 to 3% during the early morning hours. Meanwhile, moisture at the 5-cm depth steadily increases over the three-day period. This phenomenon is explained in Figure 9.10.

Figure 9.10 shows the three-day history of the noon moisture profile. The moisture discontinuity created at the interface at 8 a.m. of the first day readjusts itself to a continuous gradient by the third day. The top layers of soil dry out, but the rate of drying slows by the third day. Moistures at depths below 3 cm actually increase over the 3-day period. Moisture collects below the interface as vertical movement from below proceeds but movement across the

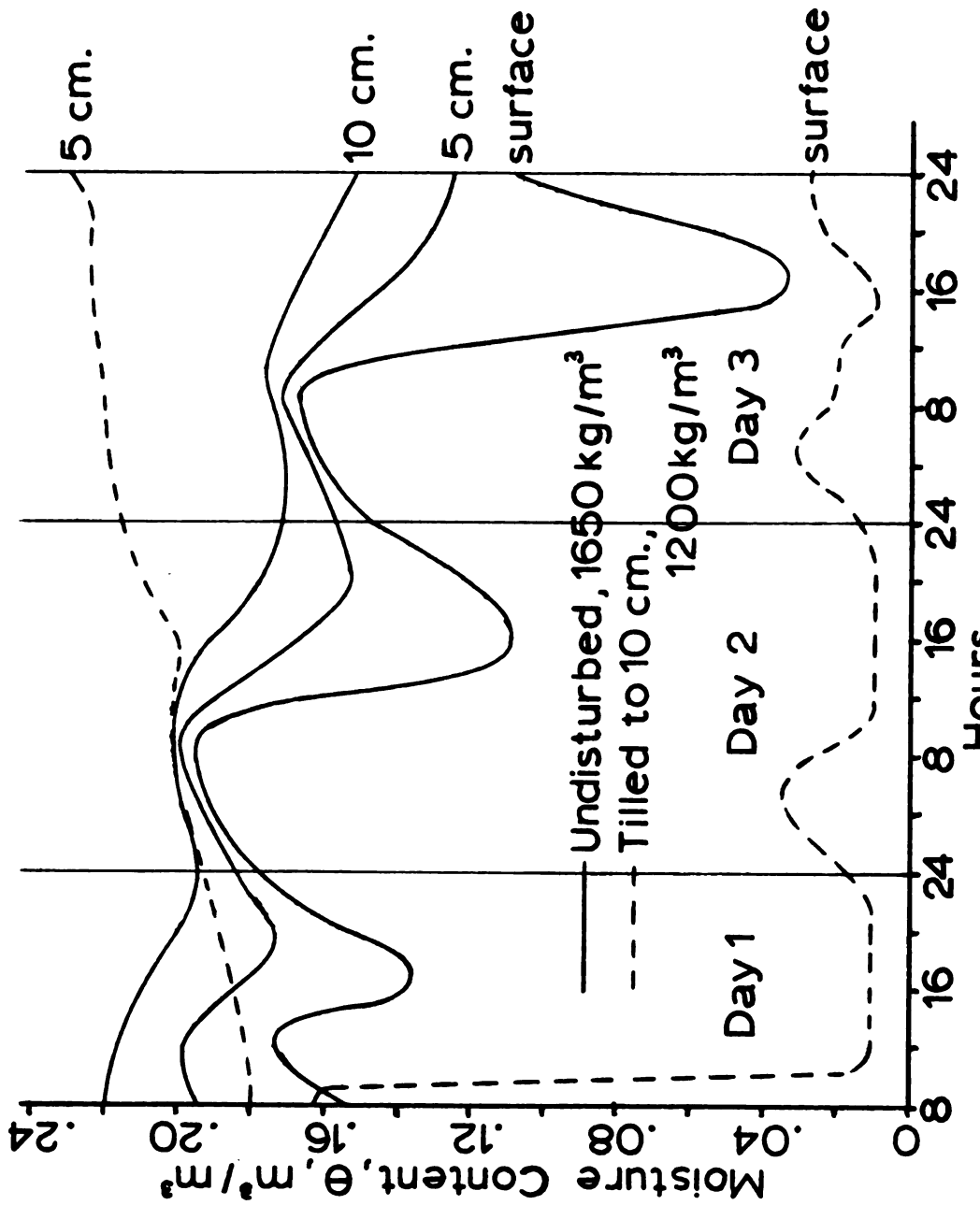


Figure 9.9. Moistures at Various Depths for Metea Sandy Loam Comparing Undisturbed and Tilled

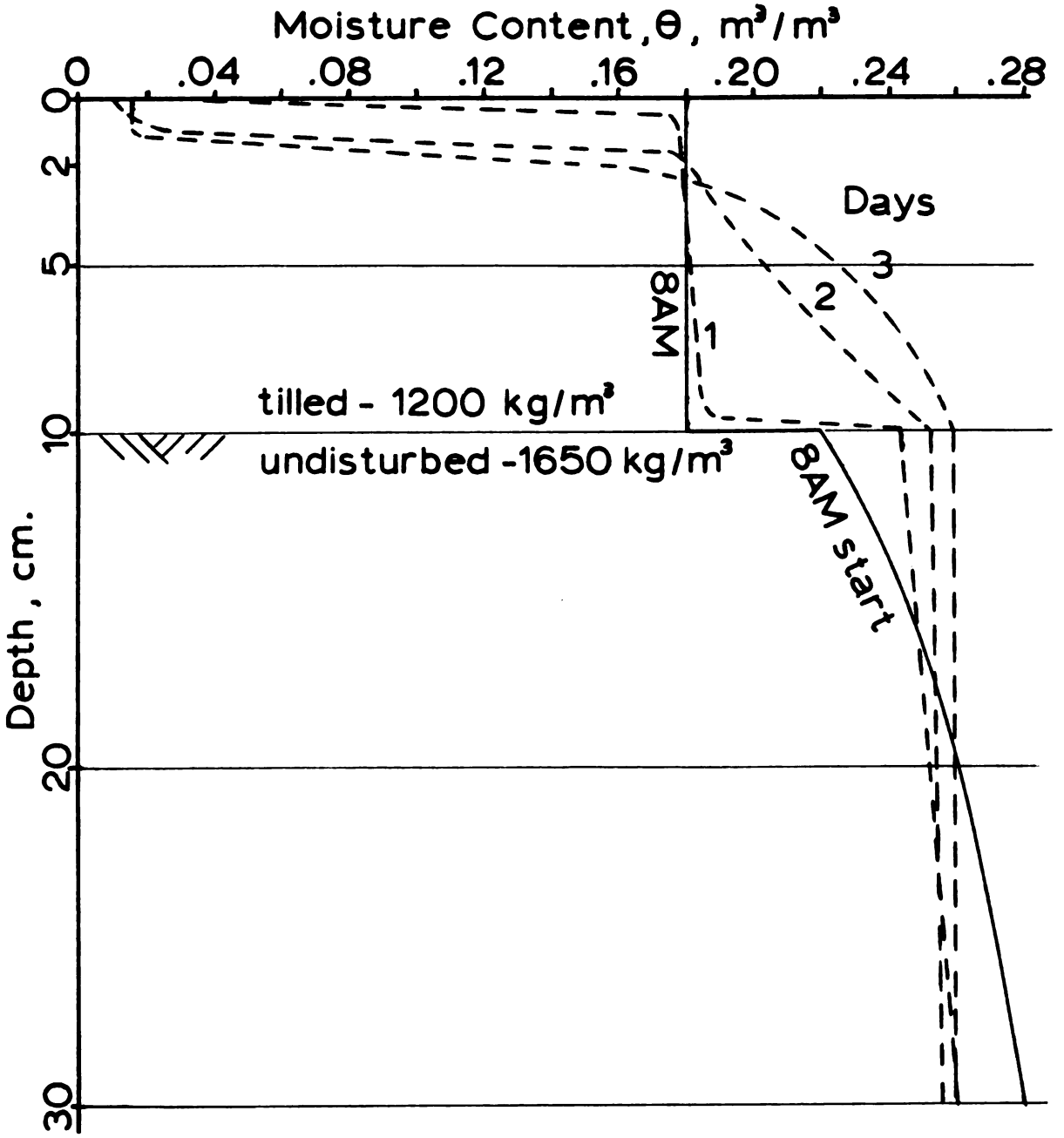


Figure 9.10. Noon Moisture Profiles in Metea Loam with a Tilled Bulk Density of 1200 Kg/m$^3$

interface is impeded. Moisture content has reached a uniform level throughout the profile below ten centimeters.

Figure 9.11 compares temperatures between the undisturbed and tilled condition. Tilling warms up the entire profile by the third day. The 10-cm tilled layer warms up faster, creating a slight discontinuity in the temperature gradient at the 10-cm depth.

9.2.4 Tilled Density and Tillage Passes Comparisons in Metea Loam.

Figure 9.12 compares the effects of bulk density. A bulk density of 1200 $Kg/m^3$ is representative of a single pass of a tillage implement, whereas 1350 $Kg/m^3$ is more representative of two passes. Here again moisture trends reverse at a depth of about 3 centimeters. Below this point moisture contents by the third day are higher for the lower bulk density, possibly due to lower liquid movement. Above this point moisture is lower for the lower bulk density, probably due to higher vapor flow, the predominant mechanism in dried surface layers.

9.2.5 Minimum Tillage Furrow Shape Comparisons. Figure 9.13 shows several furrow dimensions and shapes which were modeled using the grid of Figure 6.3. The oval at the base of each furrow is the planted seed. Different combinations of the small elements in the upper right hand corner of the grid in Figure 6.3 were used to simulate the furrows.

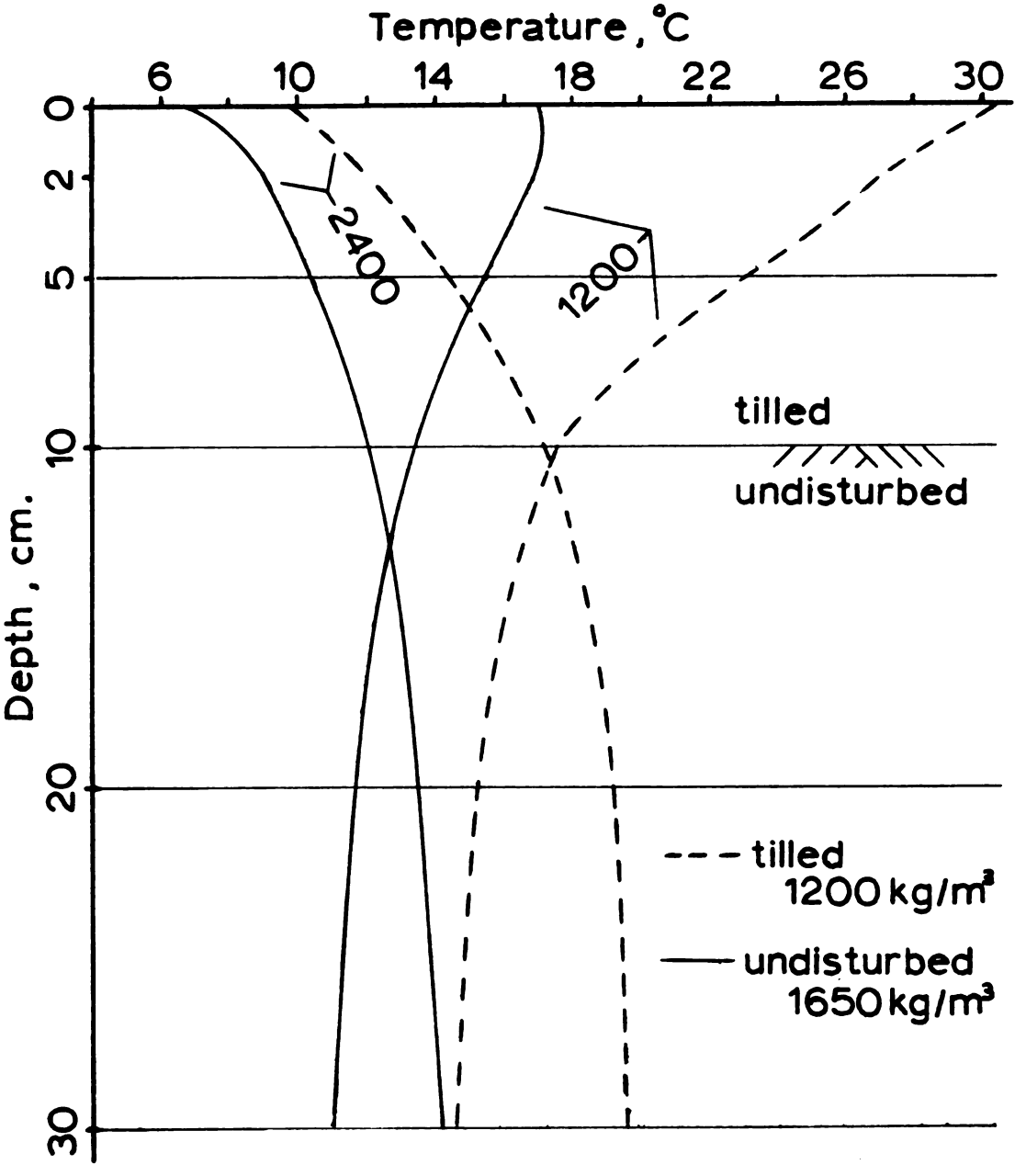


Figure 9.11. Third Day Temperatures in Metea Loam Comparing Undisturbed and Tilled Condition

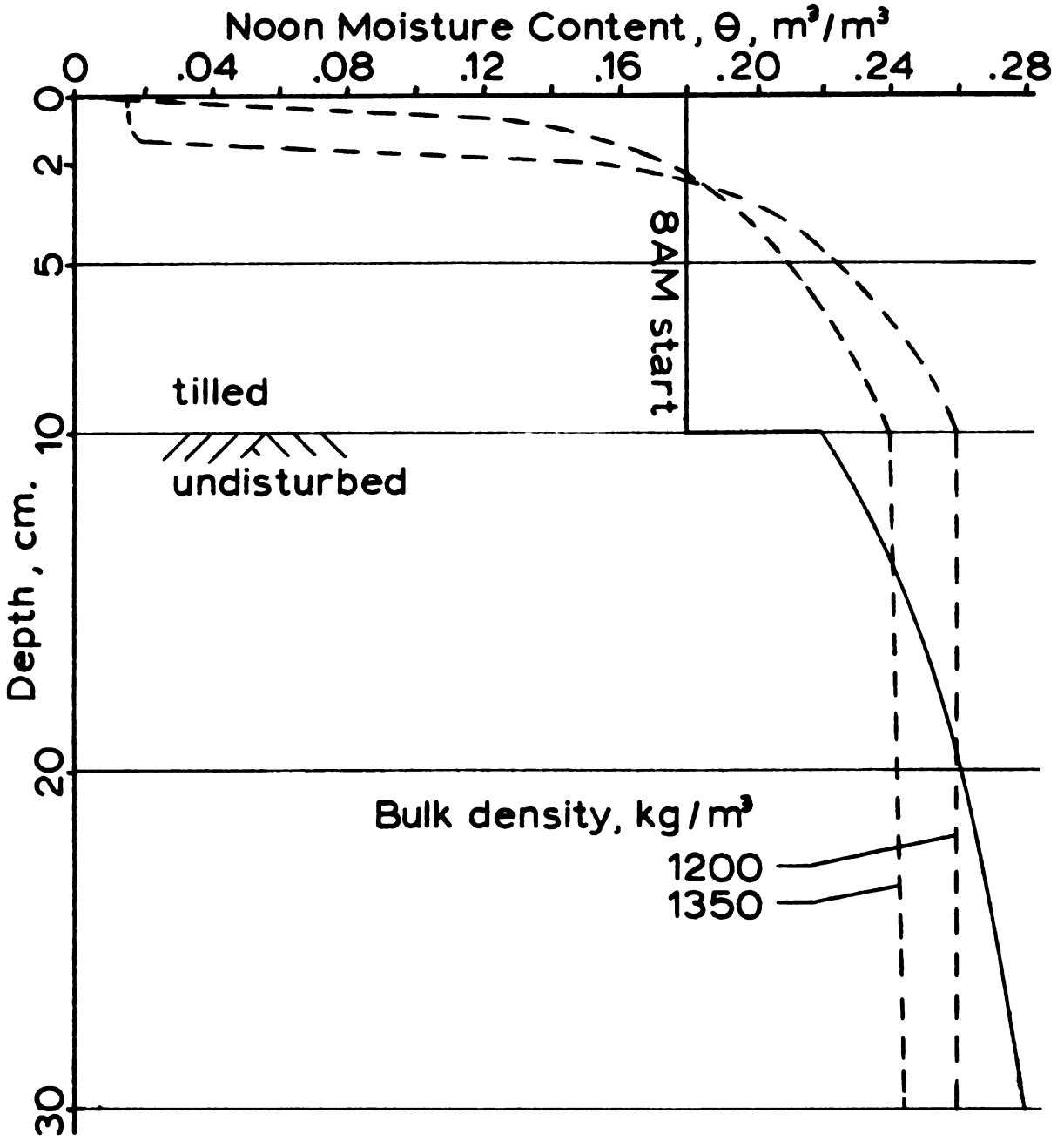


Figure 9.12. Third Day Moisture Profiles in Metea Loam Comparing Tilled Bulk Densities

The results of the simulations of these furrow shapes are exhibited in Figure 9.14. Moisture content at the seed point decreases at the same rate for all furrow shapes for the undisturbed condition. However, the seed point stays wetter by 1 to 2% when at the base of a tilled furrow as compared to when in the undisturbed profile. This, again, is due to moisture movement from lower layers up to the seed, but impedance to moisture movement through the furrow. Although there is a difference of up to 1% moisture content between the wide rectangular and narrow furrows, there is essentially no difference between the two narrow profiles. This might suggest that moisture at the seed is more dependent on furrow width than furrow shape.

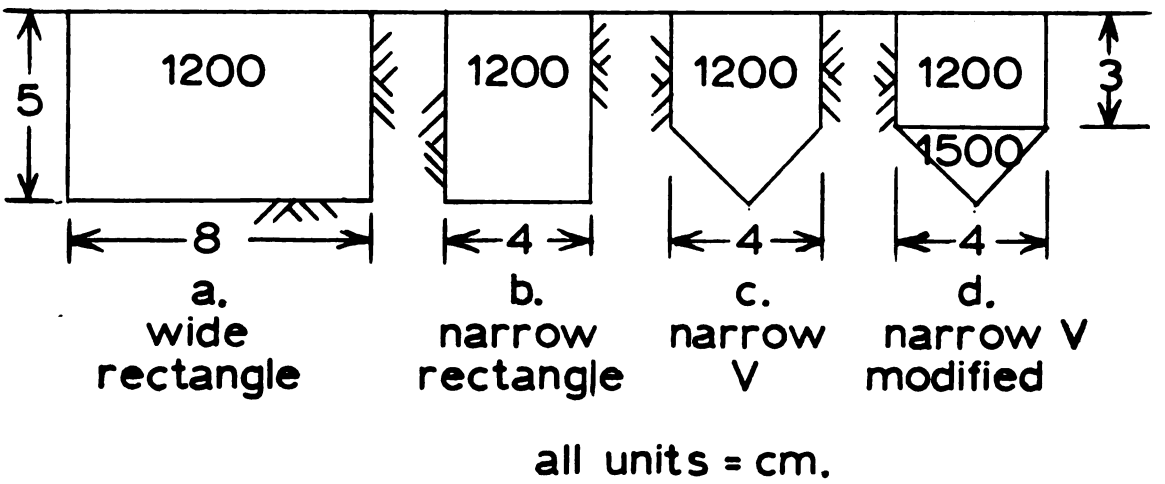


Figure 9.13. Minimum tillage furrows modeled.

Figure 9.13(d) shows a narrow V furrow simulating a condition where some loose soil fell into the furrow in

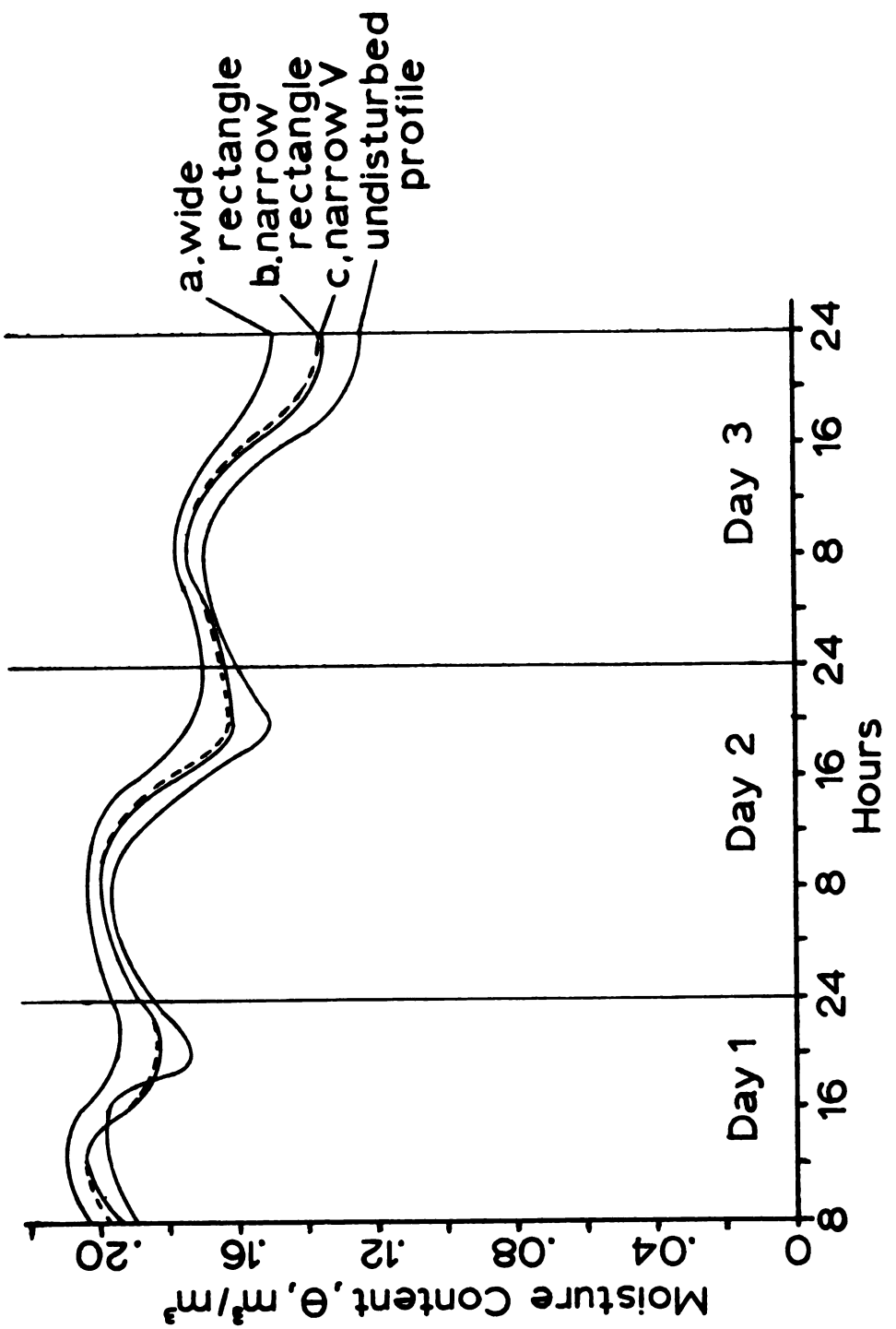


Figure 9.14. Moisture at Seed Point (5 cm) for Several Tilled Furrow Profiles with Metea Sandy Loam and Average May Climate

front of the seed firming wheel and was firmed immediately over the seed to 1500 Kg/m$^3$, followed by loose soil backfill. This furrow condition was simulated on the computer and compared with the narrow V shape of Figure 9.13(c). Three nodes of the grid, all on the furrow centerline, were compared. The node at the surface for both conditions dried to 1% and remained there for the 3-day period. The node representing the seed did not vary more than 0.2% between conditions for the simulation period.

The largest difference was experienced with the node at the interface of the two densities. In the modified furrow, this node, in the first day, was 4 to 5% higher in moisture content than the narrow V furrow. However, by the end of the third day, this had reversed where the modified furrow was 3 to 4% lower than the narrow V.

Apparently the interface created a moisture barrier early in the period, and water accumulated at the interface. Later, after continuity had been restored, the 1500 Kg/m$^3$ section of soil dried out further than had it been at 1200 Kg/m$^3$. The narrow V of Figure 9.13(c) had built up a barrier to liquid flow earlier in the period, where as the modified condition allowed additional moisture to be "trapped" in the triangular section to be lost later. The two conditions simulated had no effect on moisture at the seed, suggesting it had received adequate moisture from lower depths throughout the 3-day period.

9.2.6 Varying Meteorological Conditions. Figures 9.15 and 9.16 show the effect different meteorological conditions have on the temperature and moisture profiles. Average May and hot June conditions for Michigan, as outlined in Table 9.5, were used in this simulation. With average air temperatures increased by 6.5°C, the soil temperature by the third day has increased by 6°C throughout most of the profile. However, with a corresponding reduction of average air relative humidity by 7%, most of the moisture profile remains unchanged. Only the top one centimeter has dried further.

## 9.3 Summary.

This chapter exhibited the results of simulations of soil conditions comparing soil types, structure, tilled furrow shapes and dimensions, and meteorological conditions. Chapter 10 presents concluding remarks and recommendations for future work.

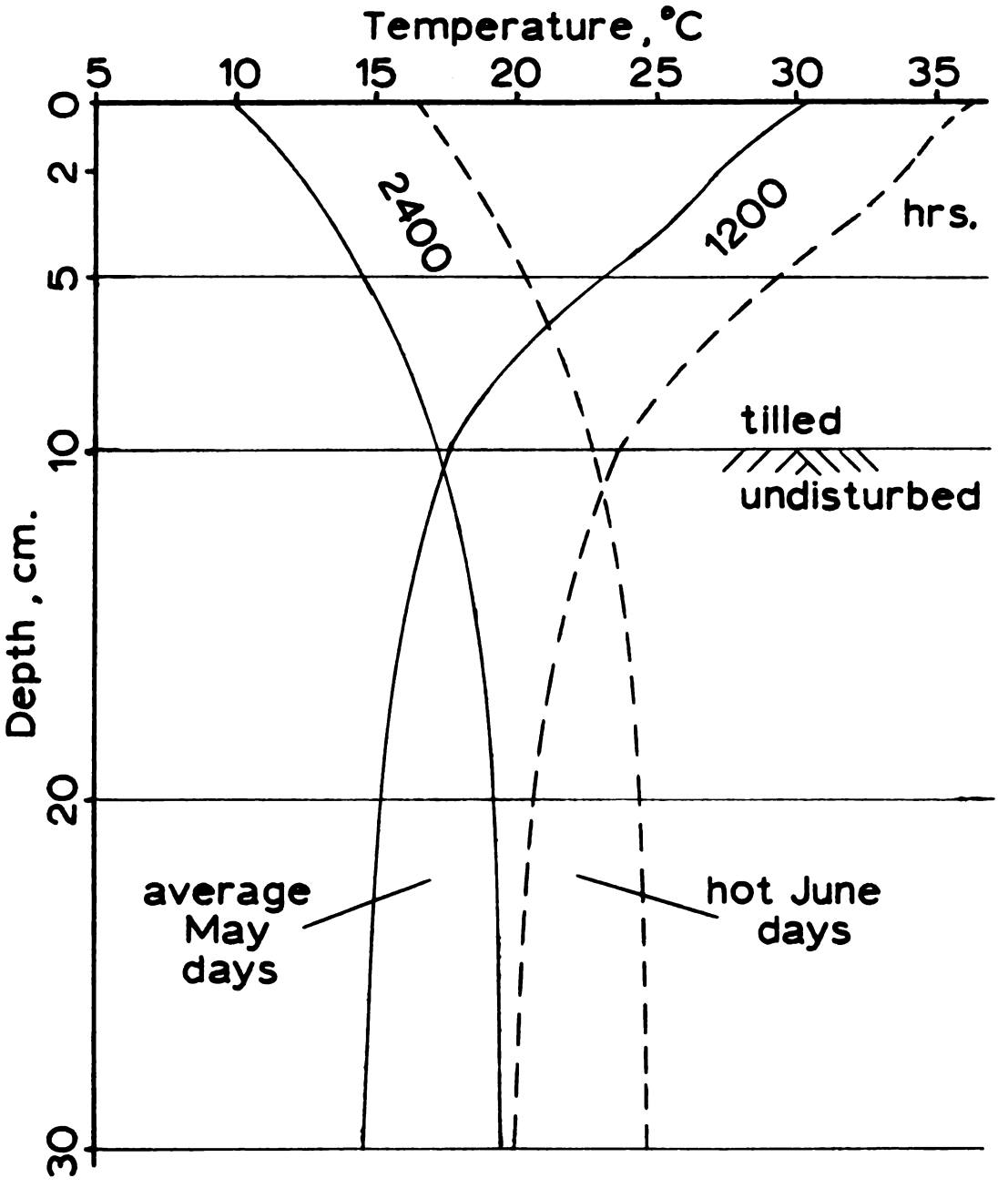


Figure 9.15. Third Day Temperature Profiles in Metea Loam Tilled to 1200 Kg/$m^3$ Exposed to Varying Meteorological Conditions

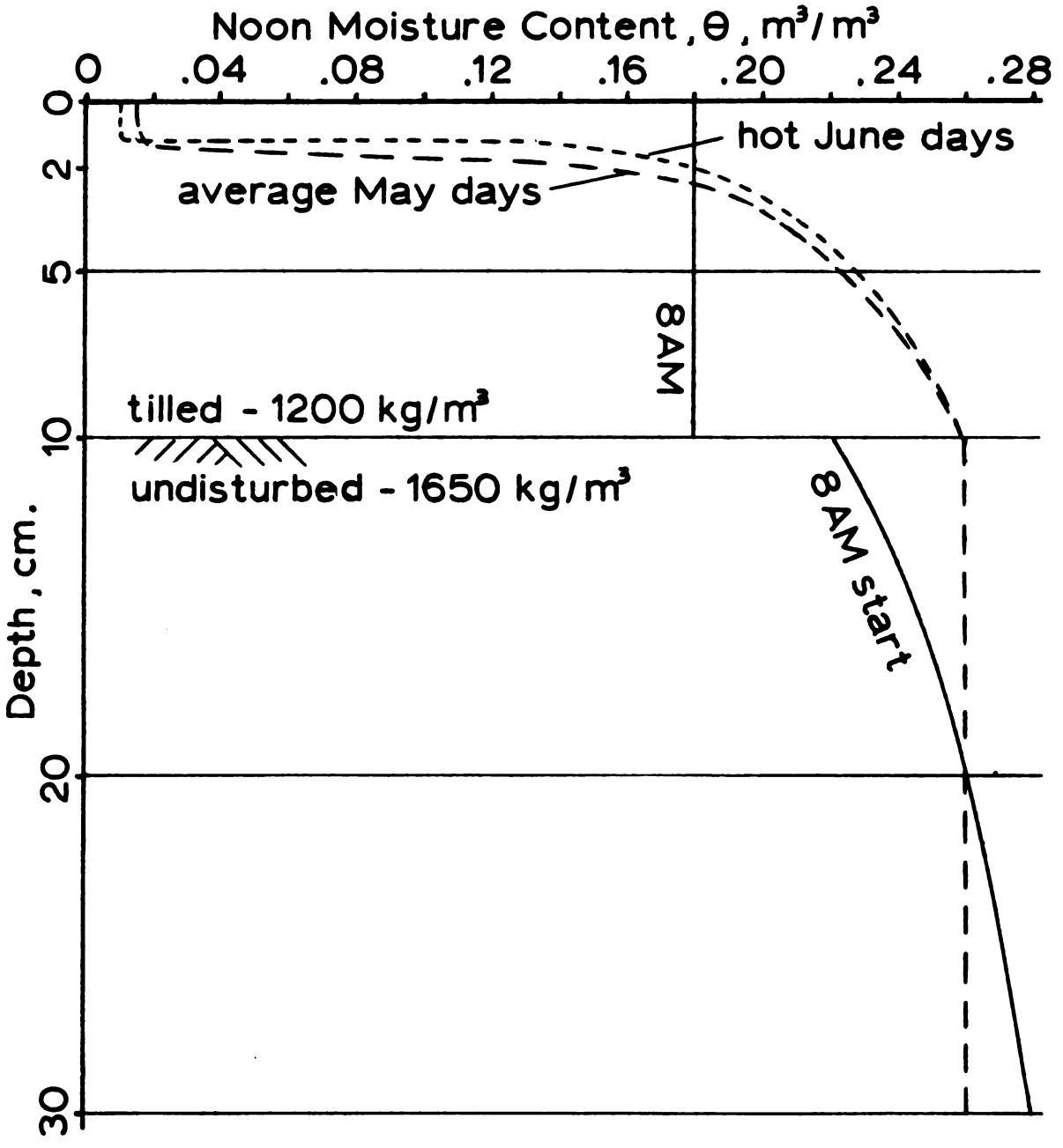


Figure 9.16. Third Day Moisture Profiles in Metea Loam Tilled to 1200 Kg/m$^3$ Exposed to Varying Meteorological Conditions

# 10. CONCLUSIONS AND FUTURE WORK

## 10.1 Summary

This study produced the following, in reference to the seed-soil system model of Figure 1.1:

a. the two-dimensional soil physical model

b. the meteorological model

c. the soil surface interface tying the boundary conditions of the soil model to the meteorological inputs

The model was based on the Galerkin approximation of the finite element method of numerical solutions to simultaneous differential equations relating moisture and temperature interactions. The computer program was developed in the FORTRAN language and run on the IBM 360 computer at Delta College. It was validated with actual field data extracted from the literature, and with few modifications, exhibited good agreement with the data.

Although simultaneous interactions of two phenomena and time-dependent problems have previously been modeled with the finite element method, the model of this study is unique due to the combination outlined below:

1. Uses Galerkin approximation to finite element numerical solution
2. Is two-dimensional and time-dependent
3. Includes simultaneous moisture and temperature interactions
4. Includes heterogeneous soil grid
5. Interfaces with real meteorological model
6. Applies to seed furrow and tillage practice studies

Simulation results shown in Chapter 9 demonstrate that the model can be used to study the following parameters and their effects on soil moisture and temperature:

1. Soil texture of $A_p$ and $B_1$ horizons
2. Soil structure and tillage effects on structure
3. Furrow geometry
4. Meteorological conditions
5. Albedo

## 10.2 Conclusions

The objective of this study was to develop a realistic model of soil moisture and temperature, not to develop new theory. Nevertheless, several conclusions can be drawn from the experience gained in developing the model.

a. Moisture diffusivity due to vapor flow induced by moisture gradients cannot be ignored, and in fact is a significant factor at low moisture content in the surface layers, especially during mid afternoon.

b. The "mass enhancement factor" added to the soil thermal conductivity term in equation [57] fully accounts for heat convection through the soil due to vertical air movement. A separate air convection term using the vertical air velocity gradient $\partial V/\partial z$ in addition to the mass enhancement factor produces excessive heat flow conditions.

c. The soil air mass flow term due to vertical air density gradients, obtained from equation [68],

produces excessive moisture movement. Whereas the theory underpredicts this phenomenon, the model developed in this study overpredicts.

d. The soil moisture diffusivity due to temperature gradients is several orders of magnitude smaller than that due to moisture gradients. Only at very dry conditions below the wilting point does $D_\theta$ sink to a level where $D_T$ becomes significant.

## 10.3 Future Work

The models developed from this work could be considered a good start towards the attainment of the long-range goal identified in Section 1.3. Yet a great deal of work needs to be done before the seed-soil system model of Figure 1.1 can be realized. This work can be categorized as follows:

1. Second validation of the present models
2. Refinement of parameters of present models
3. Expansion of utility of present models
4. Development of three-dimensional seed model
5. Development of three-dimensional soil model with moisture, temperature and oxygen parameters.
6. Linking of all models into seed-soil system model.

### 10.3.1 Second Validation

Although the soil model has shown good agreement with field data from one study, a second validation with a different soil under different weather conditions would add credibility to the model. Field data for such a validation

would need to supply the inputs listed in Sections 4.7 and 5.3. At the time of this study, sufficient published data were not available for a second validation. The field study by Jackson, et al. (1973, 1975) came the closest to supplying all inputs, but several key parameters were missing.

### 10.3.2 Refinement of Parameters

Chapter 8 dealt with model refinements conducted during this study. Although refining a model is virtually a continuous process as experience with it accumulates, several specific suggestions are listed here which could improve the accuracy of the model.

a. Surface conditions. Section 8.2.1 explained the physical constraint imposed on the surface temperature in order to suppress oscillations in the finite element solution. The surface condition requires further development and may justify a separate model to be interfaced with the soil model.

Closely coupled with this are the evaporation and sensible heat flux terms in the surface energy balance equation explained in Section 8.2.3. Although these were taken directly from the literature, closer study of their interactions would possibly benefit the overall seed-soil system model.

b. Soil moisture diffusivity $D_\theta$. The moisture diffusivity $D_\theta$ was used with relationships based on the most advanced theory to date. However, these relationships,

embodied in equations [44] and [47], are still only approximations, with limitations to their applicability to all soil classes. The expression for saturated hydraulic conductivity as a function of density, equation [86], is also an approximation. The soil model will have to incorporate improvements in these relationships as theory is refined in the future.

c. Hysteresis. Although the model incorporates hysteretic effects in the soil, virtually no field data are available to verify this parameter. The development of adsorption data in the field for modeled soils is necessary to quantify this part of the model.

10.3.3 Model Expansion

a. The use of the soil model to simulate conservation tillage or minimum tillage practices will be enhanced with the incorporation of a surface model which represents corn stalks and other surface residue. It will affect such parameters as albedo and surface roughness, and would create a separate layer of finite thickness with a unique moisture diffusivity, thermal conductivity and heat capacitance. Literature on this topic is still sketchy, and considerable research is implied.

b. The model in its present form accepts a diurnal cycle of weather conditions which is the same every day. More realistic conditions can be simulated if the average and amplitude of each cycle can be changed from day to day.

c. Presently the model does not accept a rainfall. The incorporation of this weather condition is important when expanding the model's use to the study of seed response to oxygen deficiency.

10.3.4 The Three-Dimensional Seed Model.

Referring back to Figure 1.1, a three-dimensional seed biophysical model must be developed to determine the hourly viability of the seed in response to its environment. This model must represent the biophysical processes within a given seed which would include temperature, moisture, and oxygen cause-effect relationships. Throughout the past few decades, a number of investigators have studied the biophysical processes of germinating seeds. The author has literature on seed studies dating to 1916, and recent partial models advanced, exemplified by that by Waggoner and Parlange (1976), would indicate at least a crude model could be developed, drawing from submodels found in the literature.

10.3.5 The Three-Dimensional Soil Model.

A spherical soil shell wrapped around the spherical seed model needs to be developed to interact directly with the seed. According to Figure 1.1, at each time step, this soil shell receives its moisture and temperature distribution from the two-dimensional soil model. The shell's radius extends out from the seed center only to the extent

of the seed's influence. This model would include a spherical seed-soil interface providing impedance to heat, moisture and oxygen exchange between the seed and soil.

The author is aware of several studies of seed imbibition as affected by seed-soil contact area. Earlier investigations are represented by Collis-George and Hector (1966) and Hadas (1969). More recent work is represented by Bruckler (1983) and Boiffin, et al. (1983).

### 10.3.6 The Seed-Soil System Model.

Once the various component models have been verified and refined, a final linking together is necessary to obtain a harmonious flow as outlined in Figure 1.1.

# LIST OF REFERENCES

## LIST OF REFERENCES


1. Allmaras, R.R. et al.
1977. Surface energy balance and soil thermal property modifications by tillage-induced soil structure. Minnesota Agric. Exp. Sta. Technical Bulletin 306.

2. Arkin, G.F. et al.
1980. Forecasting grain sorghum yields using simulated weather data and updating techniques. Transactions of American Society of Agricultural Engineers, 23(3):676-680.

3. Baker, D.G. and D.A. Haines.
1969. Solar radiation and sunshine duration relationships in the North-Central Region and Alaska. North Central Regional Research Publication 195, Technical Bulletin 262. Agric. Exp. Sta. Univ. of Minnesota.

4. Baker, D.G. and J.C. Klink.
1975. Solar radiation reception, probabilities, and areal distribution in the North-Central Region. North Central Regional Research Publication 225, Technical Bulletin 300. Agric. Exp. Sta. Univ. of Minnesota.

5. Boiffin, J. et al.
1983. Role des proprietes physiques du lit de semences sur l'imbibition et al germination. III. Valeur previsionnelle d'un modele d'imbibition au champ et caracterisation des lits de semences. Agronomie 3(4):291-302.

6. Bresler, E. et al.
1969. Infiltration, redistribution and subsequent evaporation of water from soil as affected by wetting rate and hysteresis. Soil Science Society of America Proceedings, 33:832-839.

7. Bruce, R.R.
1972. Hydraulic conductivity evaluation of the soil profile from soil water retention relations. Soil Science Society of America Proceedings, 36:555-561.

8. Bruce, R.R. et al.
1977. Diurnal soil water regime in the tilled plow layer of a warm humid climate. Soil Science Society of America Journal, 41:455-460.

9. Bruckler, L.
1983. Role des proprietes physiques du lit de semences sur l'imbibition et la germination. I. Elaboration d'un modele du systeme terre-graine. II. Controle experimental d'un modele d'imbibition des semences et possibilites d'applications. Agronomie 3(3):213-222 and 223-232.

10. Cary, J.W. and S.A. Taylor.
1962a. The interaction of the simultaneous diffusions of heat and water vapor. Soil Science Society of America Proceedings, 26:413-416.

11. Cary, J.W. and S.A. Taylor.
1962b. Thermally driven liquid and vapor phase transfer of water and energy in soil. Soil Science Society of America Proceedings, 26:417-420.

12. Cary, J.W.
1965. Water flux in moist soil: thermal versus suction gradients. Soil Science, 100 (3):168-175.

13. Collis-George, N. and J.B. Hector.
1966. Germination of seeds as influenced by matrix potential and by area of contact between seed and soil water. Australian Journal of Soil Research, 4:145-164.

14. Cruse, R.M. et al.
1980. A model to predict tillage effects on soil temperature. Soil Science Society of America Journal, 44:378-383.

15. Cushman, J.H. and Kirkham, D.
1978. A two-dimensional linearized view of one-dimensional unsaturated-saturated flow. Water Resources Research, 14(2):319-323.

16. Cushman, J.H. et al.
1979. A Galerkin in time, linearized finite element model of two-dimensional unsaturated porous media drainage. Soil Science Society of America Journal, 43:638-641.

17. DeVries, D.A.
1958. Simultaneous transfer of heat and moisture in porous media. Transactions of American Geophysical Union, 39(5):909-915.

18. DeVries, D.A.
1963. Thermal properties of soils. In: VanWijk, Physics of Plant Environment. North-Holland Publishing Co. Amsterdam, Div. of John Wiley & Son, NY:210-235.

19. Farrell, D.A. et al.
1966. Vapor transfer in soil due to air turbulence. Soil Science, 102:305-313.

20. Fukuda, H.
1955. Air and vapor movement in soil due to wind gustiness. Soil Science, 79:249-258.

21. Gebhart, B.
1961. Heat Transfer. McGraw-Hill Book Co., Inc. New York.

22. Ghosh, R.K.
1980. Estimation of soil-moisture characteristics from mechanical properties of soils. Soil Science, 130(2):60-63.

23. Gray, W.G. and G.F. Pinder.
1974. Galerkin approximation of the time derivative in the finite element analysis of groundwater flow. Water Resources Research, 10(4):821-828.

24. Gustafson, R.J. et al.
1979. Temperature and stress analysis of corn kernel-finite element analysis. Transactions of American Society of Agricultural Engineers, 22(4):955-960.

25. Hadas, A.
1968. Simultaneous flow of water and heat under periodic heat fluctuations. Soil Science Society of America Proceedings, 32(3):297-301.

26. Hadas, A.
1969a. A comparison between predicted and measured values of the thermal conductivity of a moist soil under steady and fluctuating thermal regimes. Israel Journal of Agricultural Research, 19(4):151-159.

27. Hadas, A.
1969b. Effects of soil moisture stress on seed germination. Agronomy Journal, 61(2):325-327.

28. Hadas, A.
1977a. Evaluation of theoretically predicted thermal conductivities of soils under field and laboratory conditions. Soil Science Society of America Journal, 41:460-466.

29. Hadas, A.
1977b. Heat transfer in dry aggregated soil: I. Heat conduction. Soil Science Society of America Journal, 41:1055-1059.

30. Haghighi, K. and L.J. Segerlind.
1978. Computer simulation of the stress cracking of soybeans, American Society of Agricultural Engineers paper no. 78-3560. St. Joseph, MI.

31. Haghighi, K.
1979. Finite element formulation of the thermo-hydro stress problem in soybeans, Unpublished Ph.D. Thesis, Michigan State University, East Lansing, MI.

32. Hanks, R.J. and N.P. Woodruff.
1958. Influence of wind on water vapor transfer through soil, gravel, and straw mulches. Soil Science, 86:160-165.

33. Harper, L.A. et al.
1976. Soil and microclimate effects on Trifluralin volatilization. Journal of Environmental Quality, 5(3), July-Sept.

34. Hillel, D.
1971. Soil and Water: Physical Principles and Processes. Academic Press, New York.

35. Hillel, D.
1977. Computer Simulation of Soil-Water Dynamics. International Development Research Center, Ottawa, Canada. -082e:35-78.

36. Hirschi, M.C. and I.D. Moore.
1980. Estimating soil hydraulic properties from soil texture. American Society of Agricultural Engineers paper no. 80-2523. St. Joseph, MI.

37. Hollman, J.P.
1976. Heat Transfer. McGraw-Hill Publishing, New York.

38. Jackson, R.D. et al.
1973. Diurnal soil-water evaporation:time-depth-flux patterns. Soil Science Society of America Proceedings, 37:505-509.

39. Jackson, R.D. et al.
1975. Heat and water transfer in a natural soil environment. In: Heat and Mass Transfer in the Biosphere. John Wiley & Sons, New York:67-76.

40. Judah, O.M. et al.
1975. Finite element simulation of flood hydrographs. Transactions of American Society of Agricultural Engineers, 18(3):518-522.

41. Jury, W.A. and J. Letey.
1979. Water vapor movement in soil: Reconciliation of theory and experiment. Soil Science Society of America Journal, 43:823-827.

42. Kimball, B.A. et al.
1976. Comparison of field-measured and calculated soil-heat fluxes. Soil Science Society of America Proceedings, 40:18-24.

43. Laroussi, C. et al.
1975. Experimental investigation of the diffusivity coefficient. Soil Science, 120 (4):249-255.

44. Luikov, A.V.
1966. Heat and Mass Transfer in Capillary-Porous Bodies. Pergamon Press Ltd. London.

45. Malik, R.S. et al.
1979. Physical components of the diffusivity coefficient. Soil Science Society of American Journal, 43:633-637.

46. Mark's Mechanical Engineers' Handbook. McGraw-Hill Book Co., New York.

47. Merva, G.
1975. Physioengineering Principles. AVI Publishing Co., Westport, Conn.

48. Misra, R.N. and J.H. Young.
1979. The finite element approach for solution of transient heat transfer in a sphere. Transactions of American Society of Agricultural Engineers, 22(4):944-949.

49. Misra, R.N. and J.H. Young.
1980. Numerical solution of simultaneous moisture diffusion and shrinkage during soybean drying. Transactions of American Society of Agricultural Engineers, 23(5):1277-1282.

50. Misra, R.N. et al.
1981. Finite element procedures for estimating shrinkage stresses during soybean drying. Transactions of American Society of Agricultural Engineers, 24(3):751-755.

51. Mualem, Y.
1978. Hydraulic conductivity of unsaturated porous media: Generalized macroscopic approach. Water Resources Research, 14(2):325-334.

52. Ojeniyi, S.O. and A.R. Dexter.
1979. Soil structure changes during multiple pass tillage. Transactions of American Society of Agricultural Engineers, 22(5):1068-1072.

53. Pall, R. and Mohsenin, N.N.
1980. A soil air pycnometer for determination of porosity and particle density. Transactions of American Society of Agricultural Engineers, 23(3):735-741, 745.

54. Pall, R. et al.
1980. Comparison of one-dimensional flow simulation by two numerical methods. American Society of Agricultural Engineers paper no. 80-2526, St. Joseph, MI.

55. Philip, J.R. and D.A. DeVries.
1957. Moisture movement in porous materials under temperature gradients. Transactions of American Geophysical Union, 38(2):222-231.

56. Potter, M.C. and J.F. Foss.
1975. Fluid Mechanics. John Wiley & Sons, New York.

57. Rawls, W.J. et al.
1982. Estimation of soil water properties. Transactions of American Society of Agricultural Engineers, 25(5):1316-1320, 1328.

58. Rose, C.W.
1968a. Water transport in soil with a daily temperature wave: I: Theory and experiment. Australian Journal of Soil Research, 6:31-44.

59. Rose, C.W.
1986b. Water transport in soil with a daily temperature wave: II. Analysis. Australian Journal of Soil Research, 6:45-57.

60. Segerlind, L.J.
1976. Applied Finite Element Analysis. John Wiley & Sons, New York.

61. Sepaskhah, A.R. and L. Boersma.
1979. Thermal conductivity of soils as a function of temperature and water content. Soil Science Society of America Journal, 43:439-444.

62. Townsend, J.S. and P. Migchels.
1981. Albedo of wheatfields under five tillage systems in Manitoba. American Society of Agricultural Engineers paper no. 81-1014. St. Joseph, MI.

63. Tscheschke, P.D. and J.R. Gilley.
1979. Status and verification of Nebraska's corn growth model - CORNGRO. Transactions of American Society of Agricultural Engineers, 22(6):1329-1337.

64. Van Bavel, C.H.M. and D.I. Hillel.
1976. Calculating potential and actual evaporation from a bare soil surface by simulation of concurrent flow of water and heat. Agricultural Meteorology, 17:453-476.

65. VanWijk, W.R.
1963. Physics of Plant Environment. North-Holland Publishing Co., Amsterdam, Division of John Wiley & Sons, New York.

66. Waggoner, P.E. and J. Parlange.
1976. Water uptake and water diffusivity of seeds. Plant Physiology, 57:153-156.

67. Woodside, W. and J.M. Kuzmak.
1958. Effect of temperature distribution on moisture flow in porous materials. Transactions of American Geophysical Union, 39(4):676-680.

68. Zienkiewicz, O.C.
1971. The Finite Element Method in Engineering Science. McGraw-Hill, London.

# APPENDICES

# APPENDIX A

## COMPUTER FLOW DIAGRAM

The flow of information, processing and key decision points of the computer program are outlined in diagram form. This serves as a "bird's eye" view of the total program.

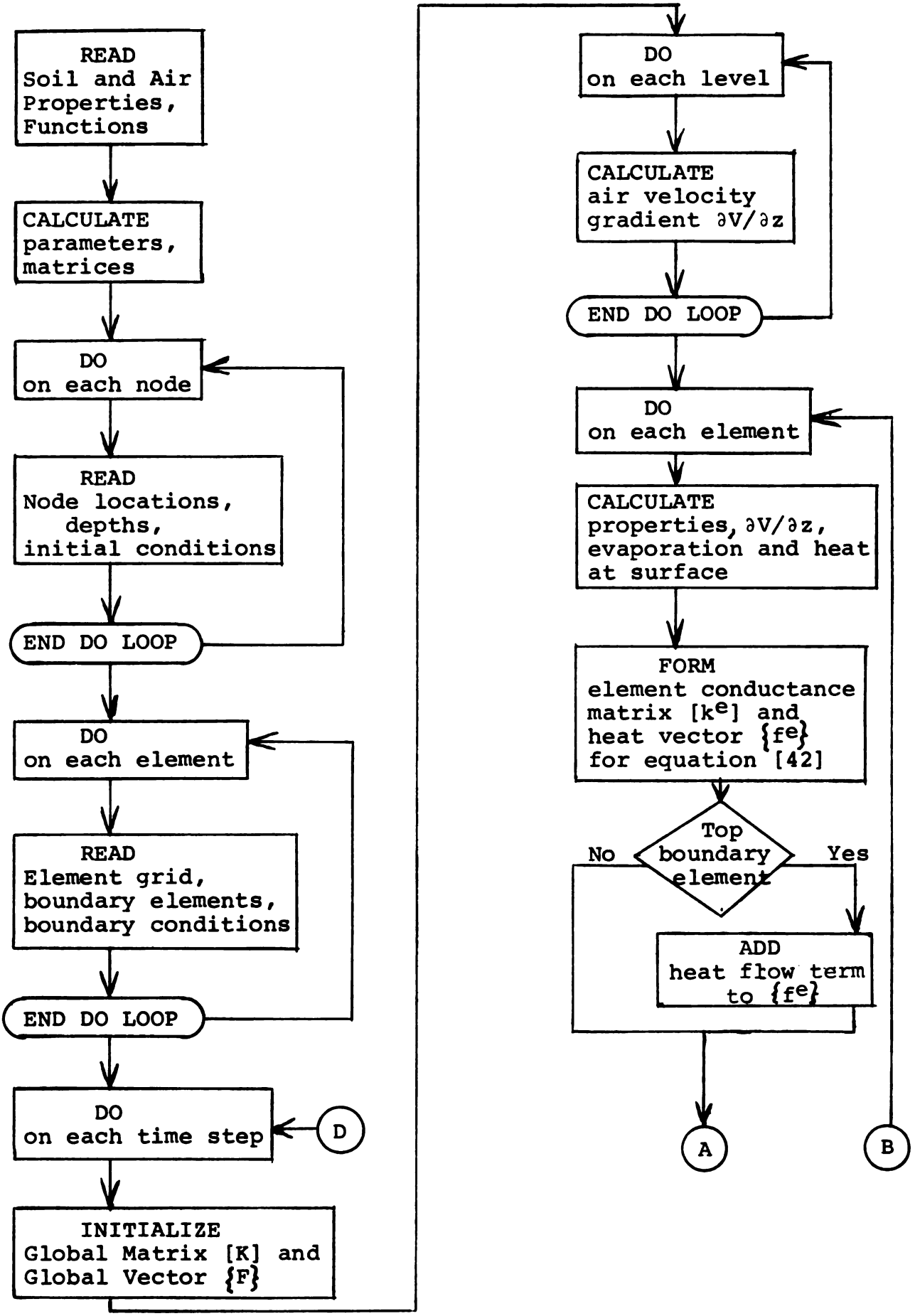


Figure A.1 Computer Flow Diagram

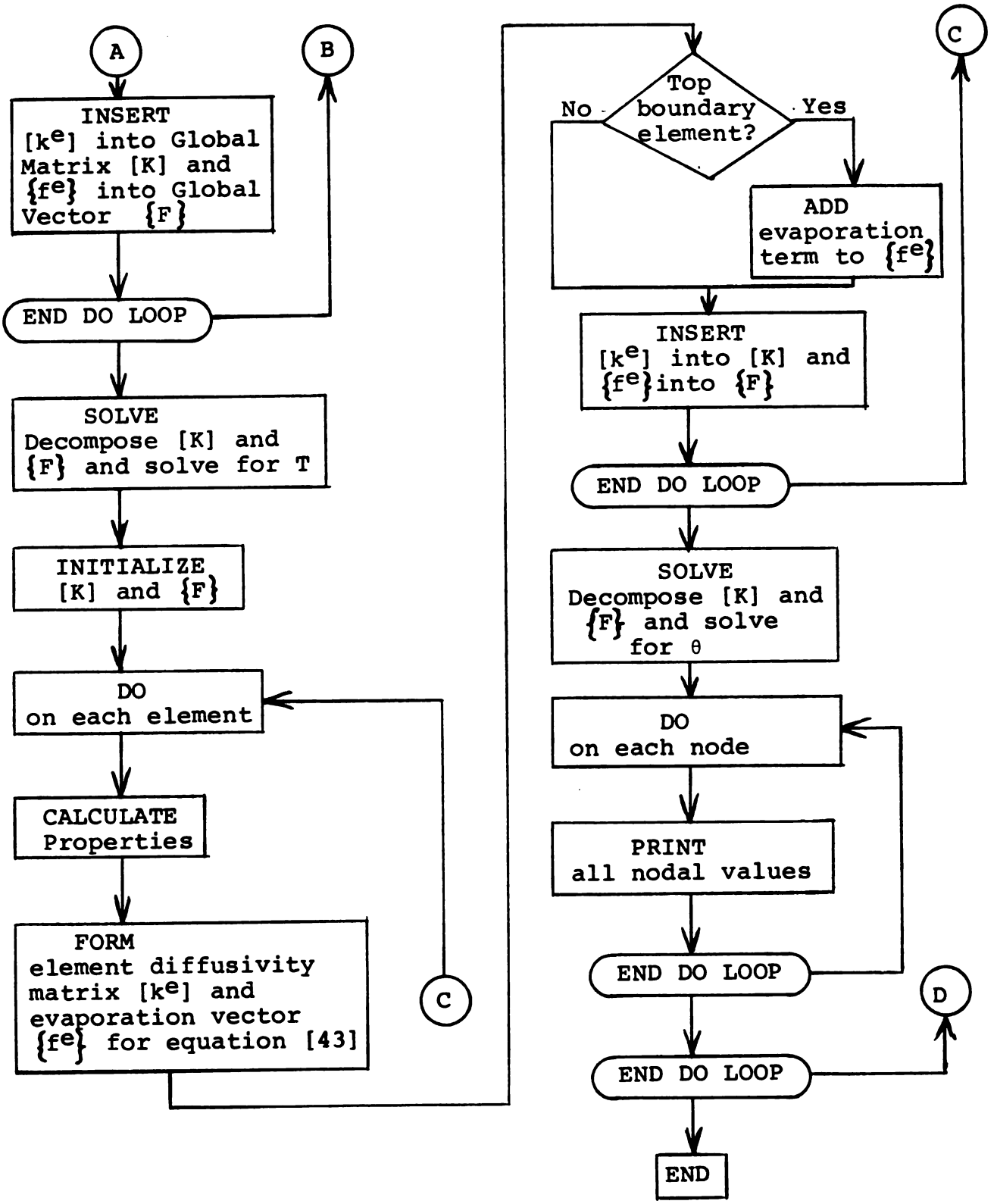
A
B
INSERT
[k^e] into Global
Matrix [K] and
{f^e} into Global
Vector {F}
END DO LOOP
SOLVE
Decompose [K] and
{F} and solve for T
INITIALIZE
[K] and {F}
DO
on each element
CALCULATE
Properties
FORM
element diffusivity
matrix [k^e] and
evaporation vector
{f^e} for equation [43]
C
C
Top
boundary
element?
No
Yes
ADD
evaporation
term to {f^e}
INSERT
[k^e] into [K] and
{f^e} into {F}
END DO LOOP
SOLVE
Decompose [K] and
{F} and solve
for θ
DO
on each node
PRINT
all nodal values
END DO LOOP
D
END DO LOOP
END

# APPENDIX B

## COMPUTER PROGRAM LISTING

The main program and its eight subroutines are listed, complete with sufficient documentation on variables and data entry for the reader to engage in future work.

MAIN PROGRAM DOCUMENTATION

| Computer Variable | Explanation |
|---|---|
| A | vector used to arrange global field variables in column form conducive to solutions in subroutines DCMPBD and SLVBD |
| AM | $\begin{bmatrix} 2 & 1 & 1 \\ 1 & 2 & 1 \\ 1 & 1 & 2 \end{bmatrix}$ |
| AMP | amplitude of horizontal air pressure waves at surface, $sec^{-1}$ |
| AREA | area of element considered |
| B and CI vectors | elements in the BC matrix |
| BC | common matrix used to build element conductance and diffusion matrices |
| BLK | bulk density of tilled soil, $kg/m^3$ |
| BULK | soil bulk density, $kg/m^3$, generally of undisturbed soil |
| C, $C_g$ | heat capacity of total soil volume and air-vapor mixture, product of subroutine CAP |
| DIFM | element moisture diffusivity $D_\theta$, product of subroutine DIFFM |
| DIFT | element moisture diffusivity $D_T$, product of subroutine DIFFT |

| | |
|---|---|
| DVDDZ | vector of $\partial V_D/\partial z$ values for all depths in grid |
| DVDZ | $\partial V/\partial z$ value for element considered, product of subroutine VEL |
| DVS | volume surface mean diameter of soil aggregates of element considered |
| E | surface evaporation vector |
| ECM | element heat conductance matrix [S], 3X3 |
| EDM | element moisture diffusion matrix [R], 3X3 |
| EEV | surface element evaporation force vector |
| EF | intermediate force vector for surface elements used to build final force vectors EHV and EEV<br>build final force vectors EHV and EEV |
| EHV | surface element heat flux force vector |
| ELEV | elevation, meters, where wind, vapor pressure, etc. were measured |
| FREQ | frequency of horizontal air pressure waves at surface, $sec^{-1}$ |
| GCM, GHV | global conductance matrix and global force vector used to store variables in preparation for A vector |
| GGF (no. nodes), GGSM (no. nodes , bandwidth) | global stiffness matrix and global force vector used to solve equations in subroutines DCMPBD and SLVBD |

| | |
|---|---|
| GPHI | field variables (temperature or moisture content) produced from solutions in subroutines DCMPBD and SLVBD |
| HCON | element hydraulic conductivity, product of subroutine DIFFM |
| HCONS | saturated hydraulic conductivity for element considered, m/sec |
| HONS | saturated hydraulic conductivity of tilled soil, m/sec |
| ISP | index to indicate status of soil properties; 0 = all elements same, 1 = some elements are different |
| IT | time increment between successive steps, minutes |
| ITIMET | total time of simulation run, minutes |
| JEND | a pointer indicating the last storage location for [K] in {A} |
| JGF | a pointer indicating the last storage location for {$\phi$} in {A} |
| JGSM | a pointer indicating the last storage location for {F} and {A} |
| LEV | total no. of horizontal levels in grid (surface included) |
| NBW | bandwidth ((R+1)NDOF) used in subroutines DCMPBD and SLVBD (see Segerlind (1976)) |
| NE | total no. of elements |

| | |
|---|---|
| NEB | no. of elements which have boundary conditions |
| NEV | no. elements having soil structure different from the majority. Program allows two different sets of properties (i.e. tilled vs. undisturbed) |
| NEVT | no. elements with texture different from majority (usually $B_1$ horizon) |
| NI, NJ, NK | three nodes of element considered |
| NIP | no. implement passes |
| NLEV1 | first node at specific depth considered |
| NLEV2 | second node at specific depth considered |
| NN | total no. of nodes |
| NNV | no. nodes having initial $\theta$ or T different from majority |
| NP | no. global degrees of freedon used in subroutines DCMPBD and SLVBD (no. unknowns per node X NN) |
| NS vector | node number variable used to build A vector |
| P | soil air porosity |
| PSI | element matric potential $\psi$, product of subroutine DIFFM |
| PSIE, PSIEA | air-entry soil matric potential for element considered, desorption and adsorption, m $H_2O$ |
| QAV, QAM | average, amplitude of total global |

| | |
|---|---|
| | irradiance, $W/m^2$ |
| QM | matrix used to build EF vector for moisture |
| QRGA | time-varying function for global radiation |
| QS | surface sensible heat flow vector |
| RAV, RAM | average, amplitude of air relative humidity |
| RHA | time-varying function for air relative humidity |
| RM2 | matrix used to build EF vector for moisture |
| S | total soil porosity |
| SAA | time-varying function for air wind speed |
| SAND, SILT, CLAY | % sand, silt, clay of $B_1$ horizon |
| SAV, SAM | average, amplitude of air wind speed, m/sec |
| SIE, SIEA | air-entry matric potential, m $H_2O$, of tilled soil, desorption and adsorption |
| SM2 | matrix used to build EF vector for temperature |
| SND, SLT, CLY | % sand, silt, clay of $A_p$ horizon |
| TAV, TAM | average, amplitude of air temperature,°C |
| TCON | thermal conductivity, product of subroutine THCON |
| TE1, TH1 | nodal temperature and moisture content from previous time step, used as |

| | |
|---|---|
| | initial conditions |
| TE2, TH2 | nodal temperature and moisture content calculated at present time step |
| TEAA | time-varying function for air temperature |
| TESO | temperature of surface nodes at previous time step, used for averaging for surface T's |
| TH, TE | moisture content and temperature (°C) of element |
| THØ | moisture content of element's nodes from two time steps back, used in subroutine DIFFM to identify whether element is adsorbing or desorbing |
| THØS | moisture content of surface element from two time steps back |
| THI, TEI | initial moisture content and temperature of tilled nodes |
| THO | vector used to build EF vector for moisture |
| THSO | moisture content of surface nodes at previous time step used for averaging for surface θ's |
| THV | element volumetric vapor content, $\theta_v$, product of subroutine CAP |
| THWP | immobile moisture content level in soil |
| TITLE | title of mainprogram |

| | |
|---|---|
| TO | vector used to build EF vector for temperatures |
| TOF | vector used to build EF vector for moistures |
| TS, THS | temperature, moisture content of surface of surface element considered for present time step |
| X, Z | x and z coordinates of node considered |
| ZLEV | vector of z coordinates of depths in grid (surface z = 0) |
| ZO | surface roughness, m |

## ADDITIONAL EXPLANATIONS

| Reference | Explanation |
|---|---|
| After statement 28 | These are special input statements to build initial $\theta$, T, and $\rho_B$ gradients throughout the soil profile |
| Comment statement after statement 35 | This calculates $\partial V_D/\partial z$ at each horizontal level in the profile. Soil profile is first divided into at most 10 horizontal levels. The levels are numbered 1, 2, 3, etc. from the surface down, with surface as no. 1. Using air velocity at bottom level as 0, calculate the velocity VDU at upper boundary of the bottom slab. Calculate $\partial V_D/\partial z$ for that slab and record. Go to the next slab, above it. Using previously calculated VDU now as VDL, recalculate VDU for new slab, record new $\partial V_D/\partial z$, etc. |
| Comment statement before statement 750 | This calculates $\partial V_D/\partial z$ for each element considered. Find the element vertically in the soil profile between two recorded levels, assign the $\partial V_D/\partial z$ of that slab to the element considered. |

Table B.1. Computer Program

MAINPGM

```
C    TIME-DEPENDENT BOUNDARY CONDITIONS.
       RHA(TME,RV,RM)=RV+RM*COS(3.1416*(TME/12.0-0.25))
       QRGA(TME,QV,QM)=QV+QM*SIN(3.1416*(TME/12.0-0.583))
       SAA(TME,SV,SM)=SV+SM*SIN(3.14159*(TME/12.0-0.583))
       TEAA(TME,TV,TM)=TV+TM*SIN(3.1416*(TME/12.0-0.583))
       DIMENSION B(3),CI(3),NS(3),E(12),QS(12),TO(3),TITLE(20),TOF(3)
       DIMENSION THO(3),EEV(3),AM(3,3),ECM(3,3),EHV(3),ECM(3,3)
       DIMENSION SM2(3,3),RM2(3,3),QM(3,3)
       DIMENSION ZLEV(10),NLEV1(10),NLEV2(10),DVDDZ(9)
       DIMENSION NI(54),NJ(54),NK(54),BULK(54),DVDZ(54),AREA(54)
       DIMENSION PSIE(54),PSIEA(54),HCONS(54),BC(54,3,3),DVS(54)
       DIMENSION THSO(40), TESO(40),THO(40)
       DIMENSION SND(54),SLT(54),CLY(54)
       DIMENSION X(40),Z(40),TH1(40),TE1(40),TH2(40),TE2(40),A(36C)
       DIMENSION GGSM(36,6),GGF(36),GPHI(36),GCM(36,36),GHV(36)
C   ENTER GRID DATA,SOIL AND AIR PROPERTIES, INITIAL CONDITIONS.
       DATA BULK/54*1080.0/,PSIE/54*-.1017/,PSIEA/54*-.1017/
       DATA IN/1/,IC/3/
       DATA SND/54*.635/,SLT/54*.218/,CLY/54*.147/
       DATA TH1/40*0.03/,TE1/40*23.0/,HCONS/54*7.19E-6/
       DATA ID1/0/
       READ(IN,7) TITLE
     7 FORMAT(20A4)
       WRITE(ID,780) TITLE
   780 FORMAT(1H1///1X,20A4)
C BUILD AM MATRIX.
       DO 794 I=1,3
       DO 794 J=1,3
   794 AM(I,J)=0.0
       DO 795 I=1,3
   795 AM(I,I)=1.0
       READ(IN,10) NN,NE,ISP,NEV,NNV,NEB,NBW,LEV,ITIMET,IT,NEVT,NIP
    10 FORMAT(12I5)
       TNIP=NIP
       READ(IN,11) FREQ,AMP,ZO,SANC,SILT,CLAY,ELEV,THWP
    11 FORMAT(8F10.5)
       JP=NE-NEVT+1
       DO 12 J=JP,NE
       SNC(J)=SAND
       SLT(J)=SILT
       CLY(J)=CLAY
    12 CONTINUE
       PVS=(1.025**3*SAND+0.026**3*SILT+0.001**3*CLAY)*0.001/(1.025**2*SA
      1ND+0.026**2*SILT+0.001**2*CLAY)
       DO 13 N=1,NE
    13 DVS(N)=PVS
       READ(IN,16) RAV,RAM,TAV,TAM,SAV,SAM,QAV,QAM
    16 FORMAT(8F10.4)
       NP=NN
       JGF=NP
       JGSM=JGF*2
       JENC=JGSM+NP*NBW
       DO 760 N=1,NN
   760 READ(IN,17) X(N),Z(N)
```

```
 17 FORMAT(2F5.3)
    IF(ISP.EQ.0) GO TO 30
    READ(IN,18) BLK,SIE,SIEA,HONS,THI,TEI
 18 FORMAT(6F10.5)
    DO 24 J=1,NEV
    READ(IN,22) N
 22 FORMAT(I5)
    BULK(N)=BLK
    DVS(N)=0.0252*EXP(-0.192*TNIP)
    PSIE(N)=SIE
    PSIEA(N)=SIEA
    HCONS(N)=HONS
 24 CONTINUE
    DO 28 J=1,NNV
    READ(IN,25) N
 25 FORMAT(I5)
    TH1(N)=THI
    TE1(N)=TEI
 28 CONTINUE
    DO 417 J6=43,54
417 BULK(J6)=1600.0
    DO 418 J6=13,18
418 BULK(J6)=1200.0
    DO 419 J6=19,24
419 BULK(J6)=1250.0
    DO 420 J6=25,30
420 BULK(J6)=1340.0
    DO 421 J6=31,36
421 BULK(J6)=1415.0
    DO 422 J6=37,42
422 BULK(J6)=1570.0
    DO 423 J6=9,12
    TH1(J6)=.095
    TE1(J6)=25.0
423 CONTINUE
    DO 424 J6=13,16
    TH1(J6)=.12
    TE1(J6)=25.5
424 CONTINUE
    DO 425 J6=17,20
    TH1(J6)=.14
    TE1(J6)=25.5
425 CONTINUE
    DO 426 J6=1,NN
426 THO(J6)=TH1(J6)
    DO 427 J6=21,24
    TH1(J6)=.165
    TE1(J6)=26.0
427 CONTINUE
    DO 428 J6=25,28
    TH1(J6)=.18
    TE1(J6)=27.0
428 CONTINUE
    DO 429 J6=29,32
```

```
      TH1(J6)=.20
      TE1(J6)=27.0
  429 CONTINUE
      DO 411 J6=33,40
      TE1(J6)=27.0
      TH1(J6)=.20
  411 CONTINUE
C  CONNECT NODES TO ELEMENTS.
   30 DO 761 I=1,NE
  761 READ(IN,29) NI(I),NJ(I),NK(I)
   29 FORMAT(3I5)
      DO 740 I=1,LEV
  740 READ(IN,741) ZLEV(I),NLEV1(I),NLEV2(I)
  741 FORMAT(F10.4,2I5)
C BUILD BC MATRIX.
      DO 788 N=1,NE
      N1=NI(N)
      N2=NJ(N)
      N3=NK(N)
      AREA(N)=(X(N2)*Z(N3)+X(N1)*Z(N2)+X(N3)*Z(N1)-X(N2)*Z(N1)-X(N3)*Z(N
     12)-X(N1)*Z(N3))*0.5
      B(1)=Z(N2)-Z(N3)
      B(2)=Z(N3)-Z(N1)
      B(3)=Z(N1)-Z(N2)
      CI(1)=X(N3)-X(N2)
      CI(2)=X(N1)-X(N3)
      CI(3)=X(N2)-X(N1)
      DO 50 I=1,3
      DO 50 J=1,3
   50 BC(N,I,J)=B(I)*B(J)+CI(I)*CI(J)
  788 CONTINUE
C  START DO LOOP FOR TIME STEP.
      DO 200 ITIME=IT,ITIMET,IT
      DO 35 I=1,JEND
   35 A(I)=0.0
      TIME=ITIME
      TIME=TIME/60.0
      TIT=IT
      TIT=TIT/60.0
      RH=RHA(TIME,RAV,RAM)
      TEA=TEAA(TIME,TAV,TAM)
      SA=SAA(TIME,SAV,SAM)
      QRG=QRGA(TIME,QAV,QAM)
      IF(QRG.LT.0.0) QRG=0.0
      AMP=AMP*SA/(SAV+SAM)
C CALCULATE DVDDZ FOR EACH LEVEL.
      VDL=0.0
      K=LEV-1
      DO 745 I=1,K
      J1=LEV-I
      J2=J1+1
      NUP1=NLEV1(J1)
      NUP2=NLEV2(J1)
      NLO1=NLEV1(J2)
```

```
      NLO2=NLEV2(J2)
      TEJ1=(TE1(NUP1)+TE1(NUP2))/2.0
      TEJ2=(TE1(NLO1)+TE1(NLC2))/2.0
      DELT=TEJ2-TEJ1
      IF(DELT.LE.0.0) DELT=0.0
      DELZ=ZLEV(J2)-ZLEV(J1)
      VCL=SQRT(0.0667*DELT*DELZ+VDL**2)
      DVDDZ(I)=(VDU-VDL)/DELZ
      IF(DVDDZ(I).LT.0.0) DVDDZ(I)=0.0
      VDL=VDU
  745 CONTINUE
      DO 811 I=1,NN
      GHV(I)=0.0
      DO 810 J=1,NN
      GCP(I,J)=0.0
  810 CONTINUE
  811 CONTINUE
C   START DO LOOP FOR EACH ELEMENT FOR TEMPERATURES.
      DO 80 N=1,NE
      N1=NI(N)
      N2=NJ(N)
      N3=NK(N)
C CALCULATE DVDDZ FOR THE ELEMENT.
      ZAVG=(Z(N1)+Z(N2)+Z(N3))/3.0
      K=LEV-1
      DO 750 I=1,K
      J1=LEV-I
      J2=J1+1
      IF(ZAVG.LE.ZLEV(J2).AND.ZAVG.GT.ZLEV(J1)) DDZ=DVDDZ(I)
  750 CONTINUE
      TH=(TH1(N1)+TH1(N2)+TH1(N3))/3.0
      TE=(TE1(N1)+TE1(N2)+TE1(N3))/3.0
      S=1.0-BULK(N)/2650.0
      P=S-TH
C   CALCULATE THERMAL CONDUCTIVITY, HEAT CAPACITY.
      CALL THCON(TH,S,P,TE,SND(N),SLT(N),CLY(N),TCON)
      CALL CAP(S,P,TH,TE,CG,C,THV)
C   CALCULATE VELOCITY GRADIENT.
      CALL VEL(DDZ,Z(N1),P,DVS(N),FREQ,AMP,DVDZ(N))
      IF(N.GT.NE8) GO TO 48
C   CALCULATE EVAPORATION AND HEAT FLOW AT SURFACE.
      TS=(TE1(N1)+TE1(N2))/2.0
      THS=(TH1(N1)+TH1(N2))/2.0
      THCS=(THO(N1)+THO(N2)+THO(N3))/3.0
      CALL DIFFM(S,PSIE(N),PSIEA(N),THOS,TE,P,SND(N),SLT(N),CLY(N),TH,TH
     1WP,HCONS(N),HCON,DIFF,PSI)
      CALL EVAP(RH,TEA,ZO,ELEV,SA,ORG,PSI,TS,E(N),THS,QS(N),N)
C CALCULATE ELEMENT COND. MATRIX,HEAT VECTOR FOR TEMP.EQUATIONS.
   48 PZ=TCON*TIT*150.0/AREA(N)
      QZ=C*AREA(N)/24.0
      DO 61 I=1,3
      DO 60 J=1,3
      ECP(I,J)=3.0*PZ*BC(N,I,J)+8.0*QZ*AM(I,J)
      SM2(I,J)=3.0*PZ*BC(N,I,J)-8.0*QZ*AM(I,J)
```

```
   60 CONTINUE
   61 CONTINUE
      TO(1)=TE1(N1)
      TO(2)=TE1(N2)
      TO(3)=TE1(N3)
      DO 71 I=1,3
      EF=0.0
      DO 70 J=1,3
      ST=SM2(I,J)*TO(J)
      EF=EF+ST
   70 CONTINUE
      EHV(I)=-EF
   71 CONTINUE
      IF(N.GT.NEB) GO TO 72
      DO 67 I=1,2
   67 EHV(I)=EHV(I)+(X(N2)-X(N1))*TIT*1800.0*QS(N)
   72 DO 821 I=1,3
      IF(I.EQ.1) K=N1
      IF(I.EQ.2) K=N2
      IF(I.EQ.3) K=N3
      GHV(K)=GHV(K)+EHV(I)
      DO 820 J=1,3
      IF(J.EQ.1) L=N1
      IF(J.EQ.2) L=N2
      IF(J.EQ.3) L=N3
      GCM(K,L)=GCM(K,L)+ECM(I,J)
  820 CONTINUE
  821 CONTINUE
C  INSERT ELEMENT PROPERTIES INTO GLOBAL A VECTOR.
      NS(1)=N1
      NS(2)=N2
      NS(3)=N3
      DO 77 I=1,3
      II=NS(I)
      J5=NP+II
      A(J5)=A(J5)+EHV(I)
      DO 76 J=1,3
      JJ=NS(J)-II+1
      IF(JJ)76,76,75
   75 J5=JGSM+(JJ-1)*NP+II
      A(J5)=A(J5)+ECM(I,J)
   76 CONTINUE
   77 CONTINUE
   80 CONTINUE
      WRITE(IO,84)TIME
   84 FORMAT(//3X,30HTEMPERATURES(C) FOR HOUR NUM. ,F6.2//)
      DO 660 I=1,NP
  660 GGF(I)=A(JGF+I)
      DO 675 J=1,NBW
      DO 670 I=1,NP
      K=(J-1)*NP+I
      GGSM(I,J)=A(JGSM+K)
  670 CONTINUE
  675 CONTINUE
```

```
      CALL DCMPRD(GGSM,NP,NBW)
      CALL SLVBD(GGSM,GGF,GPHI,NP,NBW,ID)
      DO 122 I=1,NN
      TE2(I)=GPHI(I)
      IF(TE2(I).LT.TE1(I)-4.0) TE2(I)=TE1(I)-4.0
      IF(TE2(I).GT.TE1(I)+4.0) TE2(I)=TE1(I)+4.0
      IF(TE2(I).LT.0.0) TE2(I)=0.0
  122 CONTINUE
      WRITE(IO,264) (I,TE2(I),I=1,NN)
  264 FORMAT(1X,I3,E14.5,3X,I3,E14.5,3X,I3,E14.5,3X,I3,E14.5,3X,I3,E14.5
     1)
      DO 120 I=1,JEND
  120 A(I)=0.0
      DO 840 I=1,NN
      GHV(I)=0.0
      DO 839 J=1,NN
      GCM(I,J)=0.0
  839 CONTINUE
  840 CONTINUE
C   START DO LOOP FOR EACH ELEMENT FOR MOISTURES.
      DO 180 N=1,NE
      N1=NI(N)
      N2=NJ(N)
      N3=NK(N)
      TH=(TH1(N1)+TH1(N2)+TH1(N3))/3.0
      TE=(TE1(N1)+TE1(N2)+TE1(N3))/3.0
      THOZ=(THO(N1)+THO(N2)+THO(N3))/3.0
      S=1.0-BULK(N)/2650.0
      P=S-TH
C   CALCULATE VAPOR , VELOCITY GRADIENT, MOISTURE DIFFUSIVITIES.
      CALL CAP(S,P,TH,TE,CG,C,THV)
      CALL DIFFM(S,PSIE(N),PSIEA(N),THOZ,TE,P,SND(N),SLT(N),CLY(N),TH,TH
     1WP,HCONS(N),HCON,DIFM,PSI)
      CALL DIFFT(HCON,PSI,S,TH,TE,P,DIFT)
C CALCULATE ELEMENT DIFFUS. MATRIX AND EVAP. VECTOR FOR MOISTURE EQUAT.
      SZ=TIT*450.0*DIFT/AREA(N)
      TZ=DIFM*TIT*450.0/AREA(N)
      DO 131 I=1,3
      DO 130 J=1,3
      EDM(I,J)=TZ*BC(N,I,J)+(4.0*AREA(N)/12.0)*AM(I,J)
      RM2(I,J)=TZ*BC(N,I,J)-(4.0*AREA(N)/12.0)*AM(I,J)
      QM(I,J)=SZ*BC(N,I,J)
  130 CONTINUE
  131 CONTINUE
      TOF(1)=TE1(N1)+TE2(N1)
      TOF(2)=TE1(N2)+TE2(N2)
      TOF(3)=TE1(N3)+TE2(N3)
      THC(1)=TH1(N1)
      THC(2)=TH1(N2)
      THC(3)=TH1(N3)
      DO 135 I=1,3
      EF=0.0
      DO 134 J=1,3
      ST=RM2(I,J)*THC(J)+QM(I,J)*TOF(J)
```

```
      EF=EF+ST
  134 CONTINUE
      EEV(I)=-EF+THV*DVDZ(N)*TIT*1200.0*AREA(N)
  135 CONTINUE
      IF(N.GT.NEB) GO TO 147
      DO 138 I=1,2
  138 EEV(I)=EEV(I)-(X(N2)-X(N1))*TIT*1800.0*E(N)
  147 DO 851 I=1,3
      IF(I.EQ.1) K=N1
      IF(I.EQ.2) K=N2
      IF(I.EQ.3) K=N3
      GHV(K)=GHV(K)+EEV(I)
      DO 850 J=1,3
      IF(J.EQ.1) L=N1
      IF(J.EQ.2) L=N2
      IF(J.EQ.3) L=N3
      GCM(K,L)=GCM(K,L)+EDM(I,J)
  850 CONTINUE
  851 CONTINUE
C  INSERT ELEMENT PROPERTIES INTO A GLOBAL VECTOR.
      NS(1)=N1
      NS(2)=N2
      NS(3)=N3
      DO 152 I=1,3
      II=NS(I)
      J5=NP+II
      A(J5)=A(J5)+EEV(I)
      DO 151 J=1,3
      JJ=NS(J)-II+1
      IF(JJ)151,151,150
  150 J5=JGSM+(JJ-1)*NP+II
      A(J5)=A(J5)+EDM(I,J)
  151 CONTINUE
  152 CONTINUE
  180 CONTINUE
      WRITE(IO,184)TIME
  184 FORMAT(//3X,24HMOISTURES FOR HOUR NUM. ,F6.2//)
      DO 680 I=1,NP
  680 GGF(I)=A(JGF+I)
      DO 685 J=1,NBW
      DO 682 I=1,NP
      K=(J-1)*NP+I
      GGSM(I,J)=A(JGSM+K)
  682 CONTINUE
  685 CONTINUE
      CALL DCMPBD(GGSM,NP,NBW)
      CALL SLVBD(GGSM,GGF,GPHI,NP,NBW,ID)
      DO 187 I=1,NN
      TH2(I)=GPHI(I)
      IF(TH2(I).LT.THWP/2.0) TH2(I)=THWP/2.0
  187 CONTINUE
      WRITE(IO,265) (I,TH2(I),I=1,NN)
  265 FORMAT(1X,I3,E14.5,3X,I3,E14.5,3X,I3,E14.5,3X,I3,E14.5,3X,I3,E14.5
     1)
```

```
      DO 190 K=1,NN
      TE1(K)=TE2(K)
      THC(K)=TH1(K)
      TH1(K)=TH2(K)
  190 CONTINUE
  200 CONTINUE
      STOP
      END
```

DIFFM

```
      SUBROUTINE DIFFM(DS,DPSIE,DPSIEA,THM,DTE,DP,DSA,DSI,DCL,DTH,DTHWP,
     1DHCCNS,DHCCN,DCFM,DPSI)
      IF((DTH-THM).GT.0.0) GO TO 4
      PSIA=DPSIE
      GO TO 6
    4 PSIA=DPSIEA
    6 D1=DSI/DSA
      D2=5.91*DCL/(DSA+DCL)
      D3=6.2*SQRT(D1)-D2
      BET=2.619*D1**0.2822*(D3+0.7)**0.0625*D3**0.125*(D2+1.1)**0.0625
      DPSDTH=-BET*PSIA*DS**BET/DTH**(BET+1.0)
      W=(PSIA/(1.0-BET))*(DS-DS**BET*DTHWP**(1.0-BET))*100.0
      W=ABS(W)
      DHCCN=DHCCNS*(DTH/DS)**(0.015*W+3.0)
      DCFML=CHCON*DPSDTH
      DCFMV=(1.467E-17*DP*((DTE+273.0)**2.3)*DPSDTH)/DTE
      DCFM=DCFML+DCFMV
      DPSI=PSIA*(DS/DTH)**BET
      RETURN
      END
```

# EVAP

```
      SUBROUTINE EVAP(H,TA,DZO,DELEV,DSA,DQRG,DPS,DTS,EVP,DTHS,DQS,NNN)
      DATA IN/1/,IC/3/
      RI=9.81*(DELEV-DZO)*(TA-DTS)/((TA+273.16)*DSA**2)
      IF(RI.GE.0.1)RI=0.09
      ST=1.0/(1.0-10.0*RI)
      RA=(ALOG(DELEV/DZO))**2/(0.168*DSA)
      RC=RA*ST
      EC=1.8*TA+32.0
      PS=0.0604*(1.0365)**EC
      HA=7.366*H*PS/(TA+273.16)
      HO=1.323*EXP(17.27*DTS/(237.3+DTS))/(273.16+DTS)
      HS=HO*EXP(DPS/(46.97*(DTS+273.16)))
      EM=(HS-HA)/RC
      DE=2451150.0*EM
      EVP=EM/1000.0
      QA=1257.0*(DTS-TA)/RC
      IF(QA.LT.0.0) QA=0.0
      IF(QA.GT.30.0) QA=30.0
      QRL=5.67E-8*(TA+273.16)**4*(0.605+0.048*SQRT(1370.0*HA))
      EMIS=0.90+0.18*DTHS
      IF(DTHS.GT.0.25) AL=0.10
      IF(DTHS.LT.0.10) AL=0.25
      IF(DTHS.GE.0.10.AND.DTHS.LE.0.25) AL=0.10+(0.25-DTHS)
      QRN=(1.0-AL)*DQRG+QRL-EMIS*5.67E-8*(DTS+273.16)**4
      IF(QRN.LT.0.0) DE=0.0
      IF(QRN.GT.0.0.AND.DE.GT.QRN*0.75) DE=QRN*0.75
      DQS=QRN-DE-QA
      IF(QRN.GT.0.0.AND.DQS.LT.0.01) DQS=0.0
      IF(NNN.GT.1) GO TO 902
      WRITE(IO,900) QRN,QA,QRL,DQS,DE
  900 FORMAT(/2X,6HQRN = ,E12.3,2X,5HQA = ,E12.3,2X,6HQRL = ,E12.3/2X,5H
     1QS = ,E12.3,2X,4HE = ,E12.3)
  902 RETURN
      END
```

# DIFFT

```
      SUBROUTINE DIFFT(DHCON,DPSI,DS,DTH,CTE,DA,DDT)
      DDTL=-2.09E-3*DHCON*DPSI
      THLK=0.40*DS
      IF(DTH.GT.THLK) GO TO 400
      F=DS
      GA=1.0
      GO TO 410
  400 F=DA*(1.0+DTH/(DS-THLK))
      GA=DA/(DS-THLK)
  410 DATM=5.801E-11*(DTE+273.0)**2.3
      DTADT=0.24*DTH-1.53*DS+2.46
      DE=((DA+DTH*GA)/(DA+0.124*DTH/GA))**2
      DDTV=F*DATM*1.024*1.05E-3*DTADT/1.0E3
      DDT=DDTL+DDTV
      RETURN
      END
```

VEL

```
      SUBROUTINE VEL(DDDZ,Z2,DA,DCVS,DFR,CAMP,DDVDZ)
      DKAS=DDVS**2*1.111E6*DA**3/(1.0-DA)**2
      EX=SQRT(DFR*DA/(20.70*DKAS))*Z2
      DVPDZ=(DFR*DAMP/10.35)*EXP(-EX)
  480 DDVDZ=DVPDZ+DDDZ/40.0
  475 RETURN
      END
```

THCON

```
      SUBROUTINE THCON(DTH,CS,DA,CTE,DSA,CSI,DCL,DL)
      THLK=0.40*DS
      SO=1.0-DS
      PSAN=SO*DSA
      PSIL=SO*DSI
      PCLA=SO*DCL
      Q2=.274
      S2=.611
      C2=.527
      DLV=1.024*1.05E-3*5.801E-11*(DTE+273.0)**2.3*2.451E6
      DLAV=0.2577E-1+1.3*DLV
  450 DKAV=0.333*(2.0/(0.971-0.248*DTH/DS)+1.0/(0.226+0.496*DTH/CS))
      DL=(DTH*.595+DKAV*DA*DLAV+Q2*PSAN*8.799+S2*PSIL*2.179+C2*PCLA*2.97
     15)/(DTH+DKAV*DA+Q2*PSAN+S2*PSIL+C2*PCLA)
  451 RETURN
      END
```

CAP

```
SUBROUTINE CAP(DS,DA,DTH,DTE,DCG,CC,DTHV)
DCG=3.771*DTE**1.015+1.257E3*(1.0-0.90E-6*DTE**1.015)
DC=(1.0-DS)*2.011E6+DTH*4.19E6+DA*DCG
DTHV=0.90E-6*DTE**1.015
RETURN
END
```

# DCMPBD

```
      SUBROUTINE DCMPBD(GSM,NP,NBW)
      DIMENSION GSM(NP,NBW)
      NP1=NP-1
      DO 226 I=1,NP1
      MJ=I+NBW-1
      IF(MJ.GT.NP) MJ=NP
      NJ=I+1
      MK=NBW
      IF((NP-I+1).LT.NBW) MK=NP-I+1
      ND=0
      DO 225 J=NJ,MJ
      MK=MK-1
      ND=ND+1
      NL=ND+1
      DO 225 K=1,MK
      NK=ND+K
  225 GSM(J,K)=GSM(J,K)-GSM(I,NL)*GSM(I,NK)/GSM(I,1)
  226 CONTINUE
      RETURN
      END
```

```
      SUBROUTINE SLVBD(GSM,GF,PHI,NP,NBW,IC)
      DIMENSION GSM(NP,NBW),GF(NP),PHI(NP)
      DATA IN/1/,IO/3/
      NP1=NP-1
C  DECOMPOSITION OF THE COLUMN VECTOR GF( )
      DO 250 I=1,NP1
      MJ=I+NBW-1
      IF(MJ.GT.NP) MJ=NP
      NJ=I+1
      L=1
      DO 250 J=NJ,MJ
      L=L+1
  250 GF(J)=GF(J)-GSM(I,L)*GF(I)/GSM(I,1)
C  BACKWARD SUBSTITUTION FOR DETERMINATION OF PHI( )
      PHI(NP)=GF(NP)/GSM(NP,1)
      DO 252 K=1,NP1
      I=NP-K
      MJ=NBW
      IF((I+NBW-1).GT.NP) MJ=NP-I+1
      SUM=0.0
      DO 251 J=2,MJ
      N=I+J-1
  251 SUM=SUM+GSM(I,J)*PHI(N)
  252 PHI(I)=(GF(I)-SUM)/GSM(I,1)
      RETURN
      END
```

# APPENDIX C

## CONVERSION TABLE

The table lists pertinent metric-metric and metric-English unit conversions.

## APPENDIX C

### Table C.1. Conversion Table

| To get ← | Divide by ← | If you have |
|---|---|---|
| If you have → | Multiply by → | To get |
| bar | 0.987 | atmosphere |
| bar | 1017 | cm water |
| bar | 100 | joule/kg |
| calorie/$cm^3$ | 4.186E6 | joule/$meter^3$ |
| calorie/gm | 4186 | joule/kg |
| cm water | 0.0009703 | atmosphere |
| gram/$cm^3$ | 1000 | kg/$meter^3$ |
| inch mercury | 0.03386 | bar |
| joule | 0.2389 | calorie |
| langley | 1.0 | calorie/$cm^2$ |
| langley/minute | 697.5 | watt/$meter^2$ |
| millibar | 0.01017 | meter water |
| watt/$meter^2$ | 2.389E-5 | calorie/sec.$cm^2$ |
| watt/$meter^2$ | 86400 | megajoule/$meter^2$·day |

# APPENDIX D

## CALCULATION OF METEOROLOGICAL INPUTS

Explained here is the process by which the diurnal cycle inputs for air relative humidity, air temperature, air wind speed, and total global short-wave irradiance were calculated.

## APPENDIX D

Calculation of meteorological inputs.

Air temperature, global irradiance and wind speed all were modeled in the following form:

$$V = M + A \sin \pi (t/12 - k)$$

and relative humidity as the form:

$$V = M + A \cos \pi (t/12 - k)$$

where V = meteorological variable

M = daily mean

A = amplitude

t = time (hrs)

k = phase shift to peak in early afternoon

Air temperature, wind speed and relative humidity data were found in the literature in enough detail where M and A could be calculated directly. However, global irradiance is normally published as daily, or even monthly, averages.

To fit a diurnal cycle to a daily average figure for radiation (see Figure D1), area A was set equal to area B using integral calculus. Published values by Bruce, et al. (1977) and Van Bavel and Hillel (1976) indicated that area B was larger than that under half a sine wave, thus QAV was set equal to a value greater than 0, and the sine wave for radiation was truncated below the 0 line. Thus:

$$\int_{6}^{18} [QAV + QAM \sin \pi (t/12 - 0.5)]\, dt \overset{\text{set}}{=} Q(\text{published daily avg.}) \times 24 \text{ hours}$$

The integration produces one equation with 2 unknowns QAM and QAV:

$$12\ QAV + 7.64\ QAM = Q\ (published) \times 24$$

Fitting to published data, the author chose QAV = 50 $W/m^2$, and used the equation to calculate the corresponding QAM.

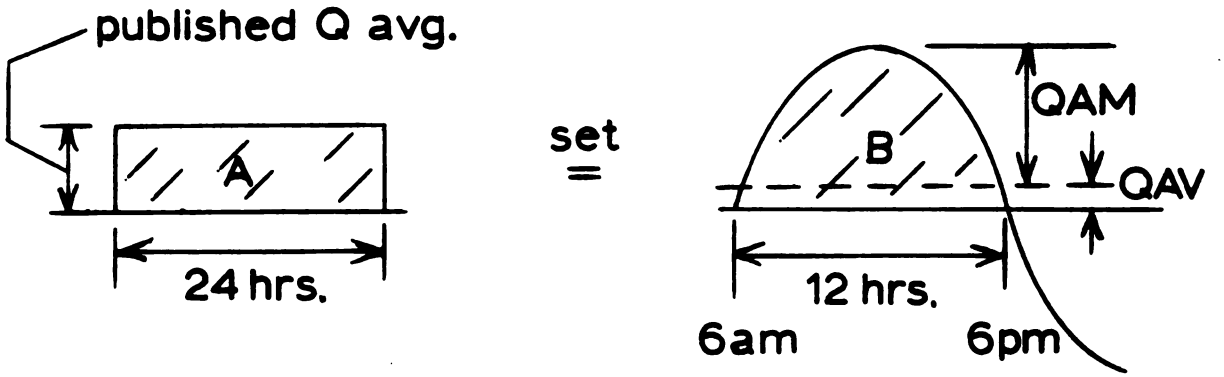


Figure D.1. Global irradiance cycle computation.